THERMODYNAMIC MODELING AND TRANSIENT SIMULATION OF A LOW-PRESSURE HEAT RECOVERY STEAM GENERATOR USING SIEMENS T3000

by

ANDRES M. CAESAR
B.S. University of Florida, 2015

A thesis submitted in partial fulfillment of the requirements
for the degree of Master of Science
in the Department of Mechanical and Aerospace Engineering
in the College of Engineering and Computer Science
at the University of Central Florida
Orlando, Florida

Summer Term
2018

Major Professor: Tuhin K. Das

ABSTRACT

With world energy consumption rising, and nonrenewable energy resources quickly depleting, it is essential to design more efficient power plants and thereby economically utilize fossil fuels. To that end, this work focuses on the thermodynamic modeling of steam power systems to enhance our understanding of their dynamic and transient behavior. This thesis discusses the physical phenomena behind a heat recovery steam generator (HRSG) and develops a mathematical description of its system dynamics. The model is developed from fundamentals of fluid dynamics, phase change, heat transfer, conservation laws and unsteady flow energy equations. The resulting model captures coupled physical phenomena with acceptable accuracy while achieving fast, and potentially real-time, simulations. The computational HRSG model is constructed in the Siemens T3000 platform. This work establishes the dynamic modeling capability of T3000, which has traditionally been used for programming control algorithms. The validation objective of this project is to accurately simulate the transient response of an operational steam power system. Validation of the T3000 model is carried out by comparing simulation results to start-up data from the low-pressure system of a Siemens power plant while maintaining the same inlet conditions. Simulation results well correlate with plant data regarding transient behavior and equilibrium conditions. With a comprehensive HRSG model available, it will allow for further research to take place, and aid in the advancement of steam power system technology. Some future research areas include the extension to intermediate and high-pressure system simulations, combined simulation of all three pressure stages, and continued improvement of the boiler model. In addition to enabling model-based prediction and providing further insight, this effort will also lead to controller design for improved performance.

This thesis is dedicated to my parents, my siblings, and to the love of my life; everything that I have and everything that I am, I owe it all to them.

ACKNOWLEDGMENTS

I would like to thank the many people who have contributed to this body of work and helped an idea transcend into a thesis. First and foremost I would like to express my sincere gratitude to my advisor, Professor Tuhin Das, for accepting me into his lab. I cannot thank you enough for giving me this incredible opportunity, and the continuous support that has changed my life. I could not imagine having a better teacher, advisor, and mentor for my graduate studies. I would like to extend my appreciation to the rest of my thesis committee, Professor Samik Bhattacharya, and Professor Shawn Putnam, for their interest in my work. I want to sincerely thank my colleague and labmate Singith Abeysiriwardena for assisting me at every turn in my studies. His daily attention to my work gave me the motivation and focus necessary to complete this research. I am thankful for the support of Bilal Salih and Farzad Aalipour-Hafshejani, who have been outstanding labmates during my time at the University of Central Florida. I would like to acknowledge the tireless work of Vaahini Ganesan whose previous efforts laid a foundation for the research in this thesis.

A special thank you to my colleagues at Siemens, Prithvi Veeravalli, and James Hoy, who have invested a tremendous amount of time and effort into this research. I am genuinely grateful for their commitment to this project, and the encouragement that I have received since the start. Without their support and expertise, this thesis would not have been possible.

TABLE OF CONTENTS

LIST OF FIGURES

LIST OF TABLES

LIST OF ACRONYMS

ACC	Air-Cooled Condenser
CCGT	Combined-Cycle Gas Turbine
CCPP	Combined-Cycle Power Plant
CV	Control Volume
DB	Deadband
DCS	Distributed Control System
FBD	Function Block Diagram
FD	Forced-Draft
FG	Flue Gas
GT	Gas Turbine
HP	High-Pressure
HRSG	Heat Recovery Steam Generator
HTC	Heat Transfer Coefficient
HX	Heat Exchanger
ID	Induced-Draft
IP	Intermediate-Pressure
LHS	Left-Hand Side
LMTD	Logarithmic Mean Temperature Difference
LP	Low-Pressure
PI	Proportional-Integral
PID	Proportional-Integral-Derivative
RHS	Right-Hand Side
SCPP	Simple-Cycle Power Plant

SPPA	Siemens Power Plant Automation
SPS	Steam Power System
ST	Steam Turbine
VPL	Visual Programming Language
WCC	Water-Cooled Condenser

LIST OF SYMBOLS

A	Area	m^2
C_p	Specific Heat at Constant Pressure	KJ Kg^{-1} K^{-1}
C_v	Specific Heat at Constant Volume	KJ Kg^{-1} K^{-1}
Δ	Difference Operator	-
$\dot{E}$	Energy Rate of Change	KJ s^{-1}
ϵ	Constant Tuning Parameter	-
f	Function Operator	-
g	Gravity	m s^{-2}
H	Enthalpy	KJ Kg^{-1}
$\dot{H}$	Enthalpy Rate of Change	KJ Kg^{-1} s^{-1}
h	Heat Transfer Coefficient	W m^{-2} K^{-1}
K_f	Flow Coefficient	-
M	Molecular Weight	mol
m	Mass	Kg
$\dot{m}$	Mass Flow Rate	Kg s^{-1}
n	Mole	mol
$\dot{n}$	Molar Flow Rate	mol s^{-1}
P	Pressure	bar(g)
ρ	Density	Kg m^{-3}
$\dot{Q}$	Heat Transfer Rate	KJ s^{-1}
R	Gas Constant	J K^{-1} mol^{-1}
T	Temperature	K
$\dot{T}$	Temperature Rate of Change	K s^{-1}

t	Time	s
U	Internal Energy	KJ Kg^{-1}
$\dot{U}$	Internal Energy, Rate of Change	KJ Kg^{-1} s^{-1}
V	Volume	m^3
v	Specific Volume	m^3 Kg^{-1}
$\dot{W}$	Work Rate of Change	KJ s^{-1}
X	Mole Fraction	-
z	Elevation	m

CHAPTER 1: INTRODUCTION

1.1 Research Motivation

Over the past 200 years, electricity has blossomed from scientific curiosity, into an essential component of modern life. As a result, energy production has become one of the most significant topics in scientific study today. The primary focus of power generation research is to improve power plant efficiency continually, and sparingly use the fossil fuels we have remaining. This effort has caused a global shift toward the increased application of combined-cycle power plants (CCPPs). While simple-cycle power plants (SCPPs) have a typical efficiency range between 25% and 40%, a CCPP can achieve electrical efficiencies from 50% to over 60%. A combined-cycle plant generally has a higher efficiency because SCPPs do not utilize any waste heat that comes from the turbine exhaust gas. Instead, this energy is immediately released to the atmosphere, in the form of flue gas, and not applied to do any additional work. In a CCPP, this waste heat is recovered and exploited to operate a steam power system (SPS); repurposing exhaust heat before expelling flue gas into the atmosphere will effectively increase electrical efficiency. However, the addition of a heat recovery mechanism will dramatically elevate the plant complexity. To further our understanding of how these intricate systems behave, we can develop comprehensive thermodynamic models. This work is not only for educational purposes, but to conduct research which will support the progression of power plant technology.

The rapid advancement in computer science has provided a computational platform which made this research possible. Thanks to the accessibility of high-speed processors, and the limitless capability of programming software, there has never been a more opportune time to create thermodynamic plant models. The application of modern computer technology will allow for plant

models to more accurately represent an actual system. From this, we can deepen our understanding of the dynamic characteristics of power plants. Furthermore, we can analyze plant behavior when subject to a disturbance. Since power plants are crucial to the daily operation of society, it is imperative that they do not falter or fail. Assessing simulations can be helpful, not only in preventing plant disturbance, but developing controllers to manage a plant if perturbed.

1.2 Research Objective

The objective of this project is to develop a comprehensive, physics-based model which represents a Siemens combined-cycle power plant. This type of power station is composed of three main components: gas turbine (GT), heat recovery steam generator (HRSG), and steam turbine (ST). The majority of modeling effort in this thesis will be on the HRSG system. This model will be developed on the Siemens Power Plant Automation (SPPA) T3000 platform and simply referred to as T3000 throughout this document. While this program is traditionally applied as a distributed control system, it has the potential to become a powerful graphical programming environment. For this project to be possible, we must be able to establish that T3000 is indeed a feasible modeling platform capable of handling complex multi-physics models. The complete physics-based power plant model will integrate fundamental physical phenomena which contribute to the dynamic behavior of a power system. The following sections will highlight some of the physics concepts which will be present in the HRSG model.

1.2.1 Flow Characteristics

Modeling the flow of fluid will largely depend on the principle of mass conservation, and the analysis of pressure change within the HRSG. Both topics are significant and will affect the

migration of flue gas in ducting, as well as the transport of fluid throughout piping. These topics also incorporate the physical parameters of the plant including component geometry, elevation changes, and material properties.

1.2.2 Thermodynamic Characteristics

Modeling the thermodynamics of a HRSG will primarily involve temperature changes and enthalpy balance within control volumes. The presence of phase change and accompanying enthalpy change over the flow path of flue gas, liquid water, and vapor is also considered.

1.2.3 Heat Transfer Mechanisms

The most common modes of heat transfer for the heat recovery steam generator are conduction and convection. The modeling of heat transfer will be closely related to flow and thermodynamic characteristics. Metal control volumes such as heat exchanger pipe bundles will transfer heat through conduction. While liquid, vapor, and flue gas control volumes will transmit thermal energy through forced convection.

1.2.4 Boiling and Condensation

The ability to accurately predict boiling and condensation within the HRSG can provide valuable insight into plant performance. The model can be applied to identify regions in the flow path where phase change is likely under specified operating conditions. Having this capability is invaluable considering that it is challenging, intrusive, and expensive to determine from the actual plant using sensors. Locating the domains of phase change is also significant from a plant-design perspective. These areas are associated with a dramatic change in temperature, pressure, and fluid

velocity. Therefore, a rapid change in these physical quantities could cause damage to a plant if they do not occur in the desired region.

We can expect to model phase transition taking place inside the HRSG piping using the steady flow energy equation. This formulation essentially models energy and mass conservation for open systems which operate under lasting steady-state conditions. For larger thermodynamic system (superheater, evaporator, economizer), we will adopt a control volume approach that includes mass evolution and pressure dynamics. This approach will allow us to demonstrate pressurization and depressurization, along with phenomena such as volume swell and shrink in simulations.

1.3 Research Approach

1.3.1 Physical Description

The first step in developing a comprehensive physics-based model is recognizing which principles are essential for characterizing the system. The aim is to construct a HRSG model which can simulate the transient response of plant startup, load fluctuation, and shutdown procedures. In Chapter 2 we will identify the major components of a combined-cycle power plant and give a brief description of each system. Understanding how each component of a CCPP functions will allow us to determine which concepts to apply when describing the HRSG. A lumped model approach is employed in this thesis; this will capture the essential physics of the system while making the model concise. By doing so, only the necessary physics are implemented to detail how the HRSG behaves.

1.3.2 Mathematical Formulation

Once an understanding of the HRSG is established, the physics can be expressed using the language of mathematics. In Chapter 3, each constituent of the heat recovery steam generator (economizer, evaporator, and superheater) is divided into multiple control volumes. These control volumes will contain different working fluids and thus differ in physical and mathematical description. By using balance laws and constitutive relationships, every control volume within the HRSG can be broken down into a set of equations. By relating the equations between control volumes, we can develop a network of expressions that define the HRSG.

1.3.3 Modeling in T3000

Now that a mathematical model for the HRSG is established, we can import this construct into the T3000 platform. In Chapter 4 we will implement this graphical programming environment to compute the library of equations previously developed. By simulating the mathematical model in real-time, we can view the HRSGs transient and steady-state response.

1.3.4 Model Validation

Chapter 5 is dedicated to validating the mathematical HRSG model by comparing simulation results in T3000 to start-up data from a Siemens power plant. The same operating conditions and parameters applied to the plant will also be implemented in T3000. Not only are the steady state results significant, but the transient response must also agree. By running a simulation and analyzing the results, we should see an identical response between the plant and model. With a comprehensive HRSG model developed, we can use this system as a testbed for further research to transpire.

CHAPTER 2: PLANT OVERVIEW

2.1 Combined-Cycle Power Plant

The grand-scale objective of this Siemens program is to develop a comprehensive, physics-based model which represents a combined-cycle power plant. The target CCPP is a gas turbine-based system also known as a combined-cycle gas turbine (CCGT) plant. Individually, a simple-cycle or steam-electric power plant can only achieve electrical efficiencies between 30 to 35 percent. A CCGT plant couples the gas and steam power cycles by using gas turbine exhaust heat as input energy for the steam power system. The combination of these thermodynamic cycles increases the net efficiency of a CCGT plant to around 60 percent. Throughout the remainder of this thesis, we will refer to a CCGT plant as simply a combined-cycle power plant. A typical CCPP layout is shown below in Figure 2.1 [1] to demonstrate how these systems interact.

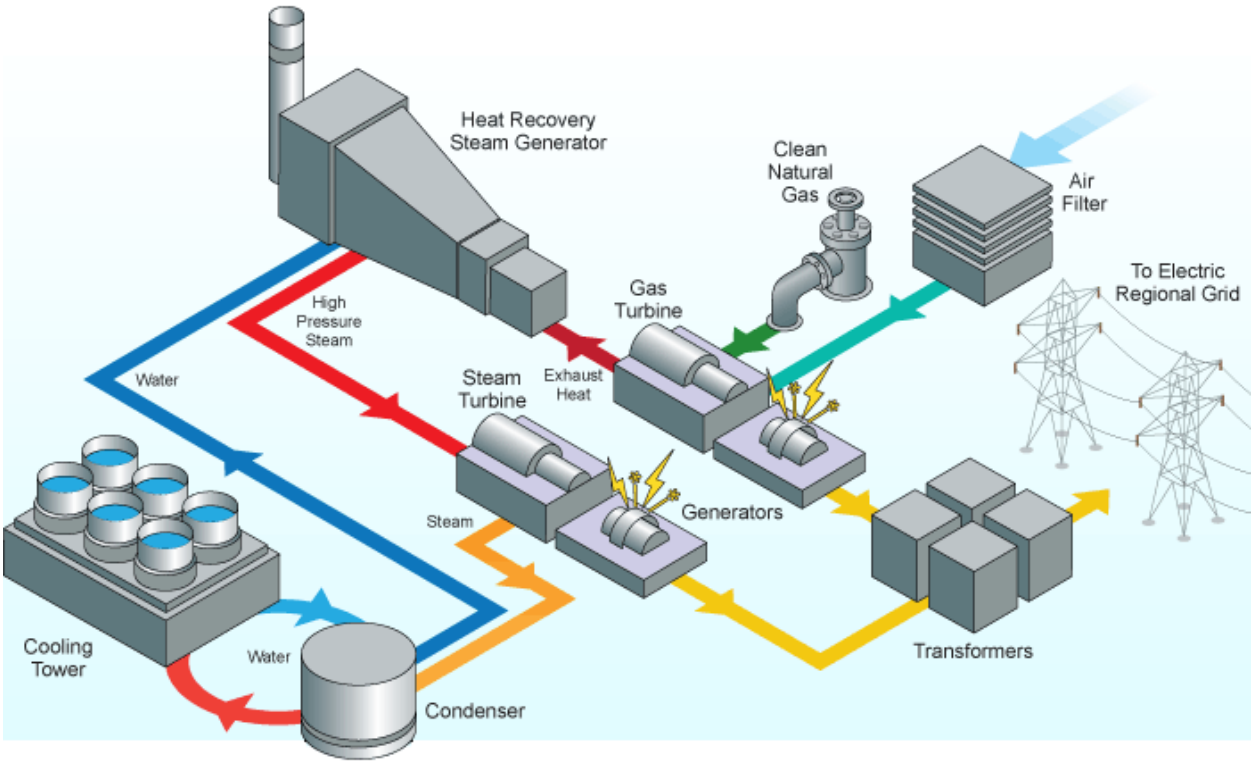

Figure 2.1: Diagram of a typical combined-cycle power plant

To give a better perception of size and plant configuration, Figure 2.2 [2] gives an aerial view of a 3x3 combined-cycle power plant. The MxN (M-on-N) notation describes a combined-cycle plant with M GT/HRSG trains supplying N steam turbines.

Figure 2.2: TVA Caledonia Combined-Cycle Plant, Mississippi

2.2 Plant Components

While a CCPP plant is composed of numerous elements, the major components of this system are as follows: gas turbine, heat recovery steam generator, steam turbine, and condenser. The rest of this chapter will give a brief overview of how these devices function within a combined-cycle power plant.

2.2.1 Gas Turbine

The operation of a CCPP starts with the gas turbine. Clean atmospheric air is drawn into the gas turbine compressor, elevating it to a higher pressure. This compressed air is then sprayed

with a fuel, typically natural gas, and ignited in the GT combustion chamber. At a high-temperature, the gas suddenly enters the turbine portion of the GT and expands quickly. The high-energy fuel-air mixture passes through the turbine blades at an accelerated velocity causing them to spin rapidly. The turbine shaft work is then used to actuate the compressor and draw additional air into the GT, as well as drive the electric generator and produce electricity. An illustration of a typical gas turbine engine is shown in Figure 2.3 [3].

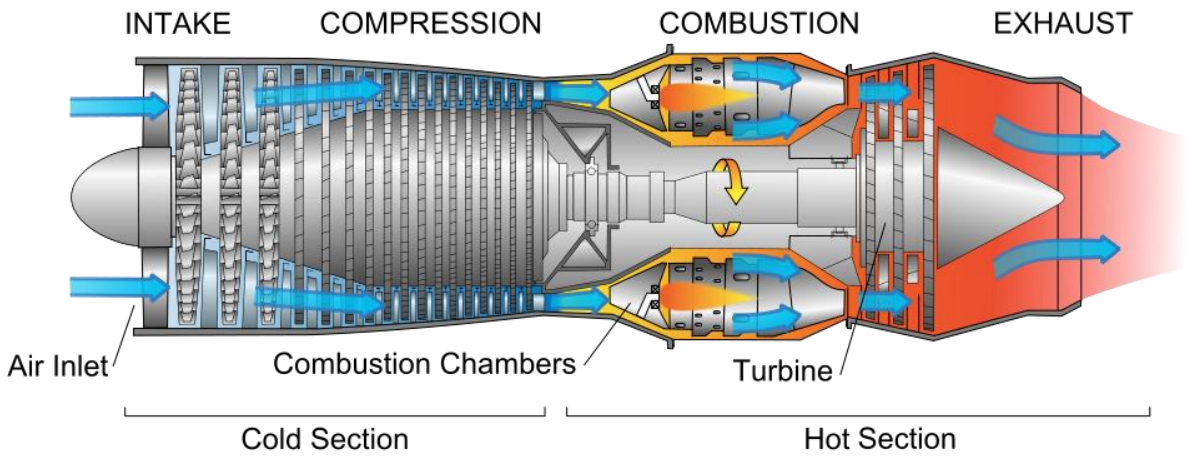

Figure 2.3: Diagram of a typical gas turbine engine

A byproduct of energy production using a combustion turbine is exhaust gas, also referred to as flue gas. In a simple-cycle gas turbine plant, the flue gas is released to the atmosphere through a stack, wasting thermal energy in the process. In a CCPP the exhaust heat is repurposed as the input energy for a heat recovery steam generator, effectively increasing electrical efficiency. An image of gas turbine assembly is shown in Figure 2.4 [4].

Figure 2.4: Assembly of a gas turbine rotor and casing

2.2.2 Heat Recovery Steam Generator

A heat recovery steam generator is essentially a heat exchanger (HX) which produces steam. This system is composed of smaller heat exchangers in series known as the economizer, evaporator, and superheater. Gas turbine exhaust flows through the HRSG casing in one direction and heats the internal piping. In the opposite direction, water travels through the heated regenerator piping and becomes steam. A more detailed description of this system and its components are given in Chapter 3.

The HRSG operates by first pumping purified feedwater into the economizer piping. In this heat exchanger, the water is preheated from a subcooled to saturated liquid state in preparation for vaporization. Heated feedwater is then propelled to the evaporator piping and further heated in the steam drum to its boiling point. This process causes water to undergo a phase transition from saturated liquid to saturated vapor. As saturated vapor proceeds through the superheater, it is

reheated past the saturation temperature to become superheated steam. Increasing the thermal energy of vapor from a saturated to a superheated state will decrease the likelihood of premature condensation and increase thermal energy. As superheated steam exits the HRSG, it is applied to drive the steam turbine and produce additional electricity. A diagram of a triple-pressure HRSG is shown below in Figure 2.5 [5]. An operational triple-pressure HRSG is captured in Figure 2.6 [6].

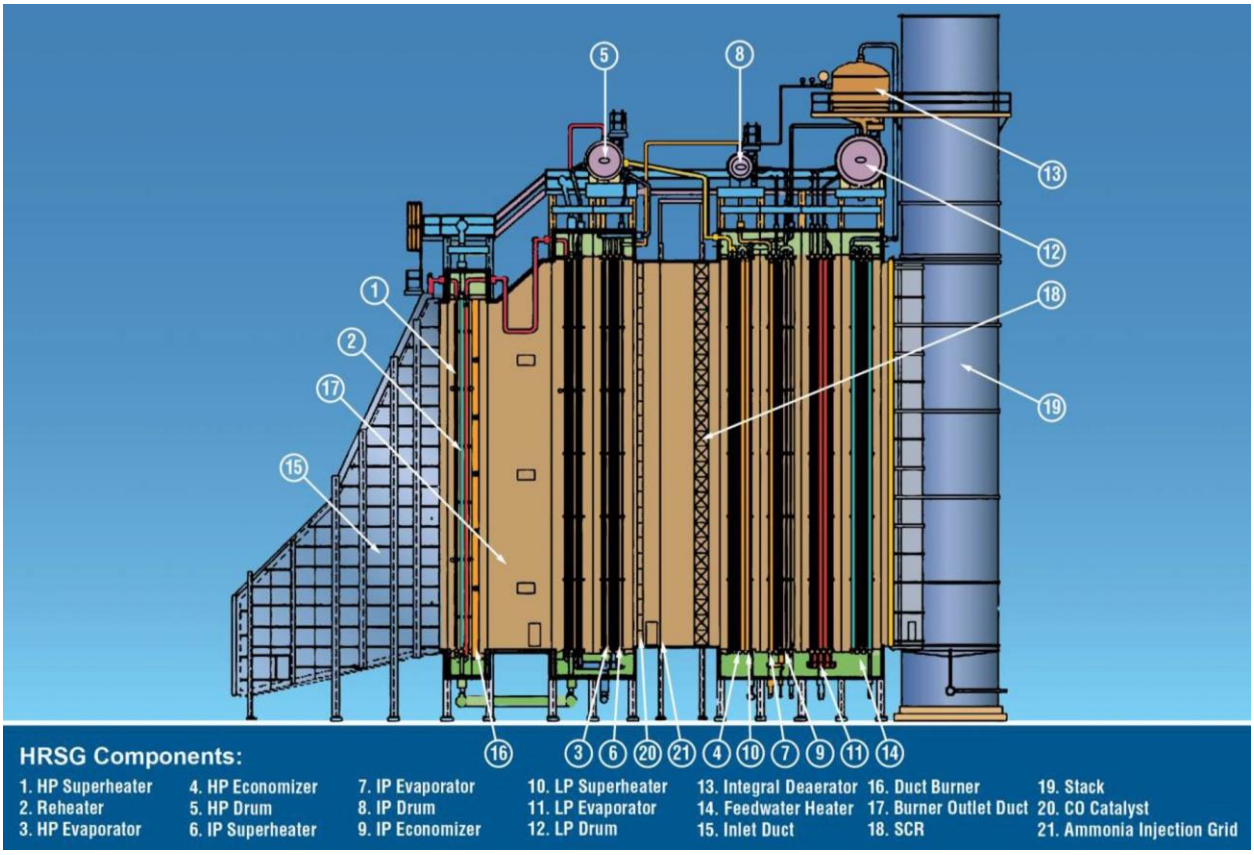

Figure 2.5: Component diagram of a triple-pressure heat recovery steam generator

Figure 2.6: Triple-pressure heat recovery steam generator

2.2.3 Steam Turbine

Gas and steam turbines operate similarly but use different working fluids to produce shaft work; while GTs use compressed air, STs are driven by superheated steam. As high-temperature high-pressure steam enters the ST, it instantly expands to occupy a greater volume. Superheated steam is forced through the turbine blades at high speed causing them to rotate and produce shaft work. The ST shaft is coupled to an electric generator and drives the production of electricity. An image of a single-case, industrial steam turbine is shown in Figure 2.7 [7].

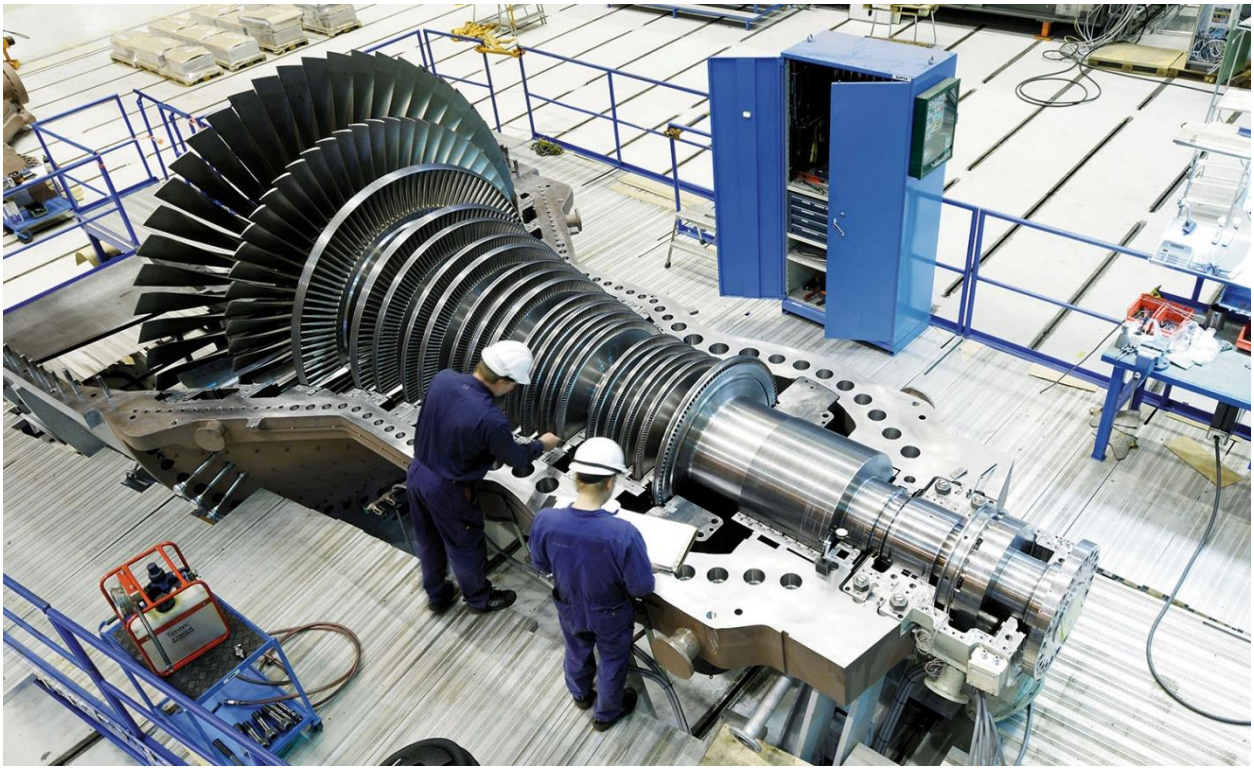

Figure 2.7: Assembly of Siemens SST-900 industrial steam turbine

In higher megawatt combined-cycle power plants, multiple steam turbines are typically connected in series; the exhaust from a higher pressure turbine is fed to operate a lower pressure turbine. These compound steam-turbine configurations fully utilize the steam and extracts as much thermal energy as possible to produce electricity. An example of a multiple-case, utility steam turbine is shown in Figure 2.8 [8]. An operational Siemens SST-6000 utility steam turbine is presented in Figure 2.9 [9].

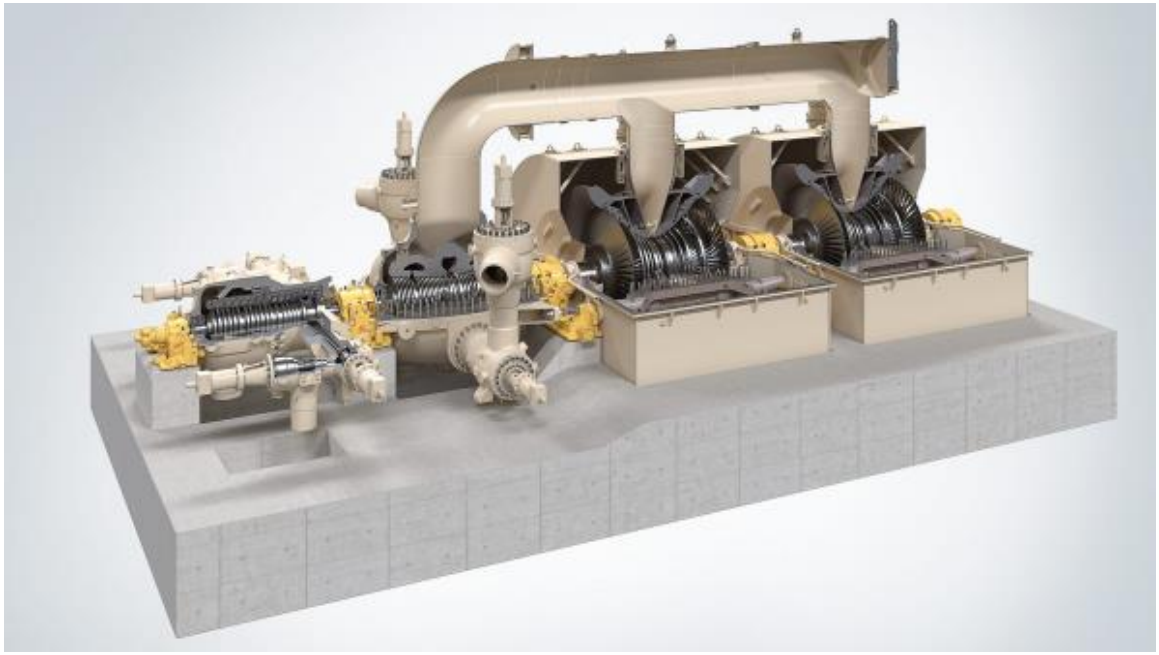

Figure 2.8: Model of a Siemens SST-6000 utility steam turbine package

Figure 2.9: Siemens SST-6000 steam turbine in Lünen Power Station, Germany

2.2.4 Condenser

In a combined-cycle power plant, the condenser is a heat exchanger which converts steam turbine exhaust steam into liquid water. This device uses a cooling medium to extract latent heat from the steam which induces condensation. The condensate (liquid water) collects in a receptacle and is then pumped back into the HRSG to be recycled as boiler feedwater. This process occurs at a pressure below atmospheric conditions with the assistance of condensate extraction pumps. The suction pressure from these pumps creates a vacuum (negative pressure) which produces the subatmospheric operating pressure within the condenser. By condensing exhaust steam below atmospheric pressure, the steam pressure drop between the inlet and outlet of the steam turbine is raised. This process enlarges steam expansion across the steam turbine and increases the amount of thermal energy available to produce electricity. The most common cooling mediums used in condensers are water and air which will be discussed in the following sections. Water-cooled condensers provide a higher vacuum pressure than air-cooled systems and can more significantly increase steam turbine efficiency. However, air-cooled condensers are low maintenance and provide a practical solution when water is scarce or expensive.

2.2.4.1 Water-Cooled Condenser

A surface condenser is a water-cooled, shell-and-tube heat exchanger which uses cooling water to condense steam into a liquid. A diagram of a typical water-cooled condenser (WCC) is shown in Figure 2.10 [10].

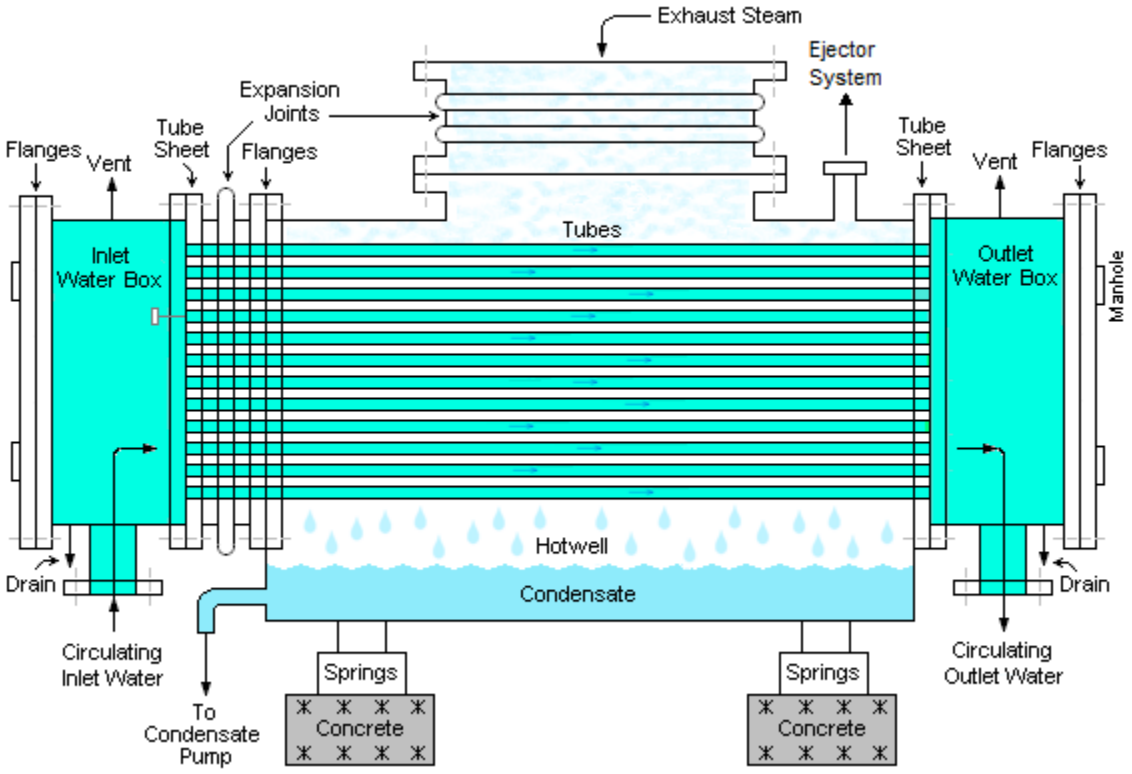

Figure 2.10: Diagram of a combined-cycle power plant single-pass surface condenser

As exhaust steam exits the steam turbine, it is fed into the shell side of the condenser. Cooling water is pumped into the condenser tube bundles which are contained within the shell. As steam flows through the tube section, it transfers thermal energy to the cooling water and condenses on the outside of the tubes. The newly formed condensate drips off of the cooling tubes and down into a liquid reservoir called the hotwell. As condensate collects in this basin, it will be pumped into the HRSG and used as boiler feedwater. The cooling water is transported to a cooling tower where its heat is rejected to the atmosphere. Once its temperature is reduced to ambient conditions, the cooling water is returned to the condenser. An air ejector system is implemented to draw air and various dissolved gases out of the condenser. This mechanism is put in place to remove contaminants which cause corrosion and interfere with steam contacting the cooling tubes. Figure 2.11 [11] shows a surface condenser used in a combined-cycle power plant.

Figure 2.11: Combined-cycle power plant surface condenser

2.2.4.2 Air-Cooled Condenser

An air-cooled condenser (ACC) uses induced-draft (ID) or forced-draft (FD) air flow to cool turbine exhaust steam and condense it into liquid water. Below in Figure 2.12 [12] is an illustration of a forced-draft air-cooled condenser.

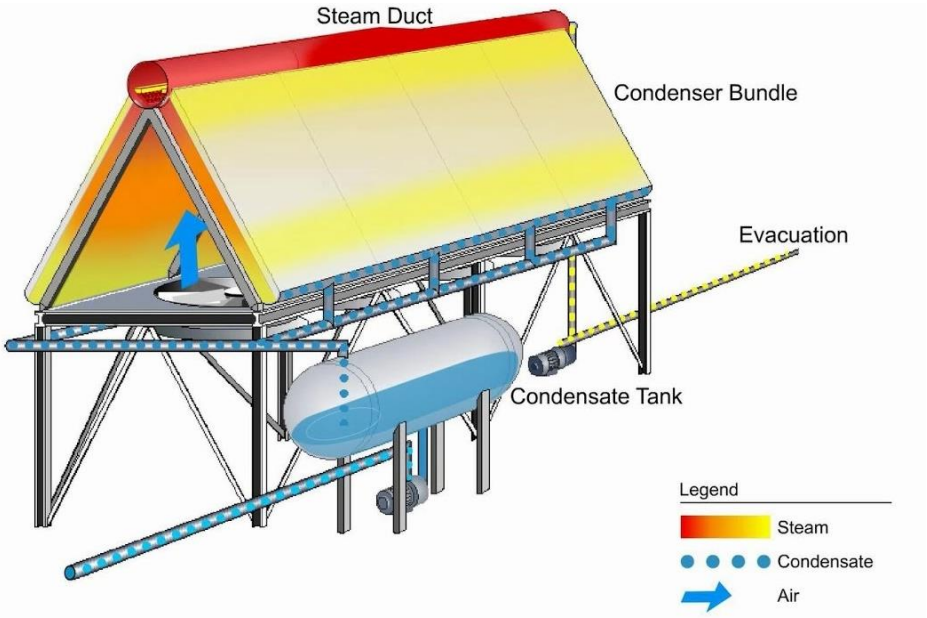

Figure 2.12: Diagram of a forced-draft air-cooled condenser

As exhaust steam leaves the steam turbine, it is directed into a large steam duct. This duct runs the length of the air-cooled condenser and channels steam into finned tubes. A fan is used to cause induced-draft or forced-draft airflow across the tube bundles. An induced-draft setup places the fan above the tube bundles so that it draws cool ambient air through the tube section. A forced-draft configuration places the fan below the tube bundles where it discharges cool ambient air across the tube section. As cool air passes over the tube bundles, thermal energy is removed from the steam which causes it to condense. This condensate drips down the tube bundle and accumulates in a header. The tube header then directs the condensate into a large collection tank where it will be pumped into the HRSG and recycled as boiler feedwater. For combined-cycle power plants, multiple air-cooled condenser sections are used to create an entire unit. This is carried out to provide the necessary cooling for large plant steam cycles. Air and non-condensable gases are removed from the steam cycle using an evacuation system. Not removing these pollutants can cause a reduction in heat transfer effectiveness and diminish power plant efficiency. The construction of a multi-section air-cooled condenser is shown in Figure 2.13 [13].

Figure 2.13: Construction of a combined-cycle power plant air-cooled condenser

CHAPTER 3: MATHEMATICAL MODELING OF THE HRSG

3.1 An Introduction to the HRSG

The heat recovery steam generator is at the heart of a combined cycle power plant, serving as a thermodynamic link between the gas and steam cycles. This system fundamentally acts as a counterflow heat exchanger and exploits heat from GT exhaust to produce steam for the ST. Inside the HRSG are three crossflow heat exchanger regimes called the economizer, evaporator, and superheater. These subsystems are shown below in the HRSG heat diagram in Figure 3.1. [14].

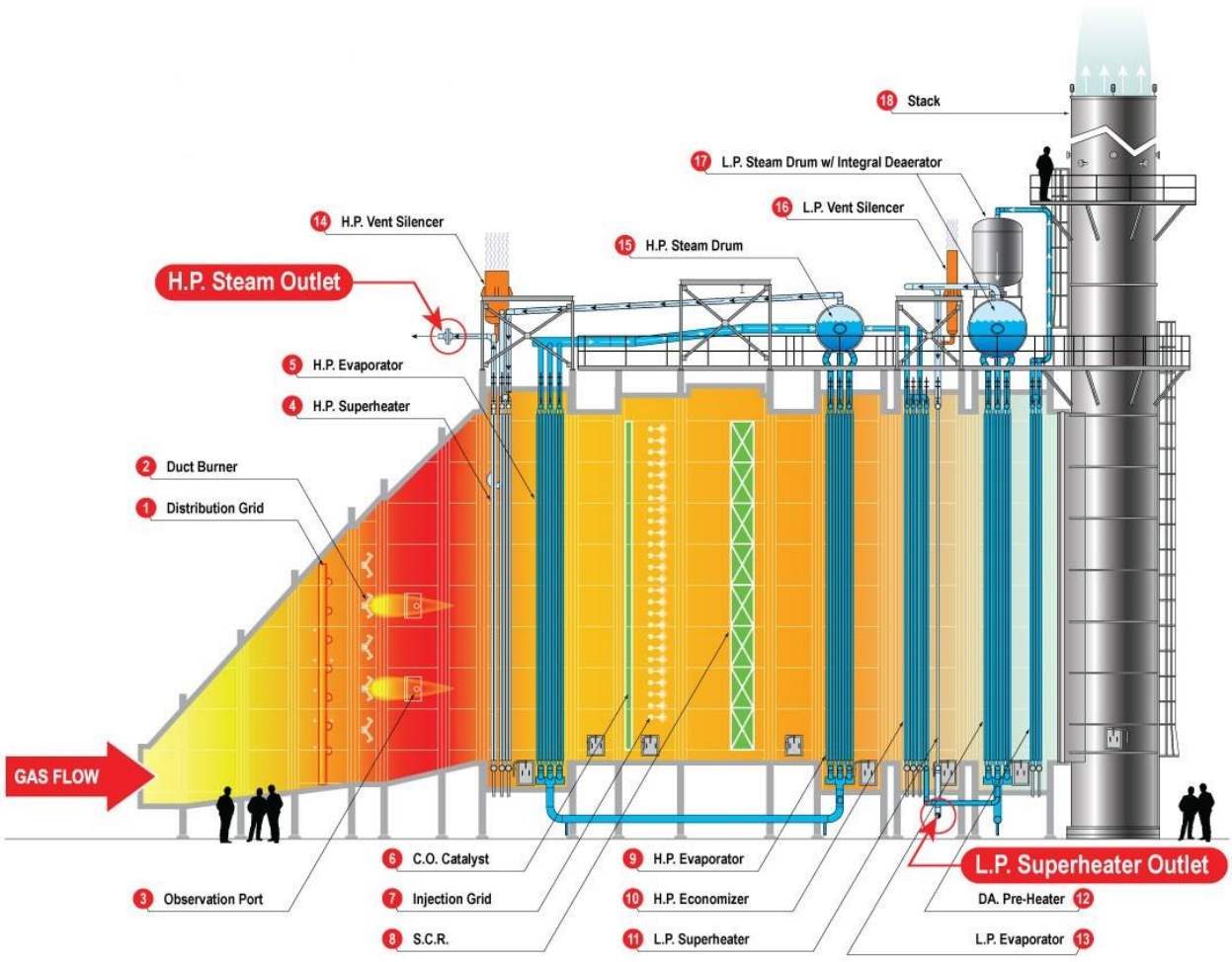

Figure 3.1: Heat diagram of a dual-pressure heat recovery steam generator

As high-energy flue gas passes through the system, energy is transferred from the exhaust to the water. Not only does this process assist in boiling, but it also reduces the flue gas temperature before exhausting to the atmosphere. This repurposing of thermal energy is key to increase plant efficiency. As a result, the HRSG is the primary focus of this thesis. The remaining sections in this chapter will give a physical and mathematical rendition of each major component of the HRSG.

3.2 Economizer

3.2.1 Physical System

The economizer (also known as feedwater preheater) is a heat exchanger which increases the temperature of feedwater before it enters the evaporator. It is positioned at the low-temperature end of the HRSG where feedwater is entering the system, and flue gas is exiting. Initially, subcooled feedwater is pumped from the condenser into the economizer piping. Low-temperature exhaust gas travels through the pipe bundles and heats them before exiting the HRSG. As the feedwater advances through the economizer pipeline, it absorbs thermal energy from the flue gas. This heat transfer raises the temperature of feedwater up to, but not beyond, the fluid saturation point. Thus, increasing the heat level of feedwater effectively lowers the input energy necessary for boiling in the evaporator and reduces plant operating costs. This process improves plant efficiency by recycling waste heat from the flue gas to preheat boiler feedwater. Additionally, the economizer further extracts thermal energy from the flue gas before it is expelled to the atmosphere. Preheating feedwater also helps to avoid thermal shock to the evaporator metal piping when the liquid is introduced back into the steam cycle.

3.2.2 Description of Parameters

This portion of the chapter details the symbols applied to describe the economizer mathematically. Table 3.1 describes the given/known economizer conditions where Table 3.2 defines the calculated/unknown parameters. Abbreviations for flue gas (*fg*), liquid (*liq*), and vapor (*vap*) are used as symbol subscripts throughout this chapter. Metric units are assumed for all variables and will be given in each table as necessary.

Table 3.1: Given Conditions for the Economizer

Description	**Symbol**	**Units**
Area of Contact	$A_{fg,met}$; $A_{met,liq}$	m^2
Flow Coefficient	K_f	-
Gas Constant	R	J K^{-1} mol^{-1}
Heat Transfer Coefficient	$h_{fg,met}$; $h_{met,liq}$	W m^{-2} K^{-1}
Inlet Mass Flow Rate of Liquid	$\dot{m}_{liq,in}$	kg s^{-1}
Inlet Molar Flow Rate of Flue Gas	$\dot{n}_{fg,in}$	mol s^{-1}
Inlet Pressure	$P_{fg,in}$; $P_{liq,in}$	bar(g)
Inlet Temperature	$T_{fg,in}$; $T_{liq,in}$	K
Mass of Metal	m_{met}	Kg
Molecular Weight	M_{fg} ; M_{liq}	mol
Specific Heat of Metal	$C_{p,met}$	KJ Kg^{-1} K^{-1}
Volume of Control Volume	V_{CV1} ; V_{CV2} ; V_{CV3}	m^3

Table 3.2: Calculated Parameters for the Economizer

Description	Symbol	Units
Inlet Enthalpy	$H_{fg,in}$; $H_{liq,in}$	KJ Kg^{-1}
Inlet Mass Flow Rate of Liquid	$\dot{m}_{liq,out}$	kg s^{-1}
Moles in Control Volume	n_{fg} ; n_{liq}	mol
Outlet Enthalpy	$H_{fg,out}$; $H_{liq,out}$	KJ Kg^{-1}
Outlet Molar Flow Rate of Flue Gas	$\dot{n}_{fg,out}$	mol s^{-1}
Outlet Pressure	$P_{fg,out}$; $P_{liq,out}$	bar(g)
Outlet Temperature	$T_{fg,out}$; $T_{liq,out}$	K
Specific Heat	$C_{v,fg}$; $C_{v,liq}$	KJ Kg^{-1} K^{-1}
Temperature of Metal	T_{met}	K

3.2.3 Mathematical Model

In this mathematical model, the economizer is represented as a massive control volume (CV) comprised of three smaller systems. The flue gas control volume (CV1) consists of gas turbine exhaust and resembles the domain around the economizer pipe bundles. The metal control volume (CV2) is made up of metal piping which runs through the economizer section. The liquid control volume (CV3) is composed of feedwater and encompasses the interior volume of the economizer piping.

3.2.3.1 Flue Gas Control Volume (CV1)

The flue gas outlet pressure is determined using the ideal gas law as shown in Equation (3.1). For this calculation, the volume of CV1 and universal gas constant are known. Yet the number of moles and temperature of flue gas at the outlet are unidentified and need to be found.

$$P_{fg,out} = \frac{n_{fg}\, R T_{fg,out}}{V_{CV1}} \tag{3.1}$$

The outlet molar flow rate of flue gas is discovered by applying Equation (3.2)

$$\dot{n}_{fg,out} = \frac{\Delta P_{fg}\, K_f}{M_{fg}} = \frac{\left(P_{fg,out} - P_{fg,in}\right) K_f\, X_{fg}}{M_{fg}} \tag{3.2}$$

The variable X_{fg} signifies the mole fraction of flue gas within the economizer. The number of moles of flue gas (n_{fg}) inside the economizer is determined by integrating the difference between inlet and outlet molar flow rates. This calculation is expressed in Equation (3.3).

$$n_{fg} = \int_{t_1}^{t_2} \left(\dot{n}_{fg,in} - \dot{n}_{fg,out}\right) dt \tag{3.3}$$

The flue gas temperature at the economizer outlet is found by applying an energy conservation balance to the flue gas control volume (CV1).

$$\begin{aligned} -\dot{Q}_{fg,met} + \sum \dot{n}_{fg,in} \left(H_{fg,in} + \frac{{v_{fg,in}}^2}{2} + g z_{fg,in} \right) \\ = \dot{E}_{CV1} + \dot{W}_{CV1} + \sum \dot{n}_{fg,out} \left(H_{fg,out} + \frac{{v_{fg,out}}^2}{2} + g z_{fg,out} \right) \end{aligned} \tag{3.4}$$

Equation (3.4) is a differential equation with respect to time. In this formula $\dot{Q}_{fg,met}$ is the rate of net heat transfer out the control volume from flue gas to metal. This variable is determined using the convection heat transfer equation shown below.

$$\dot{Q}_{fg,met} = h_{fg,met} A_{fg,met} \left(T_{fg,out} - T_{met}\right) \tag{3.5}$$

Note that in Equation (3.4) the net heat transfer occurs out of CV1. Therefore the rate of heat transfer between flue gas and metal ($\dot{Q}_{fg,met}$) will become a negative value. Assuming the net amount of mass within the control volume remains constant, there will be no mechanical work occurring. Furthermore, the kinetic and potential energies do not change between the economizer inlet and outlet. For these reasons Equation (3.4) can be rewritten in the following simplified form.

$$-\dot{Q}_{fg,met} + \dot{n}_{fg,in}H_{fg,in} = \dot{E}_{CV1} + \dot{n}_{fg,out}H_{fg,out} \tag{3.6}$$

Energy change within the control volume ($\dot{E}_{CV1}$) is found by the following expression.

$$\dot{E}_{CV1} = n_{fg}\dot{U}_{fg} = n_{fg}C_{v,fg}\dot{T}_{fg,out} \tag{3.7}$$

The specific heat of flue gas ($C_{v,fg}$) located in Equation (3.7) is determined using its mole fraction. By substituting the results from Equation (3.7) into Equation (3.6), we can formulate an expression for calculating the temperature change of flue gas in CV1.

$$-\dot{Q}_{fg,met} + \dot{n}_{fg,in}H_{fg,in} = n_{fg}C_{v,fg}\dot{T}_{fg,out} + \dot{n}_{fg,out}H_{fg,out} \tag{3.8}$$

By isolating the desired variable $\dot{T}_{fg,out}$ the proceeding solution can be given.

$$\dot{T}_{fg,out} = \frac{\dot{n}_{fg,in}H_{fg,in} - \dot{n}_{fg,out}H_{fg,out} - \dot{Q}_{fg,met}}{n_{fg}C_{v,fg}} \tag{3.9}$$

The outlet temperature of flue gas can be derived by integrating Equation (3.9) over time to give the proceeding formula.

$$T_{fg,out} = \int_{t_1}^{t_2} \frac{\dot{n}_{fg,in}H_{fg,in} - \dot{n}_{fg,out}H_{fg,out} - \dot{Q}_{fg,met}}{n_{fg}C_{v,fg}}\,dt \tag{3.10}$$

With an expression for n_{fg} and $T_{fg,out}$ now determined, we can revisit Equation (3.1) and apply these solutions to solve for the flue gas outlet pressure ($P_{fg,out}$).

3.2.3.2 Metal Control Volume (CV2)

The temperature of metal piping (T_{met}) within the economizer is influenced by a heat inflow from the flue gas (*fg*,*met*) and a heat transfer to the liquid (*met*,*liq*). This development is modeled by representing the rate of metal heat transfer as shown.

$$\dot{Q}_{met} = \dot{Q}_{fg,met} - \dot{Q}_{met,liq} \tag{3.11}$$

Equation (3.11) can be expanded by applying the simplified steady flow (left-hand side) and convective (right-hand side) heat transfer equations as formulated below.

$$m_{met}C_{p,met}\dot{T}_{met} = h_{fg,met}A_{fg,met}\left(T_{fg,out} - T_{met}\right) - h_{met,liq}A_{met,liq}\left(T_{met} - T_{liq,out}\right) \quad (3.12)$$

Equation (3.12) can be rewritten to solve for the rate of metal temperature change.

$$\dot{T}_{met} = \frac{h_{fg,met}A_{fg,met}\left(T_{fg,out} - T_{met}\right) - h_{met,liq}A_{met,liq}\left(T_{met} - T_{liq,out}\right)}{m_{met}C_{p,met}} \quad (3.13)$$

Therefore, the temperature of economizer piping is computed by integrating Equation (3.13) to produce the following solution.

$$T_{met} = \int_{t_1}^{t_2} \frac{h_{fg,met}A_{fg,met}\left(T_{fg,out} - T_{met}\right) - h_{met,liq}A_{met,liq}\left(T_{met} - T_{liq,out}\right)}{m_{met}C_{p,met}}\,dt \quad (3.14)$$

In the equation above, metal temperature is the only undetermined parameter as heat transfer coefficients, areas of contact, specific heat, and mass of metal are all known. Temperature values within the integrand are given for flue gas, metal, and liquid at the previous instance in time.

3.2.3.3 Liquid Control Volume (CV3)

Modeling the liquid control volume (CV3) will be performed similarly to that of the flue gas control volume (CV1). The significant difference between the two environments is their working fluids. CV1 contains flue gas which is more sensitive to changes in temperature. CV3 contains subcooled feedwater which is not as responsive to heat fluctuation. Therefore the following assumptions can be made for the liquid control volume to simplify the calculations.

The pressure difference between the liquid entering ($P_{liq,in}$) and exiting ($P_{liq,out}$) the economizer is negligible. This is caused by the minimal difference in liquid temperature between

the inlet and outlet of the economizer. Hence the inlet and outlet pressure for feedwater can be assumed identical as shown below.

$$P_{liq} = P_{liq,in} = P_{liq,out} \tag{3.15}$$

Furthermore, the mass flow rate of liquid incoming and leaving the economizer is pressure driven. Therefore if the liquid pressure is assumed to be constant within the economizer, then the mass flow rate of liquid can also be assumed constant. Thus, the inlet and outlet mass flow rate for feedwater can be considered identical.

$$\dot{m}_{liq} = \dot{m}_{liq,in} = \dot{m}_{liq,out} \tag{3.16}$$

To find the outlet liquid temperature, apply an energy conservation balance to the liquid control volume (CV3). The following differential equation is produced as a result.

$$\begin{aligned} &\dot{Q}_{met,liq} + \sum \dot{m}_{liq,in}\left(H_{liq,in} + \frac{{v_{liq,in}}^2}{2} + gz_{liq,in}\right) \\ &= \dot{E}_{CV3} + \dot{W}_{CV3} + \sum \dot{m}_{liq,out}\left(H_{liq,out} + \frac{{v_{liq,out}}^2}{2} + gz_{liq,out}\right) \end{aligned} \tag{3.17}$$

By analyzing Equation (3.17), we can identify that net heat transfer is going into the liquid control volume. For this reason, $\dot{Q}_{met,liq}$ is assigned a positive value. Assuming the net amount of mass inside the liquid control volume is constant, there is no mechanical work taking place.

$$\dot{W}_{CV3} = 0 \tag{3.18}$$

The kinetic and potential energies are also constant between the entrance and exit of CV3. Thus, these values will cancel each other out in the energy conservation balance. Using this information Equation (3.17) can be rewritten in the following simplified form.

$$\dot{Q}_{met,liq} + \dot{m}_{liq,in}H_{liq,in} = \dot{E}_{CV3} + \dot{m}_{liq,out}H_{liq,out} \tag{3.19}$$

The change in energy for the liquid control volume is given below.

$$\dot{E}_{CV3} = \dot{E}_{liq} = m_{liq,out}\dot{H}_{liq,out} \tag{3.20}$$

The right-hand side of Equation (3.20) can be rewritten by expanding $\dot{H}_{liq,out}$ using the first law of thermodynamics for ideal gases.

$$\dot{H}_{liq,out} = C_{p,liq}\dot{T}_{liq,out} \tag{3.21}$$

Therefore the change in energy for CV3 can be written as follows.

$$\dot{E}_{CV3} = \dot{E}_{liq} = m_{liq,out}C_{p,liq}\dot{T}_{liq,out} \tag{3.22}$$

By substituting the change in energy for CV3 into Equation (3.19) we can develop a useful expression for deriving the outlet liquid temperature.

$$\dot{Q}_{met,liq} + \dot{m}_{liq,in}H_{liq,in} = m_{liq,out}C_{p,liq}\dot{T}_{liq,out} + \dot{m}_{liq,out}H_{liq,out} \tag{3.23}$$

Since the inlet and outlet mass flow rates are identical we can apply Equation (3.16) to further simplify Equation (3.23).

$$\dot{Q}_{met,liq} + \dot{m}_{liq}H_{liq,in} = m_{liq}C_{p,liq}\dot{T}_{liq,out} + \dot{m}_{liq}H_{liq,out} \tag{3.24}$$

Solving the expression above for the desired variable $\dot{T}_{liq,out}$ creates the proceeding equality.

$$\dot{T}_{liq,out} = \frac{\dot{Q}_{met,liq} + \dot{m}_{liq}(H_{liq,in} - H_{liq,out})}{m_{liq}C_{p,liq}} \tag{3.25}$$

The outlet temperature of liquid is calculated by integrating Equation (3.25) over time to give the following solution.

$$T_{liq,out} = \int_{t_1}^{t_2} \frac{\dot{Q}_{met,liq} + \dot{m}_{liq}(H_{liq,in} - H_{liq,out})}{m_{liq}C_{p,liq}} dt \tag{3.26}$$

In Equation (3.26), $\dot{Q}_{met,liq}$ signifies the rate of net heat transfer into CV3 from metal to liquid. This parameter is calculated within the metal control volume (CV2) using the convection heat transfer formula below.

$$\dot{Q}_{met,liq} = h_{met,liq} A_{met,liq} \left(T_{met} - T_{liq,out}\right) \tag{3.27}$$

The specific heat at constant pressure of the liquid ($C_{p,liq}$) is calculated from water tables as a function of the liquid outlet temperature.

$$C_{p,liq} = f(T_{liq,out}) \tag{3.28}$$

The inlet ($H_{liq,in}$) and outlet ($H_{liq,out}$) enthalpy of liquid are also determined from water tables as a function of temperature and pressure.

$$H_{liq,in} = f(T_{liq.in}, P_{liq,in}) \tag{3.29}$$

$$H_{liq,out} = f(T_{liq,out}, P_{liq,out}) \tag{3.30}$$

The mass of liquid within CV3 is calculated using Equation (3.31).

$$m_{liq} = \frac{V_{CV3}}{v_{liq}} \tag{3.31}$$

In the expression above, V_{CV3} is a known parameter and represents the volume of CV3. The specific volume of liquid (v_{liq}) in CV3 is unknown, but this quantity can be determined from water tables as a function of outlet temperature and pressure.

$$v_{liq} = f(T_{liq,out}, P_{liq,out}) \tag{3.32}$$

3.3 Evaporator

3.3.1 Physical System

The evaporator (also referred to as a boiler) is a heat exchanger that transforms subcooled liquid into saturated vapor. This apparatus is centrally located in the HRSG and functions identically to a water-tube boiler. Initially, preheated feedwater is transferred from the economizer to the evaporator feedwater drum. From this location, the liquid is distributed through evaporator

water tubing while being heated by incoming flue gas. As liquid circulates through the water tubes, it absorbs energy and increases in temperature. When the heated water rises into the steam drum, it becomes saturated and begins to boil. A portion of this water-vapor mixture vaporizes into saturated steam and proceeds into the superheater. However, some wet steam does not undergo a complete phase transition and instead remains in a liquid-vapor state. The liquid portion travels through downcomer tubing, by natural circulation or pump assistance, and returns to the feedwater drum. At this point the downcomer water combines with incoming feedwater, preheating it in the process, and the boiling cycle repeats.

3.3.2 Description of Parameters

This section is dedicated to defining the symbols used to characterize the evaporator mathematically. Table 3.3 outlines the given/known conditions for the evaporator where Table 3.4 details the calculated/unknown parameters. Abbreviations for flue gas (*fg*), metal (*met*), liquid (*liq*), and vapor (*vap*) are used as symbol subscripts through this chapter. Metric units are assumed for all parameters and will be given in each table as necessary.

Table 3.3: Given Conditions for the Evaporator

Description	**Symbol**	**Units**
Area of Contact	$A_{fg,met}$; $A_{met,liq}$; $A_{met,vap}$; $A_{met,vap}$	m^2
Density of Liquid	ρ_{liq}	Kg m^{-3}
Flow Coefficient	K_f	-
Gas Constant	R	J K^{-1} mol^{-1}
Heat Transfer Coefficient	$h_{fg,met}$; $h_{met,liq}$; $h_{met,vap}$; $h_{met,vap}$	W m^{-2} K^{-1}
Inlet Molar Flow Rate	$\dot{n}_{fg,in}$; $\dot{n}_{vap,in}$	mol s^{-1}
Inlet Pressure	$P_{fg,in}$; $P_{liq,in}$; $P_{vap,in}$	bar(g)
Inlet Temperature	$T_{fg,in}$; $T_{liq,in}$; $T_{vap,in}$	K
Mass of Metal	m_{met}	Kg
Molecular Weight	M_{fg} ; M_{vap}	mol
Specific Heat	$C_{v,fg}$; $C_{p,met}$; $C_{v,liq}$; $C_{v,vap}$	KJ Kg^{-1} K^{-1}
Volume of Control Volume	V_{CV4} ; V_{CV5} ; V_{CV6} ; V_{CV7}	m^3

Table 3.4: Calculated Parameters for the Evaporator

Description	**Symbol**	**Units**
CV Rate of Heat Transfer	$\dot{Q}_{fg,met}$; $\dot{Q}_{met,liq}$; $\dot{Q}_{met,vap}$; $\dot{Q}_{liq,vap}$	KJ s^{-1}
Inlet Enthalpy	$H_{fg,in}$; $H_{liq,in}$; $H_{vap,in}$	KJ Kg^{-1}
Internal Energy in Vapor CV	U_{vap}	KJ Kg^{-1}
Mass Flow Rate	$\dot{m}_{liq}$; $\dot{m}_{vap}$	Kg s^{-1}
Mass Flow Rate of Evaporation	$\dot{m}_{liq,vap}$	Kg s^{-1}
Metal Rate of Heat Transfer	$\dot{Q}_{met}$	KJ s^{-1}
Moles in Control Volume	n_{fg} ; n_{liq} ; n_{vap}	mol
Outlet Enthalpy	$H_{fg,out}$; $H_{liq,out}$; $H_{vap,out}$	KJ Kg^{-1}
Outlet Mass Flow Rate of Vapor	$\dot{m}_{vap,out}$	Kg s^{-1}
Outlet Molar Flow Rate	$\dot{n}_{fg,out}$; $\dot{n}_{liq,out}$; $\dot{n}_{vap,out}$	mol s^{-1}
Outlet Pressure	$P_{fg,out}$; $P_{liq,out}$; $P_{vap,out}$	bar(g)
Outlet Temperature of Flue Gas	$T_{fg,out}$	K
Temperature of Metal	T_{met}	K
Temperature of Water	T_{liq} ; T_{vap}	K

3.3.3 Mathematical Model

Mathematically, the evaporator is designed as a large control volume (CV) consisting of four smaller systems. The flue gas control volume (CV4) encompasses gas turbine exhaust and resembles the volume around the boiler. The metal control volume (CV5) is composed of the metal pipes and drums located in the evaporator section. The liquid control volume (CV6) features the internal space in the feedwater drum, water tubing, and a portion of the steam drum that contains liquid. The vapor control volume (CV7) corresponds to the interior volume of vapor piping, and a region inside the steam drum that contains vapor.

3.3.3.1 Flue Gas Control Volume (CV4)

The flue gas control volume for the evaporator is modeled identically to that of the economizer in Section 3.2.3.1. For this reason, a majority of the equations used to describe the economizer will be applied to express the evaporator flue gas domain. The ideal gas law gives the outlet pressure for the flue gas as shown in Equation (3.33).

$$P_{fg,out} = \frac{n_{fg}\, R T_{fg,out}}{V_{CV4}} \tag{3.33}$$

While the universal gas constant (R) and flue gas volume are given (V_{CV4}), the number of moles (n_{fg}) and temperature ($T_{fg,out}$) need to be calculated. The outlet molar flow rate can be found using the following statement.

$$\dot{n}_{fg,out} = \frac{\Delta P_{fg}\, K_f}{M_{fg}} = \frac{\left(P_{fg,out} - P_{fg,in}\right) K_f\, X_{fg}}{M_{fg}} \tag{3.34}$$

The symbol X_{fg} signifies the mole fraction of flue gas within the evaporator. After solving Equation (3.34), the outlet molar flow rate is known, and the inlet molar flow rate is given.

Therefore, we can compute the number of flue gas moles (n_{fg}) by integrating their difference as shown in Equation (3.35).

$$n_{fg} = \int_{t_1}^{t_2} \left(\dot{n}_{fg,in} - \dot{n}_{fg,out}\right) dt \tag{3.35}$$

The outlet temperature of flue gas is generated by first applying an energy balance to the appropriate control volume (CV4). The result is a differential equation with respect to time.

$$\begin{aligned} &-\dot{Q}_{fg,met} + \sum \dot{n}_{fg,in}\left(H_{fg,in} + \frac{{v_{fg,in}}^2}{2} + g z_{fg,in}\right) \\ &= \dot{E}_{CV4} + \dot{W}_{CV4} + \sum \dot{n}_{fg,out}\left(H_{fg,out} + \frac{{v_{fg,out}}^2}{2} + g z_{fg,out}\right) \end{aligned} \tag{3.36}$$

Within Equation (3.36) is the rate of net heat transfer from flue gas to metal ($\dot{Q}_{fg,met}$). This parameter is described through the convection heat transfer equation as shown below.

$$\dot{Q}_{fg,met} = h_{fg,met} A_{fg,met}\left(T_{met} - T_{fg,out}\right) \tag{3.37}$$

Observe that in Equation (3.36) the net heat transfer rate occurs out of CV4, making $\dot{Q}_{fg,met}$ a negative value. If we assume that the net amount of mass inside the control volume remains constant, then no mechanical work takes place. Also, the kinetic and potential energies remain unchanged between the inlet and outlet of the CV. The result of these assumptions reduces Equation (3.36) to the following statement.

$$-\dot{Q}_{fg,met} + \dot{n}_{fg,in} H_{fg,in} = \dot{E}_{CV4} + \dot{n}_{fg,out} H_{fg,out} \tag{3.38}$$

The following formula gives the energy rate of change inside the control volume ($\dot{E}_{cv4}$).

$$\dot{E}_{CV4} = n_{fg} \dot{U}_{fg} = n_{fg} C_{v,fg} \dot{T}_{fg,out} \tag{3.39}$$

The specific heat of flue gas ($C_{v,fg}$) is found using the flue gas mole fraction (X_{fg}). By substituting the result of Equation (3.39) into Equation (3.38), we can develop an expression for computing the outlet temperature change of flue gas in CV4.

$$-\dot{Q}_{fg,met} + \dot{n}_{fg,in}H_{fg,in} = n_{fg}C_{v,fg}\dot{T}_{fg,out} + \dot{n}_{fg,out}H_{fg,out} \tag{3.40}$$

By rearranging Equation (3.40) we can isolate the desired variable $\dot{T}_{fg,out}$ as shown below.

$$\dot{T}_{fg,out} = \frac{\dot{n}_{fg,in}H_{fg,in} - \dot{n}_{fg,out}H_{fg,out} - \dot{Q}_{fg,met}}{n_{fg}C_{v,fg}} \tag{3.41}$$

The outlet temperature of flue gas can thus be derived by integrating Equation (3.41) to provide the following result.

$$T_{fg,out} = \int_{t_1}^{t_2} \frac{\dot{n}_{fg,in}H_{fg,in} - \dot{n}_{fg,out}H_{fg,out} - \dot{Q}_{fg,met}}{n_{fg}C_{v,fg}}\, dt \tag{3.42}$$

Now that a solution for n_{fg} and $T_{fg,out}$ is available, we can return to the ideal gas law in Equation (3.33) and solve for the flue gas outlet pressure ($P_{fg,out}$).

3.3.3.2 Metal Control Volume (CV5)

The temperature of evaporator metal (T_{met}) is influenced by the rate at which it absorbs heat from the flue gas. Furthermore, T_{met} is affected by the rate at which heat is released from the metal to the liquid water and saturated vapor. This relationship of heat transfer between the four mediums is modeled using the following equations. The net heat transfer of the boiler metal is given as Equation (3.43).

$$\dot{Q}_{met} = \dot{Q}_{fg,met} - \dot{Q}_{met,liq} - \dot{Q}_{met,vap} \tag{3.43}$$

Equations (3.44), (3.45), and (3.46) express the rate of heat transfer between the flue gas and metal, metal and liquid, and metal and vapor control volumes respectively.

$$\dot{Q}_{fg,met} = h_{fg,met} A_{fg,met} (T_{fg,out} - T_{met}) \tag{3.44}$$

$$\dot{Q}_{met,liq} = h_{met,liq} A_{met,liq} (T_{met} - T_{liq}) \tag{3.45}$$

$$\dot{Q}_{met,vap} = h_{met,vap} A_{met,vap} (T_{met} - T_{vap}) \tag{3.46}$$

These three convective heat transfer equations can be used to expand the right-hand side (RHS) of Equation (3.43) to create the expression below.

$$\begin{aligned} \dot{Q}_{met} = {} & h_{fg,met} A_{fg,met} (T_{fg,out} - T_{met}) - h_{met,liq} A_{met,liq} (T_{met} - T_{liq}) \\ & - h_{met,vap} A_{met,vap} (T_{met} - T_{vap}) \end{aligned} \tag{3.47}$$

Additionally the net rate of heat transfer for the evaporator metal can be described using Equation (3.48) as shown.

$$\dot{Q}_{met} = C_{p,met} m_{met} \dot{T}_{met} \tag{3.48}$$

This result can be used to expand the left-hand side (LHS) of Equation (3.47) and produce a fully augmented version of Equation (3.43).

$$\begin{aligned} C_{p,met} m_{met} \dot{T}_{met} = {} & h_{fg,met} A_{fg,met} (T_{fg,out} - T_{met}) - h_{met,liq} A_{met,liq} (T_{met} - T_{liq}) \\ & - h_{met,vap} A_{met,vap} (T_{met} - T_{vap}) \end{aligned} \tag{3.49}$$

By reorganizing Equation (3.49) we can solve for the parameter of interest.

$$\dot{T}_{met} = \frac{\begin{array}{c} h_{fg,met} A_{fg,met} (T_{fg,out} - T_{met}) - h_{met,liq} A_{met,liq} (T_{met} - T_{liq}) \\ - h_{met,vap} A_{met,vap} (T_{met} - T_{vap}) \end{array}}{C_{p,met} m_{met}} \tag{3.50}$$

The evaporator metal temperature (T_{met}) is calculated by integrating Equation (3.50) in order to obtain the final solution.

$$T_{met} = \int_{t_1}^{t_2} \frac{\begin{array}{c} h_{fg,met} A_{fg,met} (T_{fg,out} - T_{met}) - h_{met,liq} A_{met,liq} (T_{met} - T_{liq}) \\ - h_{met,vap} A_{met,vap} (T_{met} - T_{vap}) \end{array}}{C_{p,met} m_{met}} dt \tag{3.51}$$

To complete this computation, the temperature of liquid (T_{liq}), vapor (T_{vap}), and flue gas ($T_{fg,out}$) are still needed from their individual control volumes.

3.3.3.3 Liquid Control Volume (CV6)

In the evaporator, liquid water can be in one of two states: heating or boiling. Each of these states is modeled separately and calculate the liquid temperature (T_{liq}), liquid volume (V_{liq}), mass flow rate from liquid to vapor ($\dot{m}_{liq,vap}$), and net heat transfer from liquid to vapor ($\dot{Q}_{liq,vap}$). As a result, it is crucial that we identify the current mode of liquid water. This process is done by implementing a condition that compares the current liquid temperature to its saturation temperature at the vapor pressure.

If the condition in Equation (3.52) holds true, then the liquid is in heating mode. This logic is valid considering that the liquid temperature has not yet reached its boiling point at that pressure. Therefore the difference between the current and saturation temperature will be less than some positive constant (ϵ).

$$T_{liq} - T_{sat} < \epsilon \rightarrow Heating \tag{3.52}$$

If the condition in Equation (3.53) is found true, then the liquid enters into the boiling mode. The logic for this scenario is appropriate since the liquid temperature has surpassed its boiling point at that temperature. Consequently, the difference between current and saturation temperature will be greater than some positive constant (ϵ).

$$T_{liq} - T_{sat} > \epsilon \rightarrow Boiling \tag{3.53}$$

In general, a liquid begins to boil when reaching saturation conditions (P_{sat} and T_{sat}). Therefore, when the current liquid temperature is less than its respective saturation temperature, we conclude that the liquid is heating. While liquid starts boiling at T_{sat}, the implemented switching relay will

incorporate a buffer. This neutral zone will force the current liquid temperature to exceed its saturation temperature by ϵ before entering boiling mode. The allowable difference constant ϵ is a tunable parameter which can be set to any non-negative integer. This variable will allow for a more robust model when switching between heating and boiling modes.

3.3.3.3.1 Liquid Heating

While in the liquid heating phase, there is no vapor formation occurring. Hence, there is no mass flow from the liquid to vapor state. The mass flow rate of evaporation is set to zero as shown.

$$\dot{m}_{liq,vap|heat} = 0 \tag{3.54}$$

Although Equation (3.54) holds true for heating, there will be some heat transfer present between the liquid and already formed vapor. This convective heat transfer is expressed by Equation (3.55).

$$\dot{Q}_{liq,vap} = h_{liq,vap} A_{liq,vap} \left(T_{liq} - T_{vap}\right) \tag{3.55}$$

For this equation, the vapor temperature (T_{vap}) is calculated within the vapor control volume (CV7). The liquid temperature is found by applying an energy conservation balance to this control volume (CV6). The resulting differential equation with respect to time is shown below.

$$\dot{Q}_{met,liq} - \dot{Q}_{liq,vap} + \dot{m}_{pump} H_{liq,in} = \dot{m}_{liq,vap} H_{liq,out} + \dot{E}_{liq} \tag{3.56}$$

For a liquid, the internal energy and enthalpy can be considered the same. While liquid heats inside the evaporator, there will be no vapor formation. Therefore, the rate of change for liquid mass is simply the rate at which feedwater (liquid) is entering the control volume. This condition is stated in Equation (3.57).

$$\dot{m}_{pump} = \dot{m}_{liq} \tag{3.57}$$

The change in energy of the liquid during the heating phase is given as follows.

$$\dot{E}_{liq} = \dot{m}_{liq} H_{liq} + m_{liq} \dot{H}_{liq} = \dot{m}_{liq} H_{liq} + m_{liq} C_{v,liq} \dot{T}_{liq} \tag{3.58}$$

By substituting Equations (3.57) and (3.58) into Equation (3.56), and letting the mass flow rate of evaporation be zero, we can generate an expression for computing the liquid temperature during heating.

$$\dot{Q}_{met,liq} - \dot{Q}_{liq,vap} + \dot{m}_{liq} H_{liq,in} = \dot{m}_{liq} H_{liq} + m_{liq} C_{v,liq} \dot{T}_{liq} \tag{3.59}$$

The expression above can be rewritten in order to solve for the desired parameter.

$$\dot{T}_{liq} = \frac{\dot{Q}_{met,liq} - \dot{Q}_{liq,vap} + \dot{m}_{liq}(H_{liq,in} - H_{liq})}{m_{liq} C_{v,liq}} \tag{3.60}$$

The liquid temperature during heating mode is calculated by integrating Equation (3.60) to give the following solution.

$$T_{liq} = \int_{t_1}^{t_2} \frac{\dot{Q}_{met,liq} - \dot{Q}_{liq,vap} + \dot{m}_{liq}(H_{liq,in} - H_{liq})}{m_{liq} C_{v,liq}} dt \tag{3.61}$$

In Equation (3.61), the integration initial condition is the liquid temperature from the previous instant in time. The rate of heat transfer from metal to liquid ($\dot{Q}_{met,liq}$) and liquid to vapor ($\dot{Q}_{liq,vap}$) are obtained from Equations (3.44) and (3.55) respectively. The specific heat capacity of liquid ($C_{v,liq}$) is given as a constant. Water enters the evaporator in a saturated state and is maintained at these conditions while heating. Hence, the enthalpies are computed from steam tables as a function of the liquid saturation temperature.

$$H_{liq,in} = f\left(T_{sat,in}\right) \tag{3.62}$$

$$H_{liq} = f\left(T_{sat,out}\right) \tag{3.63}$$

The inlet saturation temperature ($T_{sat,in}$) is given, and the outlet saturation temperature ($T_{sat,out}$) coincides with the liquid temperature found in Equation (3.61). The mass of liquid water is obtained from its volume (V_{liq}) and density (ρ_{liq}) as shown in Equation (3.64).

$$m_{liq} = V_{liq}\rho_{liq} \tag{3.64}$$

With the liquid density is given, the volume is calculated by integrating the difference between the incoming ($\dot{m}_{liq}$) and outgoing ($\dot{m}_{liq,vap}$) water mass flow rates.

$$V_{liq} = \int_{t_1}^{t_2} \frac{\dot{m}_{liq} - \dot{m}_{liq,vap}}{\rho_{liq}} dt \tag{3.65}$$

Although the liquid mass flow rate ($\dot{m}_{liq}$) is known, the mass flow rate of evaporation ($\dot{m}_{liq,vap}$) is calculated within the liquid boiling section.

3.3.3.3.2 *Liquid Boiling*

During the liquid boiling phase, the liquid remains at the saturation temperature throughout the vaporization process. As a result, there is no change in liquid temperature as shown below.

$$\dot{T}_{liq} = 0 \tag{3.66}$$

Instead, the temperature of liquid during boiling is taken as the last calculated temperature of liquid while heating.

$$T_{liq|boil} = T_{liq} \tag{3.67}$$

Throughout the boiling process, liquid water will evaporate and become vapor. While the mass flow rate of evaporation was zero for heating, there is a significant mass transfer from liquid to vapor during boiling. Accordingly, the mass flow rate of evaporation will be a non-zero value in the boiling mode.

$$\dot{m}_{liq,vap|boil} \neq 0 \tag{3.68}$$

This parameter is calculated by performing an energy conservation balance in the liquid control volume (CV6). The result is a differential equation with respect to time as follows.

$$\dot{Q}_{met,liq} - \dot{Q}_{liq,vap} + \dot{m}_{pump} H_{liq,in} = \dot{m}_{liq,vap} H_{vap,out} + \dot{E}_{liq} \tag{3.69}$$

We can further simplify Equation (3.69) by applying the $\dot{E}_{liq}$ formula from Equation (3.58). However, the solution will be slightly modified during boiling since the liquid temperature change ($\dot{T}_{liq}$) is zero. Therefore the change in energy for liquid during the boiling phase is given as follows.

$$\dot{E}_{liq} = \dot{m}_{liq} H_{liq} + m_{liq} C_{v,liq} \dot{T}_{liq} = \dot{m}_{liq} H_{liq} \tag{3.70}$$

The mass flow rate of the pump ($\dot{m}_{pump}$) can once again be assumed to equal the mass flow rate of liquid ($\dot{m}_{liq}$) according to Equation (3.57). From these simplifications, the fully abridged version of Equation (3.69) is created as shown below.

$$\dot{Q}_{met,liq} - \dot{Q}_{liq,vap} + \dot{m}_{liq} H_{liq,in} = \dot{m}_{liq,vap} H_{vap,out} + \dot{m}_{liq} H_{liq} \tag{3.71}$$

By rewriting the expression above we can solve for the mass flow rate from liquid to vapor during the boiling mode.

$$\dot{m}_{liq,vap} = \frac{\dot{Q}_{met,liq} - \dot{Q}_{liq,vap} + \dot{m}_{liq}\left(H_{liq,in} - H_{liq}\right)}{H_{vap,out}} \tag{3.72}$$

In Equation (3.72) the inlet liquid enthalpy ($H_{liq,in}$) is calculated from steam tables at the inlet saturation temperature as shown in Equation (3.62). Similarly, the current liquid enthalpy (H_{liq}) is obtained from steam tables using the current saturation temperature as shown in Equation (3.63). The outlet vapor enthalpy ($H_{vap,out}$) is computed from steam tables at the current liquid temperature. Note that when the liquid is boiling, the volume of the liquid found in Equation (3.65) will have a non-zero mass flow rate of evaporation ($\dot{m}_{liq,vap}$).

3.3.3.4 Vapor Control Volume (CV7)

Since vapor formation is dependent on what liquid process is occurring, the vapor control volume is modeled under two conditions: liquid heating or liquid boiling. Each vapor mode is shaped individually and calculates the vapor temperature (T_{vap}), mass of vapor (m_{vap}), and number of moles of vapor (n_{vap}). For this reason, it is vital that we recognize which of the two modes liquid water is in so that the correct vapor mode can be chosen. The mode selection criteria chosen in the liquid control volume (CV6) will also be applied for the vapor control volume (CV7). If the liquid heating mode is active, it will apply for both the liquid and vapor control volume. Likewise, if the liquid boiling mode is selected, it will apply for both the liquid and vapor control volume.

3.3.3.4.1 Liquid Heating

When the liquid is heating, it is important to remember that there is no vapor formation. Therefore the mass flow from liquid to vapor will remain zero and Equation (3.54) will hold true. The vapor pressure is assumed to be at saturation conditions and is calculated from steam tables at the vapor temperature.

$$P_{vap,out} = f(T_{sat}) \tag{3.73}$$

The current vapor temperature (T_{sat}) is obtained by applying an energy balance to the vapor control volume as shown below.

$$\dot{Q}_{met,vap} + \dot{Q}_{liq,vap} + \dot{m}_{liq,vap} H_{vap,in} = \dot{m}_{vap,out} H_{vap,out} + \dot{E}_{vap} \tag{3.74}$$

The heat transfer rate from metal to liquid ($\dot{Q}_{met,liq}$) and liquid to vapor ($\dot{Q}_{liq,vap}$) are obtained from Equations (3.45) and (3.55) respectively. The change in energy for vapor during the liquid heating phase is written as follows.

$$\dot{E}_{vap} = \dot{m}_{vap}U_{vap} + m_{vap}\dot{U}_{vap} = \dot{m}_{vap}U_{vap} + m_{vap}C_{v,vap}\dot{T}_{vap} \tag{3.75}$$

During liquid heating, there is no inflow of mass from the liquid to vapor due to the absence of evaporation. The only contribution to change in vapor mass within CV7 comes from vapor flowing out of the control volume. Therefore we can define the mass flow rate of vapor as shown.

$$\dot{m}_{vap} = -\dot{m}_{vap,out} \tag{3.76}$$

By substitution of Equations (3.75) and (3.76) into Equation (3.74), and setting the mass flow rate of evaporation to zero, we can generate an expression for calculating the vapor temperature during liquid heating.

$$\dot{Q}_{met,vap} + \dot{Q}_{liq,vap} = \dot{m}_{vap,out}H_{vap,out} - \dot{m}_{vap,out}u_{vap} + m_{vap}C_{v,vap}\dot{T}_{vap} \tag{3.77}$$

The equation above can be rearranged for the sake of isolating the desired variable.

$$\dot{T}_{vap} = \frac{\dot{Q}_{met,vap} + \dot{Q}_{liq,vap} - \dot{m}_{vap,out}H_{vap,out} + \dot{m}_{vap,out}U_{vap}}{m_{vap}C_{v,vap}} \tag{3.78}$$

Thus, the vapor temperature during liquid heating can be derived by integrating Equation (3.78) to give the following.

$$T_{vap} = \int_{t_1}^{t_2} \frac{\dot{Q}_{met,vap} + \dot{Q}_{liq,vap} - \dot{m}_{vap,out}(H_{vap,out} - U_{vap})}{m_{vap}C_{v,vap}}\,dt \tag{3.79}$$

The vapor is presumed to be at saturation conditions. As a result, the outlet vapor enthalpy ($H_{vap,out}$) and internal energy (U_{vap}) are both found from steam tables as a function of vapor temperature (at saturation).

$$H_{vap,out} = f(T_{sat}) \tag{3.80}$$

$$U_{out} = f(T_{sat}) \tag{3.81}$$

The specific heat of vapor ($C_{v,vap}$) is given as a constant value, and the outlet mass flow rate of vapor ($\dot{m}_{vap,out}$) is computed from the following equation.

$$\dot{m}_{vap,out} = -\dot{m}_{vap} = \sqrt{\Delta P_{vap}}\, K_f = \sqrt{P_{vap,out} - P_{vap,in}}\, K_f \tag{3.82}$$

By integrating Equation (3.82) over time, we can generate a solution for the mass of vapor.

$$m_{vap} = \int_{t_1}^{t_2} \dot{m}_{vap,out}\, dt = \int_{t_1}^{t_2} \sqrt{P_{vap,out} - P_{vap,in}}\, K_f\, dt \tag{3.83}$$

In a similar manner, the outlet molar flow rate of vapor ($\dot{n}_{vap,out}$) can be calculated as shown.

$$\dot{n}_{vap,out} = \frac{\dot{m}_{vap}}{M_{vap}} = \frac{\sqrt{P_{vap,out} - P_{vap,in}}\, K_f}{M_{vap}} \tag{3.84}$$

By integrating Equation (3.84), the number of moles of vapor within the boiler can be found.

$$n_{vap} = \int_{t_1}^{t_2} \dot{n}_{vap,out}\, dt = \int_{t_1}^{t_2} \frac{\sqrt{P_{vap,out} - P_{vap,in}}\, K_f}{M_{vap}}\, dt \tag{3.85}$$

3.3.3.4.2 *Liquid Boiling*

The single difference between the liquid heating and boiling in the vapor control volume is an inflow of mass due to vaporization. This variation affects the vapor temperature calculation and produces a slightly altered expression to the one seen in Equation (3.79). To find the vapor temperature, begin by performing an energy balance in the vapor control volume (CV7). The resulting differential equation is shown below.

$$\dot{Q}_{met,vap} + \dot{Q}_{liq,vap} + \dot{m}_{liq,vap} H_{vap,in} = \dot{m}_{vap,out} H_{vap,out} + \dot{E}_{vap} \tag{3.86}$$

To expand the equation above, apply the $\dot{E}_{vap}$ formula found in Equation (3.75). The following expression now contains the desired variable $\dot{T}_{vap}$ and can be solved for the vapor temperature.

$$\dot{Q}_{met,vap} + \dot{Q}_{liq,vap} + \dot{m}_{liq,vap} H_{vap,in} = \dot{m}_{vap,out} H_{vap,out} + \dot{m}_{vap} U_{vap} + m_{vap} C_{v,vap} \dot{T}_{vap} \tag{3.87}$$

By reorganizing Equation (3.87) we get the proceeding formula.

$$\dot{T}_{vap} = \frac{\dot{Q}_{met,vap} + \dot{Q}_{liq,vap} + \dot{m}_{liq,vap}H_{vap,in} - \dot{m}_{vap,out}H_{vap,out} - \dot{m}_{vap}U_{vap}}{m_{vap}C_{v,vap}} \quad (3.88)$$

The vapor temperature during liquid boiling mode is computed by integrating Equation (3.88) to create the following solution.

$$T_{vap} = \int_{t_1}^{t_2} \frac{\dot{Q}_{met,vap} + \dot{Q}_{liq,vap} + \dot{m}_{liq,vap}H_{vap,in} - \dot{m}_{vap,out}H_{vap,out} - \dot{m}_{vap}U_{vap}}{m_{vap}C_{v,vap}} dt \quad (3.89)$$

The inlet vapor enthalpy ($H_{vap,in}$) is found using saturated water tables at the liquid temperature. The outlet vapor enthalpy ($H_{vap,out}$) and vapor internal energy (U_{vap}) are calculated using steam tables at the vapor temperature.

$$H_{vap,in} = f(T_{liq}) \quad (3.90)$$

$$H_{vap,out} = f(T_{sat,vap}) \quad (3.91)$$

$$U_{vap} = f(T_{vap}) \quad (3.92)$$

The mass flow rate of vapor leaving the control volume ($\dot{m}_{vap,out}$) is determined from Equation (3.82) in the liquid heating mode of CV7. Since there is an inflow of mass from liquid to vapor, and a rate of change of mass inside the vapor control volume, the mass flow rate of vapor is given as Equation (3.93).

$$\dot{m}_{vap} = \dot{m}_{vap,in} - \dot{m}_{vap,out} = \dot{m}_{liq,vap} - \dot{m}_{vap,out} \quad (3.93)$$

Therefore, the mass of vapor (m_{vap}) can be calculated by integrating the equation above.

$$m_{vap} = \int_{t_1}^{t_2} \dot{m}_{vap}\, dt \quad (3.94)$$

The molar flow rate of vapor ($\dot{n}_{vap}$) within the vapor control volume is discovered by utilizing the expression below.

$$\dot{n}_{vap} = \frac{\dot{m}_{vap}}{M_{vap}} \tag{3.95}$$

From this equation, the number of moles of vapor (n_{vap}) is measured by integrating Equation (3.95) as shown.

$$n_{vap} = \int_{t_1}^{t_2} \dot{n}_{vap}\, dt = \int_{t_1}^{t_2} \frac{\dot{m}_{vap}}{M_{vap}}\, dt \tag{3.96}$$

3.4 Superheater

3.4.1 Physical System

The superheater, also known as a reheater, is a heat exchanger which converts saturated/wet steam into superheated/dry steam. It is located at the high-temperature end of the HRSG where the flue gas is entering the system, and superheated steam is exiting. This apparatus functions in a similar capacity to the economizer and increases a mediums heat content without phase change occurring. The difference between the two is the medium they each heat. While the economizer handles subcooled feedwater, the superheater attends to wet and dry steam. As saturated vapor exits the steam drum in the evaporator, it travels through the superheater pipe bundles. High-temperature flue gas is traveling in the opposite direction, heating the piping and consequently the steam. As the steam progresses, it absorbs more energy from the flue gas which raises its temperature above saturation. By further heating steam to a superheated state, it is has a greater potential to expand and produce energy. This increased ability to do work improves the steam cycle efficiency. Additionally, a rise in steam thermal energy will minimize the chance of vapor condensing inside the turbine. Liquid water present in the steam turbine will move at a high velocity and can cause accelerated erosion to the turbine blades. If thermal energy from the GT

exhaust is not sufficient to superheat steam, then duct burning may be implemented to increase steam quantity or temperature.

3.4.2 Description of Parameters

In order to characterize the superheater mathematically, we must first define the symbol nomenclature. Table 3.5 describes given/known superheater conditions where Table 3.6 describes the calculated/unknown parameters. Abbreviations for flue gas (*fg*), metal (*met*), and vapor (*vap*) are used as symbol subscripts throughout this chapter. Metric units are assumed for all parameters and will be given in each table as necessary.

Table 3.5: Given Conditions for the Superheater

Description	**Symbol**	**Units**
Area of Contact	$A_{fg,met}$; $A_{met,vap}$	m^2
Flow Coefficient	K_f	-
Gas Constant	R	J K^{-1} mol^{-1}
Heat Transfer Coefficient	$h_{fg,met}$; $h_{met,vap}$	W m^{-2} K^{-1}
Inlet Molar Flow Rate	$\dot{n}_{fg,in}$; $\dot{n}_{vap,in}$	mol s^{-1}
Inlet Pressure	$P_{fg,in}$; $P_{vap,in}$	bar(g)
Inlet Temperature	$T_{fg,in}$; $T_{vap,in}$	K
Mass of Metal	m_{met}	Kg
Molecular Weight	M_{fg} ; M_{vap}	mol
Specific Heat of Metal	$C_{p,met}$	KJ Kg^{-1} K^{-1}
Volume of Control Volume	V_{CV8} ; V_{CV9} ; V_{CV10}	m^3

Table 3.6: Calculated Parameters for the Superheater

Description	Symbol	Units
Inlet Enthalpy	$H_{fg,in}$; $H_{vap,in}$	KJ Kg^{-1}
Moles in Control Volume	n_{fg} ; n_{vap}	mol
Outlet Enthalpy	$H_{fg,out}$; $H_{vap,out}$	KJ Kg^{-1}
Outlet Molar Flow Rate	$\dot{n}_{fg,out}$; $\dot{n}_{vap,out}$	mol s^{-1}
Outlet Pressure	$P_{fg,out}$; $P_{vap,out}$	bar(g)
Outlet Temperature	$T_{fg,out}$; $T_{vap,out}$	K
Specific Heat	$C_{v,fg}$; $C_{v,vap}$	KJ Kg^{-1} K^{-1}
Temperature of Metal	T_{met}	K

3.4.3 Mathematical Model

The superheater is mathematically modeled as a large control volume (CV) composed of three smaller systems. The flue gas control volume (CV8) encompasses gas turbine exhaust and resembles the region around the superheater pipe bundles. The metal control volume (CV9) consists of metal piping which runs through the superheater section. The vapor control volume (CV10) contains steam and features the interior volume of superheater piping.

3.4.3.1 Flue Gas Control Volume (CV8)

The flue gas outlet pressure is determined by the ideal gas law expressed by Equation (3.97). In this calculation, the volume of CV8 and universal gas constant are given. However, the number of moles and temperature of the flue gas at the outlet are unknown and must be determined.

$$P_{fg,out} = \frac{n_{fg}\, R T_{fg,out}}{V_{CV8}} \tag{3.97}$$

The outlet molar flow rate of flue gas is computed using Equation (3.98).

$$\dot{n}_{fg,out} = \frac{\Delta P_{fg}\, K_f}{M_{fg}} = \frac{\left(P_{fg,out} - P_{fg,in}\right) K_f\, X_{fg}}{M_{fg}} \tag{3.98}$$

The symbol X_{fg} represents the mole fraction of flue gas in the superheater. The number of moles of flue gas (n_{fg}) inside the superheater is found by integrating the difference between inlet and outlet molar flow rates. The integration previously stated is expressed in Equation (3.99).

$$n_{fg} = \int_{t_1}^{t_2} \left(\dot{n}_{fg,in} - \dot{n}_{fg,out}\right) dt \tag{3.99}$$

The flue gas temperature at the outlet is obtained by applying an energy conservation balance to the corresponding control volume (CV8).

$$\begin{aligned} -\dot{Q}_{fg,met} + \sum \dot{n}_{fg,in} \left(H_{fg,in} + \frac{{v_{fg,in}}^2}{2} + g z_{fg,in} \right) \\ = \dot{E}_{CV8} + \dot{W}_{CV8} + \sum \dot{n}_{fg,out} \left(H_{fg,out} + \frac{{v_{fg,out}}^2}{2} + g z_{fg,out} \right) \end{aligned} \tag{3.100}$$

Equation (3.100) is a differential equation with respect to time. In this formula $\dot{Q}_{fg,met}$ is the rate of net heat transfer out of the control volume from flue gas to metal. This variable can be described using the convection heat transfer equation as shown below.

$$\dot{Q}_{fg,met} = h_{fg,met} A_{fg,met} \left(T_{met} - T_{fg,out}\right) \tag{3.101}$$

Notice that in Equation (3.100) the net heat transfer occurs out of CV8, making it a negative value. Assuming that the net amount of mass inside the control volume remains constant, there is no mechanical work taking place. Additionally, the kinetic and potential energies do not change between the inlet and outlet. For these reasons Equation (3.100) can be rewritten as follows.

$$-\dot{Q}_{fg,met} + \dot{n}_{fg,in} H_{fg,in} = \dot{E}_{CV8} + \dot{n}_{fg,out} H_{fg,out} \tag{3.102}$$

The energy change within the control volume ($\dot{E}_{cv1}$) is given by the following relationship.

$$\dot{E}_{CV8} = n_{fg}\dot{U}_{fg} = n_{fg}C_{v,fg}\dot{T}_{fg,out} \tag{3.103}$$

In Equation (3.103) the specific heat of the flue gas ($C_{v,fg}$) is computed using its mole fraction. By substituting the result from Equation (3.103) into Equation (3.102) we can create an expression for calculating the temperature change of flue gas in CV8.

$$-\dot{Q}_{fg,met} + \dot{n}_{fg,in}H_{fg,in} = n_{fg}C_{v,fg}\dot{T}_{fg,out} + \dot{n}_{fg,out}H_{fg,out} \tag{3.104}$$

Isolating the desired variable $\dot{T}_{fg,out}$ gives the proceeding result.

$$\dot{T}_{fg,out} = \frac{\dot{n}_{fg,in}H_{fg,in} - \dot{n}_{fg,out}H_{fg,out} - \dot{Q}_{fg,met}}{n_{fg}C_{v,fg}} \tag{3.105}$$

The outlet temperature of flue gas can thus be derived by integrating the Equation (3.105) to give the following equality.

$$T_{fg,out} = \int_{t_1}^{t_2} \frac{\dot{n}_{fg,in}H_{fg,in} - \dot{n}_{fg,out}H_{fg,out} - \dot{Q}_{fg,met}}{n_{fg}C_{v,fg}}\,dt \tag{3.106}$$

With an expression for n_{fg} and $T_{fg,out}$ now available, we can return to Equation (3.97) and apply these solutions to solve for the flue gas outlet pressure ($P_{fg,out}$).

3.4.3.2 Metal Control Volume (CV9)

The temperature of superheater piping (T_{met}) is effected by a heat influx from the flue gas (*fg*,*met*) and a heat transfer to the vapor (*met*,*vap*). These phenomena can be modeled by describing the rate of metal heat transfer as shown.

$$\dot{Q}_{met} = \dot{Q}_{fg,met} - \dot{Q}_{met,vap} \tag{3.107}$$

Equation (3.107) can be expanded using the simplified steady-flow (left-hand side) and convective (right-hand side) heat transfer equation as formulated below.

$$m_{met}C_{p,met}\dot{T}_{met} = h_{fg,met}A_{fg,met}\left(T_{fg,out} - T_{met}\right) - h_{met,vap}A_{met,vap}\left(T_{met} - T_{vap,out}\right) \quad (3.108)$$

The equation above can be rewritten to solve for the desired parameter.

$$\dot{T}_{met} = \frac{h_{fg,met}A_{fg,met}\left(T_{fg,out} - T_{met}\right) - h_{met,vap}A_{met,vap}\left(T_{met} - T_{vap,out}\right)}{m_{met}C_{p,met}} \quad (3.109)$$

Therefore, the metal temperature of superheater pipes is obtained by integrating Equation (3.109) to give the following result.

$$T_{met} = \int_{t_1}^{t_2} \frac{h_{fg,met}A_{fg,met}\left(T_{fg,out} - T_{met}\right) - h_{met,vap}A_{met,vap}\left(T_{met} - T_{vap,out}\right)}{m_{met}C_{p,met}} dt \quad (3.110)$$

In this equation the temperature of the metal is the only unknown variable as heat transfer coefficients, areas of contact, specific heat, and mass of metal are all given. Temperature values within the integrand are given for flue gas, metal, and vapor at the previous instance in time.

3.4.3.3 Vapor Control Volume (CV10)

Modeling the vapor control volume (CV10) will follow a similar approach to that of the flue gas control volume (CV8). The critical difference between the two environments is that steam will not be treated as an ideal gas. Consequently, the ideal gas law found in Equation (3.97) will no longer be an appropriate pressure calculation. Instead, the outlet pressure of steam will be obtained using the Redlich-Kwong equation of state.

$$P_{vap,out} = \frac{RT_{vap,out}}{v_m - b} - \frac{a}{\sqrt{T_{vap,out}}\, v_m(v_m - b)} \quad (3.111)$$

For Equation (3.111), a = 142.59 $Nm^4\,K^{1/2}\,mol^{-2}$ and b = 0.0211 $m^3\,mol^{-1}$ are constants that correct for the attractive potential of molecules and volume respectively. These values are derived from the critical point temperature and pressure of steam. The molar volume v_m has units of m^3mol^{-1} and is given as the following.

$$v_m = \frac{V_{CV10}}{n_{vap}} \tag{3.112}$$

The vapor outlet molar flow rate ($\dot{n}_{vap,out}$) is calculated in a similar manner within the flue gas control volume using Equation (3.98).

$$\dot{n}_{vap,out} = \frac{\sqrt{\Delta P_{vap}}\, K_f}{M_{vap}} = \frac{\sqrt{\left(P_{vap,out} - P_{vap,in}\right)}\, K_f}{M_{vap}} \tag{3.113}$$

The number of vapor moles (n_{vap}) in CV10 are calculated using the same method found in the flue gas control volume. This value will be applied to Equation (3.112) and used to calculate the molar volume (v_m).

$$n_{vap} = \int_{t_1}^{t_2} \left(\dot{n}_{vap,in} - \dot{n}_{vap,out}\right) dt \tag{3.114}$$

A previously used methodology in CV8 will again be implemented to find the outlet vapor temperature. The energy conservation principle is applied to CV10 and gives the differential equation shown.

$$\begin{aligned} &\dot{Q}_{met,vap} + \sum \dot{n}_{vap,in}\left(H_{vap,in} + \frac{{v_{vap,in}}^2}{2} + g z_{vap,in}\right) \\ &= \dot{E}_{CV10} + \dot{W}_{CV10} + \sum \dot{n}_{vap,out}\left(H_{vap,out} + \frac{{v_{vap,out}}^2}{2} + g z_{vap,out}\right) \end{aligned} \tag{3.115}$$

In Equation (3.115) $\dot{Q}_{metal,vap}$ represents the rate of net heat transfer into CV10 from metal to vapor. This parameter can be calculated using the convection heat transfer expression below.

$$\dot{Q}_{met,vap} = h_{met,vap} A_{met,vap}\left(T_{met} - T_{vap,out}\right) \tag{3.116}$$

From Equation (3.115) we can determine that the net heat transfer is going into the vapor control volume. Therefore $\dot{Q}_{met,vap}$ takes a positive value. Assuming the net amount of mass inside the

vapor control volume remains unchanged, there is no mechanical work occurring. Furthermore, the kinetic and potential energies are constant between the inlet and outlet of CV10. Using this information we can rewrite Equation (3.115) in the following simplified form.

$$\dot{Q}_{met,vap} + \dot{n}_{vap,in} H_{vap,in} = \dot{E}_{CV10} + \dot{n}_{vap,out} H_{vap,out} \tag{3.117}$$

The change in energy for the vapor control volume is given below.

$$\dot{E}_{CV10} = \dot{n}_{vap,out} U_{vap} + n_{vap} \dot{U}_{vap} = \dot{n}_{vap,out} U_{vap} + n_{vap} C_{v,vap} \dot{T}_{vap,out} \tag{3.118}$$

In Equation (3.118) the specific heat of vapor ($C_{v,vap}$) is found using its mole fraction. By substituting the solution of Equation (3.118) into Equation (3.117) we can develop an expression used to derive the outlet vapor temperature.

$$\dot{Q}_{met,vap} + \dot{n}_{vap,in} H_{vap,in} = \dot{n}_{vap,out} U_{vap} + n_{vap} C_{v,vap} \dot{T}_{vap,out} + \dot{n}_{vap,out} H_{vap,out} \tag{3.119}$$

The expression above is rearranged in order to isolate the desired variable ($\dot{T}_{vap,out}$).

$$\dot{T}_{vap,out} = \frac{\dot{n}_{vap,in} H_{vap,in} - \dot{n}_{vap,out} H_{vap,out} + \dot{Q}_{met,vap} - \dot{n}_{vap,out} U_{vap}}{n_{vap} C_{v,vap}} \tag{3.120}$$

The outlet temperature of vapor is calculated by integrating Equation (3.120) to give the following.

$$T_{vap,out} = \int_{t_1}^{t_2} \frac{\dot{n}_{vap,in} H_{vap,in} - \dot{n}_{vap,out} H_{vap,out} + \dot{Q}_{met,vap} - \dot{n}_{vap,out} U_{vap}}{n_{vap} C_{v,vap}} dt \tag{3.121}$$

In the equation above, the specific heat capacity of vapor ($C_{v,vap}$) is calculated from steam tables as a function of the outlet temperature and outlet pressure of vapor.

$$C_{v,vap} = f(P_{vap,out}, T_{vap,out}) \tag{3.122}$$

Likewise, the inlet enthalpy of vapor ($H_{vap,in}$) is at saturated conditions and can be obtained from steam tables as a function of saturation temperature.

$$H_{vap,in} = f(T_{sat}) \tag{3.123}$$

However, the computation of outlet vapor enthalpy ($H_{vap,out}$) and vapor internal energy (U_{vap}) is not as straightforward. There are two potential states in which the outlet vapor could reside, saturated or superheated. For this reason, it is important to identify which of these two states the outlet vapor is currently in and correspondingly calculate $H_{vap,out}$ and U_{vap} from steam tables.

3.4.3.3.1 Outlet Vapor Enthalpy

To calculate the outlet vapor enthalpy ($H_{vap,out}$) the state of vapor at the outlet must be known. This process involves comparing the outlet vapor temperature ($T_{vap,out}$) against its saturation temperature T_{sat} (with respect to outlet vapor pressure). If the condition in Equation (3.124) holds true, then the vapor is considered superheated at the outlet. Thus, the outlet vapor enthalpy is calculated as a function of outlet temperature and pressure.

$$T_{vap,out} > T_{sat} + \epsilon \tag{3.124}$$

$$H_{vap,out} = f(P_{vap,out}, T_{vap,out}) \tag{3.125}$$

If the condition in Equation (3.126) holds true, then the vapor is saturated at the outlet, and the outlet vapor enthalpy will be calculated as a function of the saturation pressure.

$$T_{vap,out} < T_{sat} + \epsilon \tag{3.126}$$

$$H_{vap,out} = f(P_{sat}) \tag{3.127}$$

The allowable difference between the actual outlet temperature and saturation temperature is presented as a tunable parameter (ϵ). This will allow for a more accurate model of switching between a saturated and superheated vapor state.

3.4.3.3.2 *Internal Energy of Vapor*

A similar procedure to that found in Section 3.4.3.3.1 will be applied in calculating the vapor internal energy (U_{vap}). By comparing the outlet vapor temperature against its saturation temperature, we can identify whether the vapor is in a saturated or superheated state. If the condition found in Equation (3.128) is true, the outlet vapor is superheated. Therefore the outlet vapor enthalpy is calculated as a function of the outlet temperature and pressure.

$$T_{vap,out} > T_{sat} + \epsilon \tag{3.128}$$

$$U_{vap} = f(P_{vap,out}, T_{vap,out}) \tag{3.129}$$

If the condition in Equation (3.130) is found true, then the outlet vapor is saturated. As a result, the outlet vapor enthalpy is calculated as a function of saturation pressure.

$$T_{vap,out} < T_{sat} + \epsilon \tag{3.130}$$

$$U_{vap} = f(P_{sat}) \tag{3.131}$$

As previously stated, the allowable difference in actual outlet temperature and saturation temperature is denoted as a tunable parameter (ϵ). This variable will allow for a more accurate model when switching between saturated and superheated vapor states.

CHAPTER 4: MODEL IMPLEMENTATION IN T3000

4.1 T3000 Modeling Platform

Siemens Power Plant Automation T3000 (SPPA-T3000) is a distributed control system (DCS) designed to perform all power plant automation tasks. These responsibilities typically include turbine control, boiler level control, balance of plant operations, and integration of third-party systems. However, for this thesis, we will be applying T3000 in an entirely different capacity. In this chapter, T3000 will be used as a graphical programming environment to digitally model a low-pressure (LP) heat recovery steam generator.

4.1.1 Advantages of T3000

4.1.1.1 Thermodynamic Software

SPPA-T3000 employs a visual programming language (VPL) to construct system models from a library of blocks. The premise behind block-structured programming is to use various blocks which represent code, joined by connections to signify relations, to create a function block diagram (FBD) that characterizes a system. The inherent advantage that T3000 has over other visual programming languages is its focus on power plant systems. Most VPLs, including T3000, possess common block libraries such as math operators (add, divide, etc.), continuous functions (integrate, derivate, etc.) and logic operators (and, or, etc.). Since T3000 was conceived for power plant management, it contains specialized function blocks suitable for modeling a thermodynamic system. To that end, there are blocks in T3000 that calculate enthalpy, specific volume, flue gas specific heat, and saturation conditions based on temperature and pressure. While modeling a

HRSG may be possible without these specific elements, they have certainly made the process more concise and convenient.

4.1.1.2 Real-Time Analysis

Another crucial benefit that T3000 maintains over other VPLs is modeling and simulation flexibility. Since T3000 was developed to be a DCS, it was designed as a continuously running processor. By using this platform for visual programming, it allows the user to perform real-time analysis and modification to the system model while a simulation is running. This feature allows for a more transparent debugging process when the model is malfunctioning. In most visual programming languages, an incorrectly constructed model will crash when a simulation is run. This computational failure can make it difficult to pin-point modeling mistakes and resolve the issue. When a simulation is executed in T3000, it will continue to run regardless of whether the model is stable or not. This feature allows the programmer to analyze the model while it is operating and identify what areas are causing an error. Furthermore, it allows the user to make changes to the model while it is running and see in real time whether it has a positive or negative effect on stability.

4.1.1.3 Computational Power

Computer performance is an essential commodity in modeling and simulating complex thermodynamic systems. T3000 is a server-based system powerful enough to handle the controls for an entire power plant simultaneously. As a result, it was built to possess superior computational power compared to client-based programming machines. The robustness of this system presents an opportunity for users to run multiple simulations concurrently and increase productivity without

fear of being limited on computational resources. Additionally, this allows for simulations to be run seamlessly and produce accurate results in less time.

4.2 Modular Control Volumes

The development of an entire HRSG model begins by breaking down its structure into more manageable sections. The complete system was initially separated into three heat exchangers: economizer, evaporator, and superheater. These three devices are then further divided into multiple control volume modules: liquid, vapor, metal, and flue gas. Each CV consists of a single medium and does not allow phase change to occur within them. The purpose of dissecting the model in this fashion is to not only reduce its complexity but also to make it more robust. Since the control volumes are modular, it allows for all three heat exchangers to be constructed from the same set of modules. Furthermore, it makes the HRSG model easily modifiable and able to satisfy various plant configurations.

The following topics in Section 4.2 will describe the four CV types used in this thesis. Each module will model the underlying physical phenomena of that control volume including mass flow evolution, energy balance, temperature change, and pressure change. As presented in Chapter 3, these fundamental concepts characterize the system via a set of equations. By connecting these expressions in each CV, we can establish a network of equations that define the HRSG.

4.2.1 Liquid Control Volume

The liquid control volume represents water in a liquid state before evaporation takes place. Subcooled water is pumped into the liquid control volume which encompasses the interior volume of HRSG piping. As an influx of flue gas warms the metal piping, it transfers thermal energy to

the water. This convective heat transfer causes the liquid to be heated and leave the CV at a higher temperature than when it entered. A visual depiction of this control volume is shown below in Figure 4.1. Shown below in Figure 4.2 is an example of a T3000 liquid control volume block.

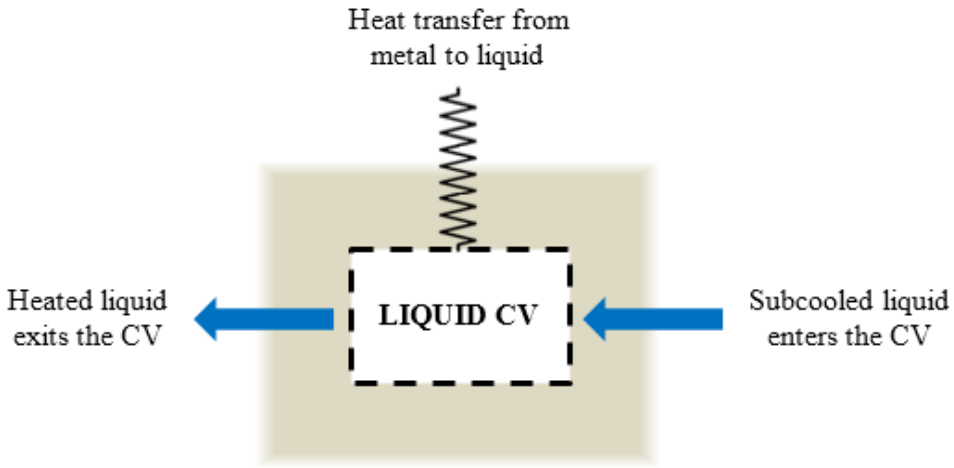

Figure 4.1: Diagram of a liquid control volume

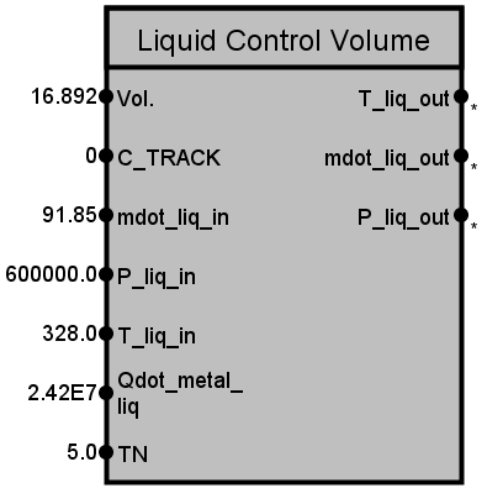

Figure 4.2: SPPA-T3000 liquid control volume block in the economizer

The economizer liquid CV block contains the mathematical description of the system represented in Section 3.2.3.3. The block diagram contained inside this liquid control volume module is shown in the following figure.

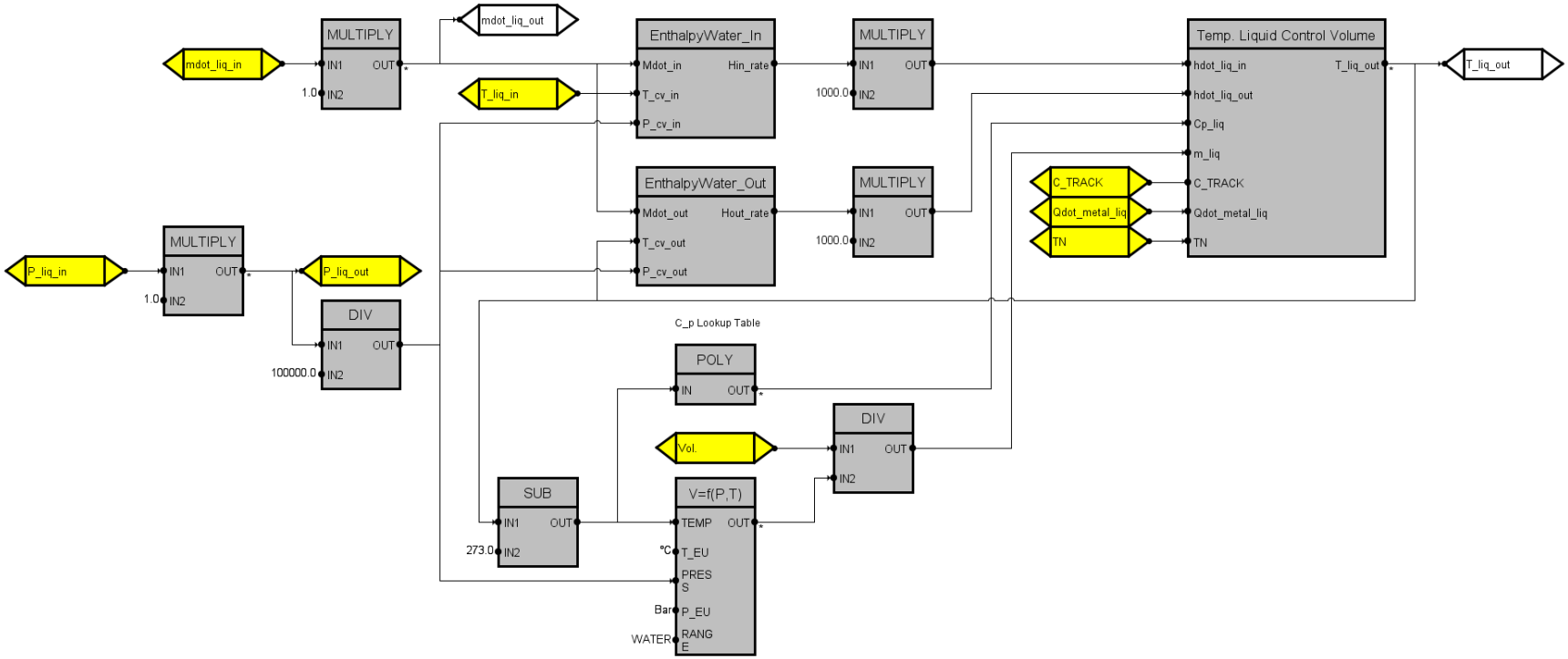

Figure 4.3: SPPA-T3000 block diagram of the liquid control volume in the economizer

4.2.2 Vapor Control Volume

The vapor control volume describes water in a gaseous state after vaporization has occurred. Water vapor enters the vapor control volume located within the interior volume of HRSG piping. As incoming flue gas warms the pipe bundles, thermal energy is absorbed by the vapor. This convective heat transfer causes an increase in vapor temperature as it exits the CV. A graphical representation of this CV is displayed in Figure 4.4.

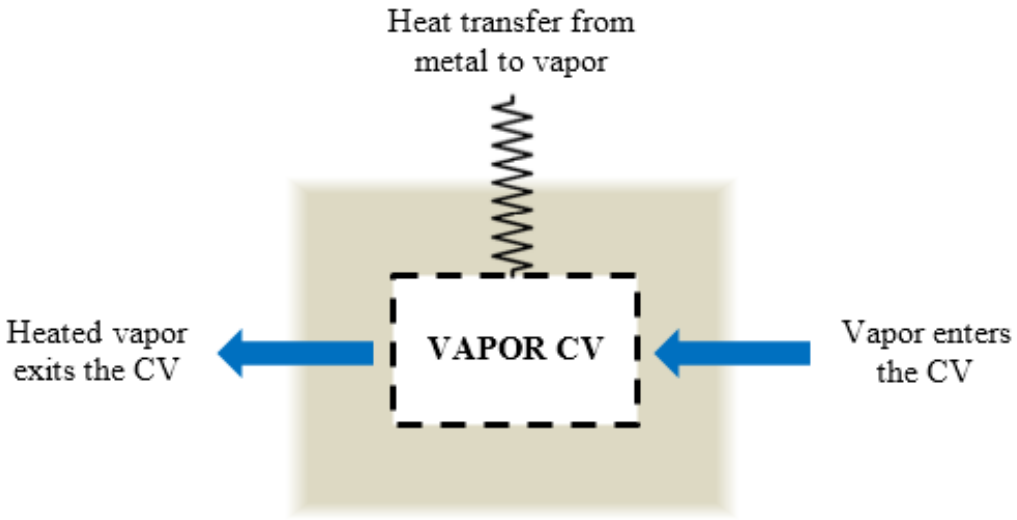

Figure 4.4: Diagram of a vapor control volume

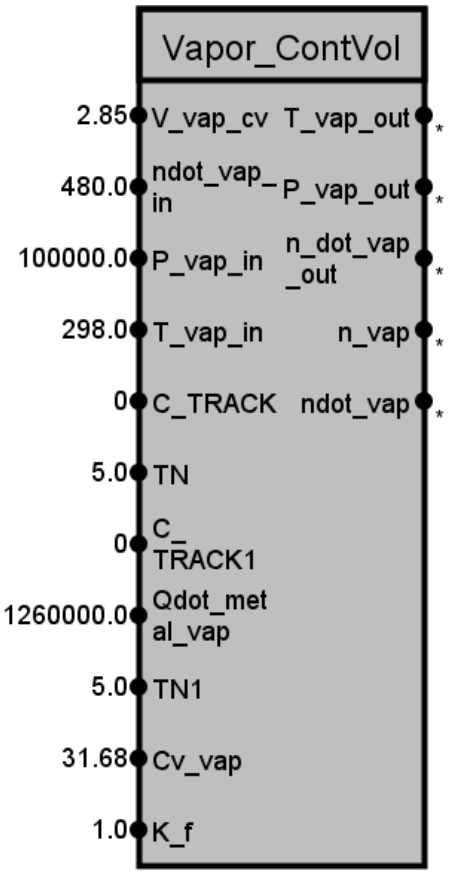

Figure 4.5: SPPA-T3000 vapor control volume in the superheater

The superheater vapor CV block is a mathematical representation of the system characterized in Section 3.4.3.3. The block diagram found within this vapor control volume module is shown in the proceeding figure.

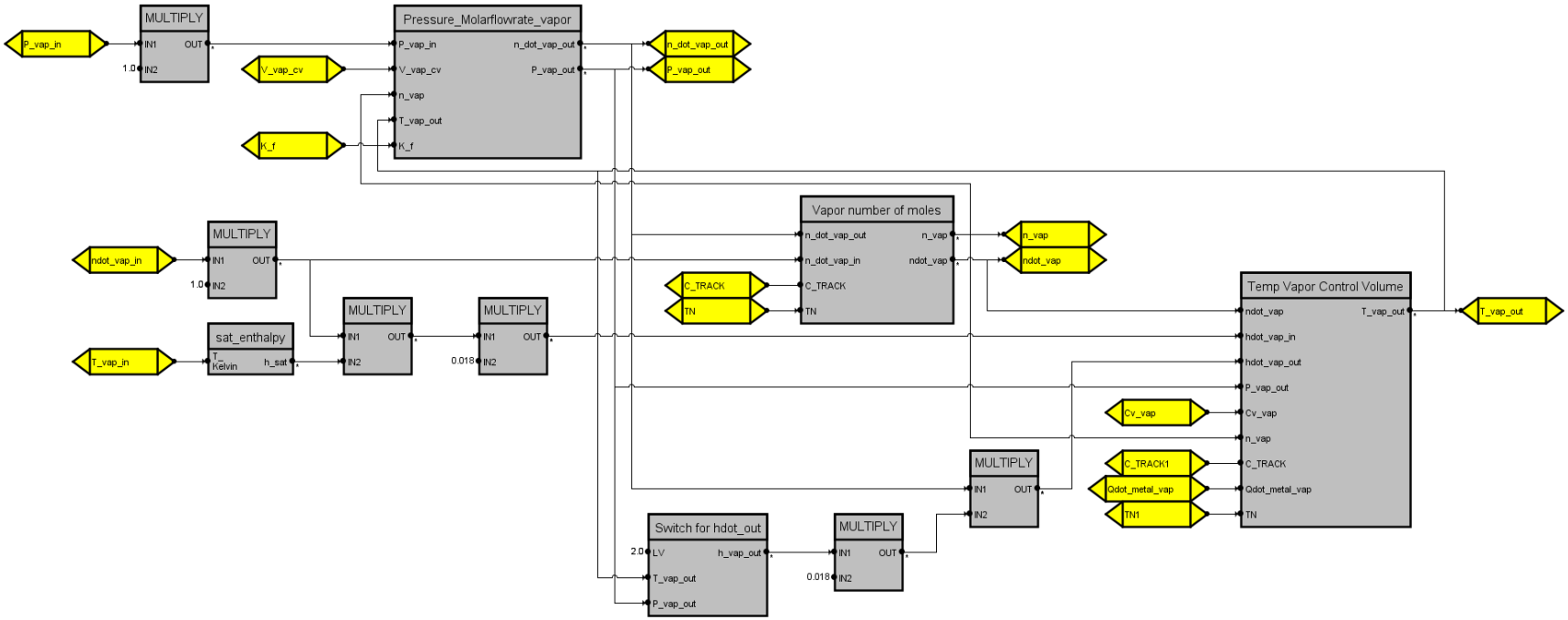

Figure 4.6: SPPA-T3000 block diagram of the vapor control volume in the superheater

4.2.3 Metal Control Volume

The metal control volume defines the pipe bundles that transport liquid and vapor water throughout the HRSG. An illustration of this control volume is found in Figure 4.7.

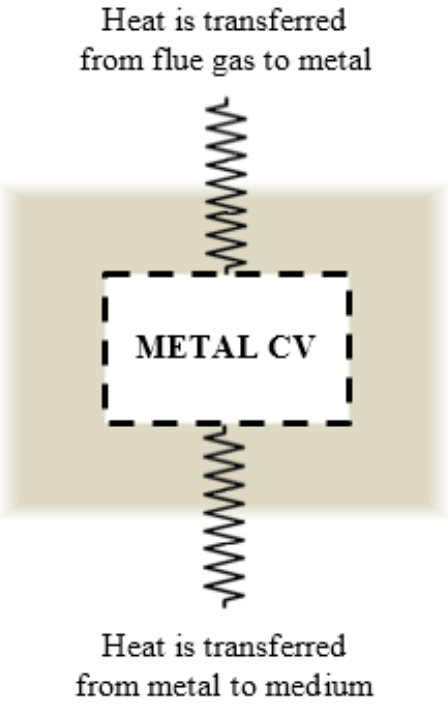

Figure 4.7: Diagram of a metal control volume

High-temperature flue gas passes through the pipe bundles and heats the exposed surface through convective heat transfer. As the piping temperature increases, heat propagates from the outer diameter to inner diameter by way of conduction. As a result, the fluid contained within the piping is heated via convection and leaves the control volume at a higher temperature. An example of a metal control volume block is displayed in Figure 4.8.

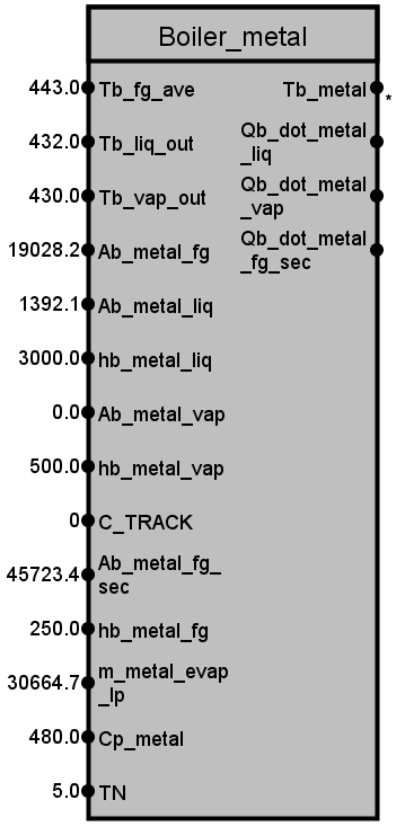

Figure 4.8: SPPA-T3000 metal control volume block in the evaporator

The evaporator metal CV block gives a mathematical description of the system expressed in Section 3.3.3.2 previously. Figure 4.9 presents the block diagram created inside this metal CV module. As shown below, the rate of heat transfer from flue gas to metal, metal to liquid, and metal to vapor are all included in the evaporator metal CV. However, direct heat transfer from the metal to vapor does not take place in the evaporator. As described in Figure 4.15, heat is transferred from the metal to liquid via convection, and from the liquid to vapor by way of boiling. Therefore, the area of contact between the metal and vapor was set to zero as shown in Figure 4.8. This adjustment would result in the rate of heat transfer from metal to vapor becoming zero. Thus, $\dot{Q}_{met,vap}$ would not influence the metal temperature calculation shown in Equation (3.51).

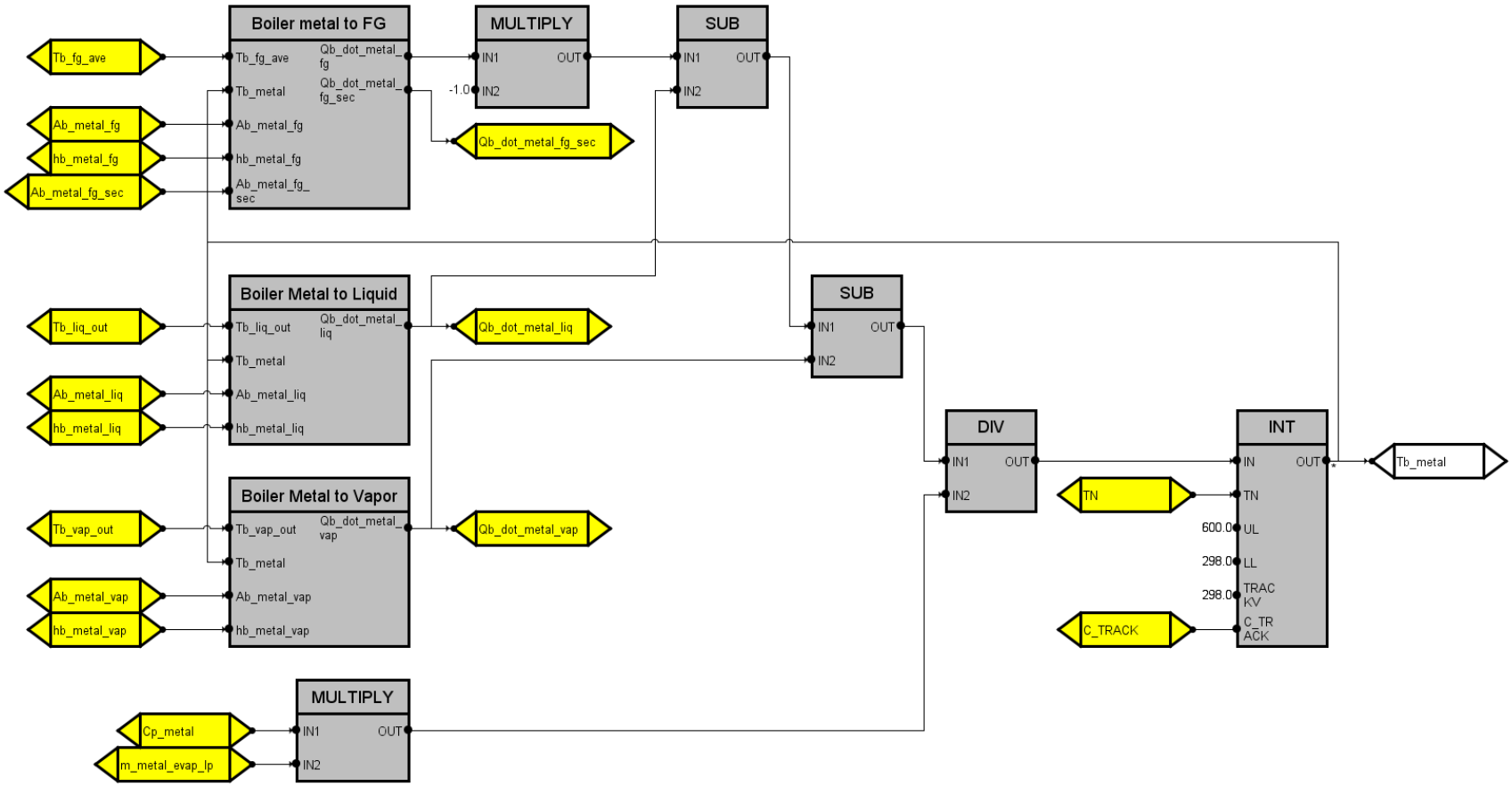

Figure 4.9: SPPA-T3000 block diagram of the metal control volume in the evaporator

4.2.4 Flue Gas Control Volume

The flue gas control volume is composed of GT exhaust gas and surrounds the pipe bundles within the HRSG ducting. A portrayal of this control volume is presented in Figure 4.10.

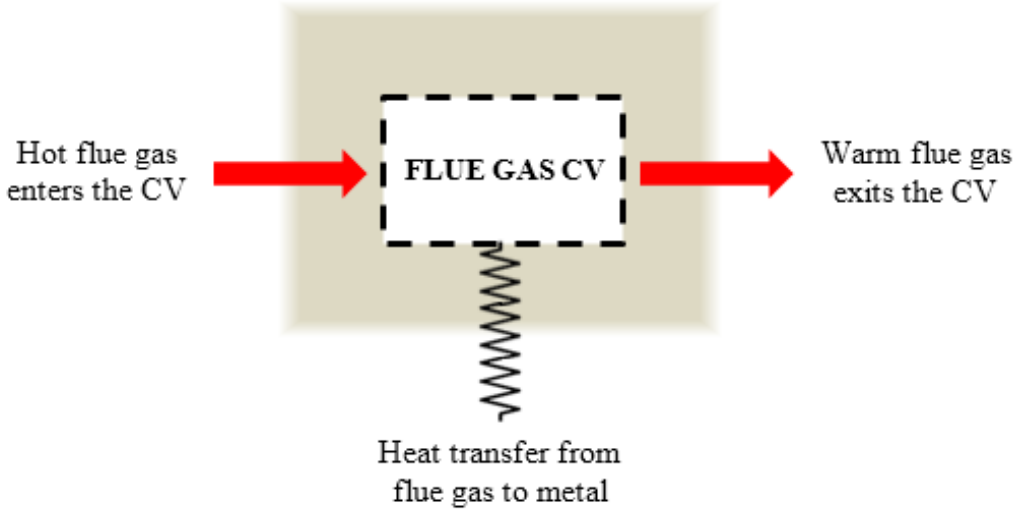

Figure 4.10: Diagram of a flue gas control volume

Gas turbine exhaust enters the flue gas control volume and comes into contact with the HRSG piping. This interaction causes a convective heat transfer where the flue gas transfers thermal energy to the metal. Consequently, the flue gas thermal energy reduces as it travels across the CV and exits at a lower temperature. The T3000 block for the flue gas control volume is shown in Figure 4.11.

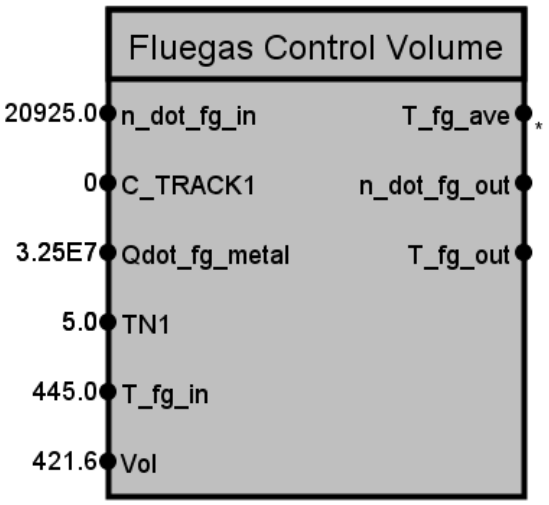

Figure 4.11: SPPA-T3000 flue gas control volume block in the economizer

The flue gas CV block within the economizer mathematically describes the system portrayed in Section 3.2.3.1. The block diagram for this flue gas control volume is depicted in Figure 4.12.

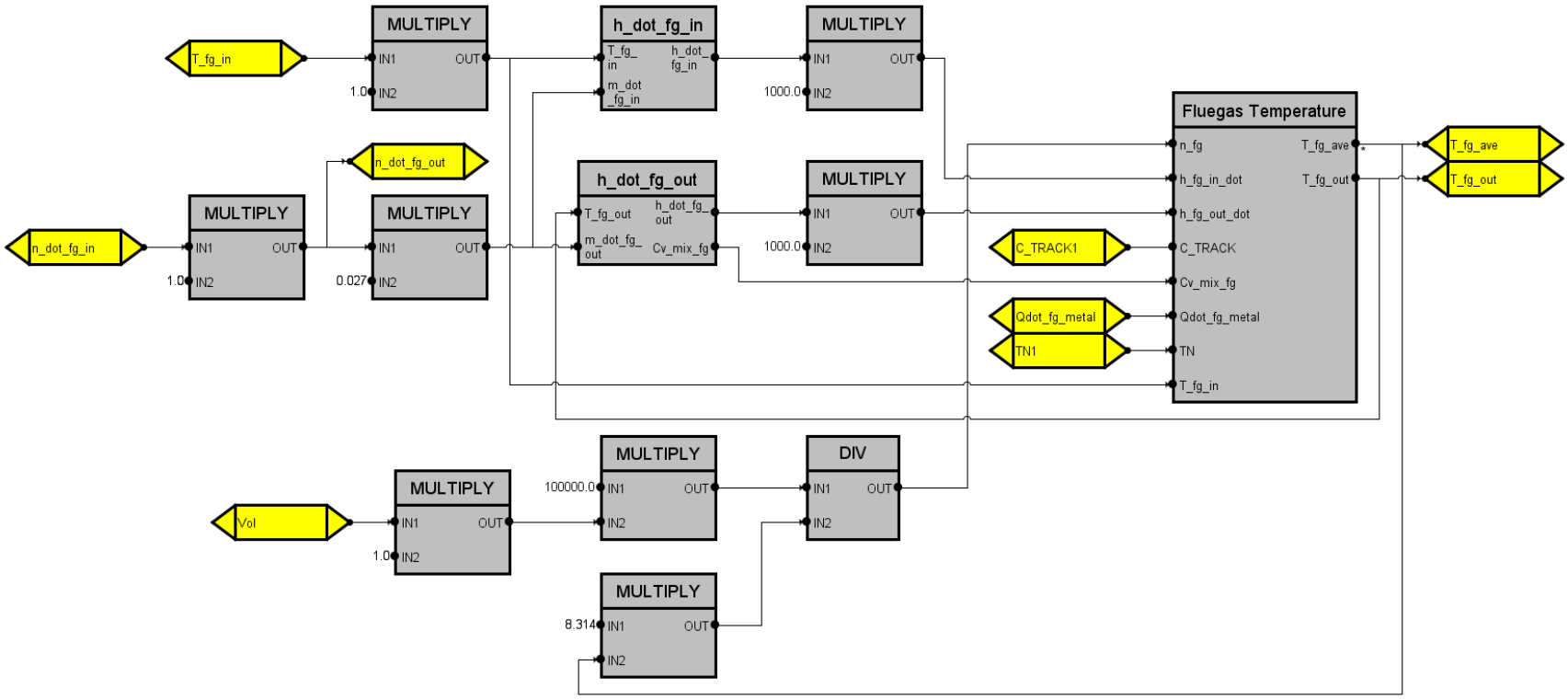

Figure 4.12: SPPA-T3000 block diagram of the flue gas control volume in the economizer

4.3 Economizer

The primary purpose of the economizer is to preheat feedwater in preparation for boiling in the evaporator. To model this heat exchanger, we will be using the flue gas, metal, and liquid control volumes. A description of these control volumes concerning the economizer can be seen in Sections 3.2.3.1, 3.2.3.2, and 3.2.3.3 respectively. A representation of this system is shown below in Figure 4.13.

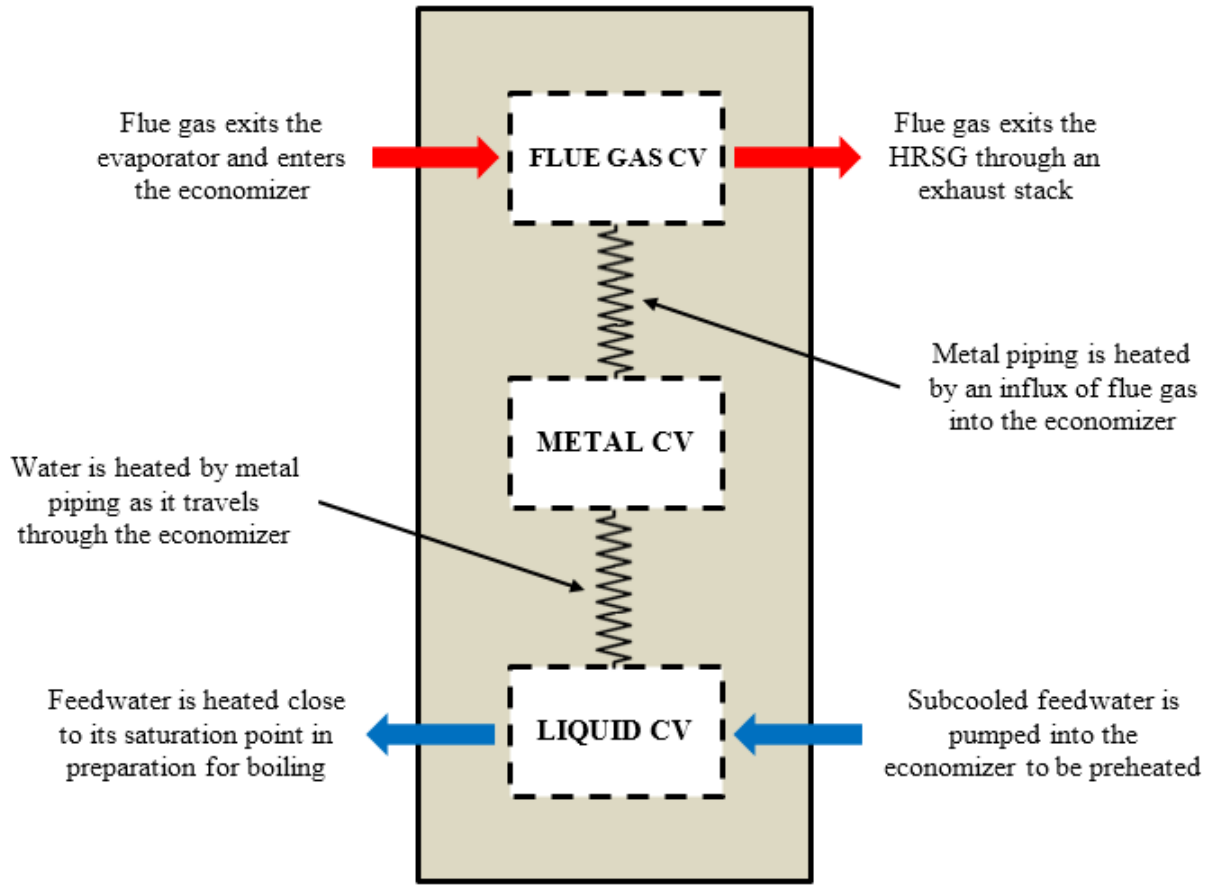

Figure 4.13: Diagram of an economizer heat exchanger

The economizer was constructed as a single entity before being fully integrated into the complete HRSG model. This T3000 heat exchanger module is shown below in Figure 4.14.

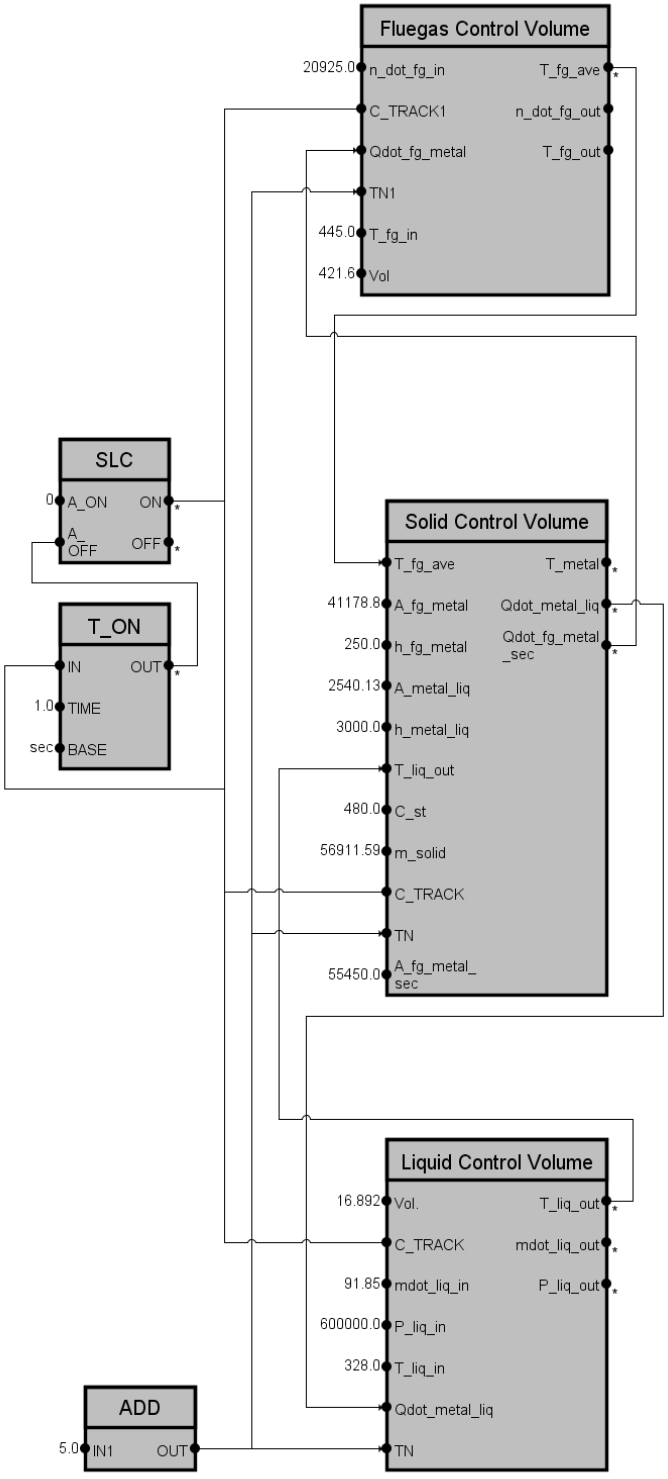

Figure 4.14: SPPA-T3000 model of the economizer heat exchanger

4.4 Evaporator

The primary responsibility of the evaporator is to facilitate the phase change of water from a liquid to gaseous state. The flue gas, metal, liquid, and vapor control volumes are all implemented to capture the system dynamics accurately. A detailed account of these control volumes relative to the evaporator is found in Sections 3.3.3.1, 3.3.3.2, 3.3.3.3, and 3.3.3.4 respectively. An illustration of this heat exchanger is presented in Figure 4.15.

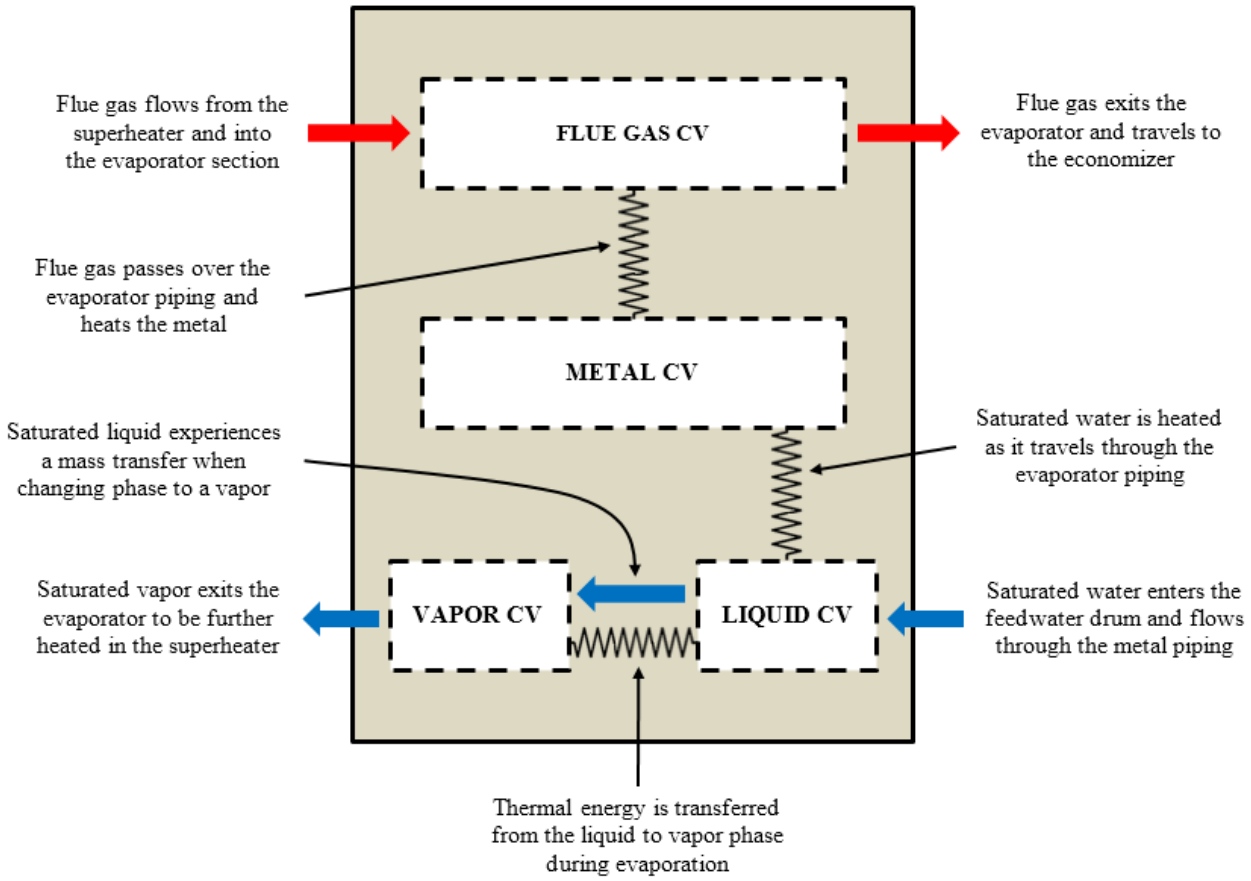

Figure 4.15: Diagram of an evaporator heat exchanger

The evaporator was created as an individual model before assimilation into the complete HRSG system. This T3000 heat exchanger module is shown below in Figure 4.16.

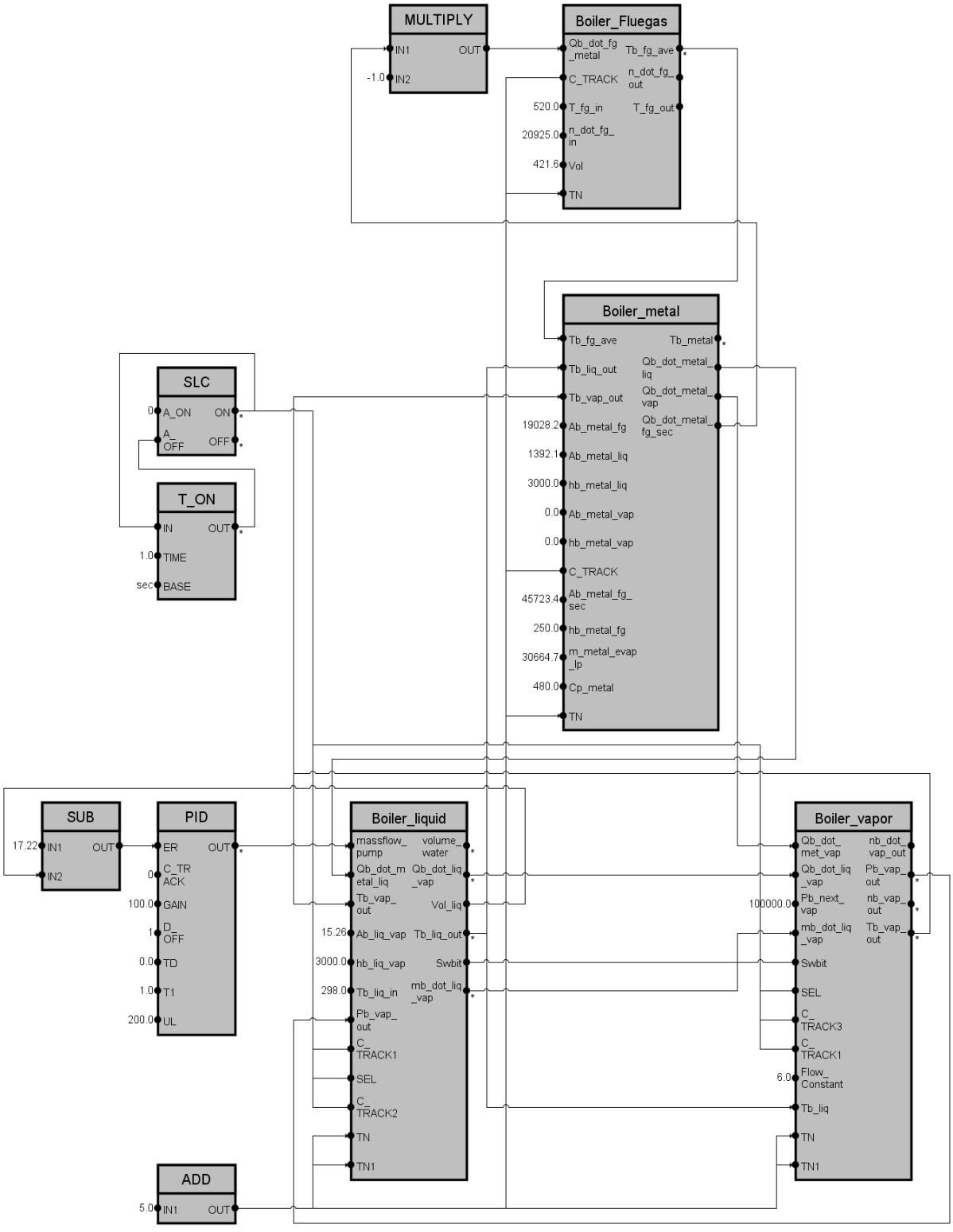

Figure 4.16: SPPA-T3000 model of the evaporator heat exchanger

4.5 Superheater

The principal function of the superheater is to increase the temperature of water vapor to go from a saturated to a superheated state. The physical phenomena occurring within this apparatus are represented by the flue gas, metal, and vapor control volumes. The definition of these control volumes regarding the superheater system are detailed in Sections 3.4.3.1, 3.4.3.2, and 3.4.3.3 respectively. Shown in Figure 4.17 is a graphical depiction of this heat exchanger.

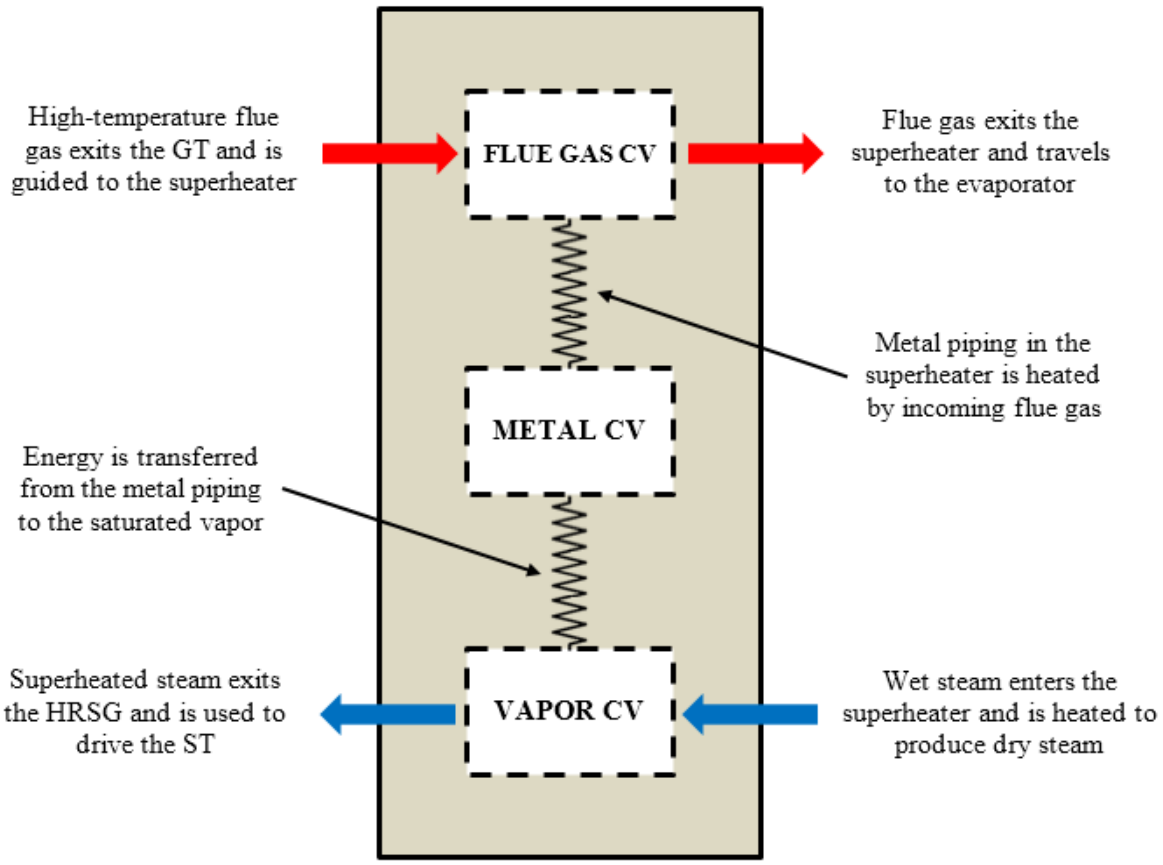

Figure 4.17: Diagram of a superheater heat exchanger

The evaporator was created as an individual model prior to integration into the complete HRSG system. This T3000 heat exchanger module is shown below in Figure 4.18.

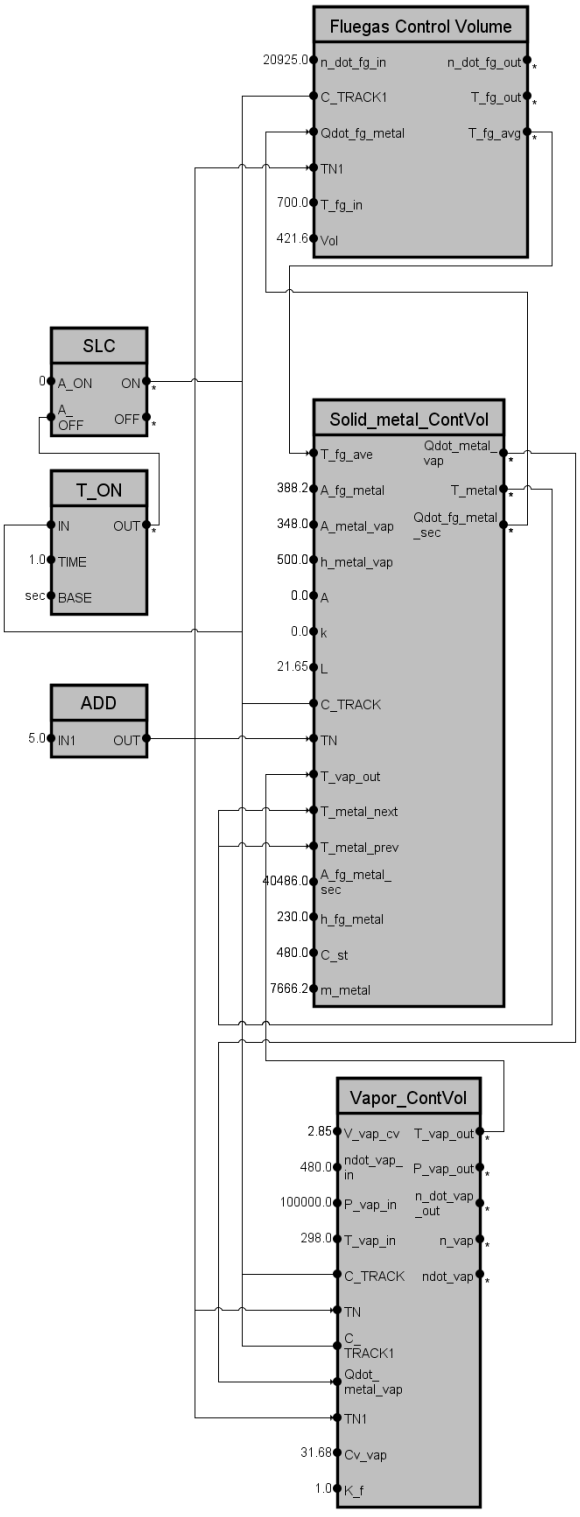

Figure 4.18: SPPA-T3000 model of the superheater heat exchanger

4.6 Combined HRSG Model

The principal objective of a HRSG is to reclaim waste heat from the GT exhaust and use that thermal energy to produce steam. Once generated, this steam can be used to drive a ST and increase plant efficiency by producing additional power. To model this thermodynamic process, we will combine the economizer, evaporator, and superheater modules. By connecting each subsystem to form one combined model, we can accurately represent the low-pressure heat recovery steam generator. A diagram of this cohesive structure is located in Figure 4.19.

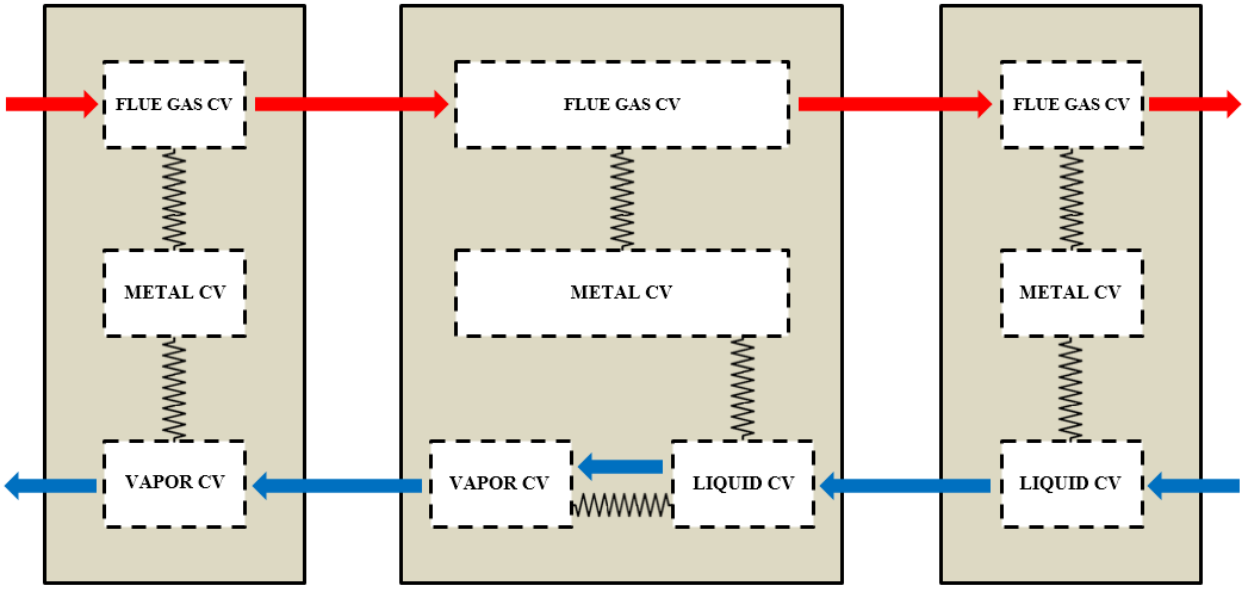

Figure 4.19: Diagram of a low-pressure heat recovery steam generator

Initially, the economizer, evaporator, and superheater were developed as individual systems before unification. Each heat exchanger was combined as shown in Figure 4.20 to manufacture the comprehensive HRSG model.

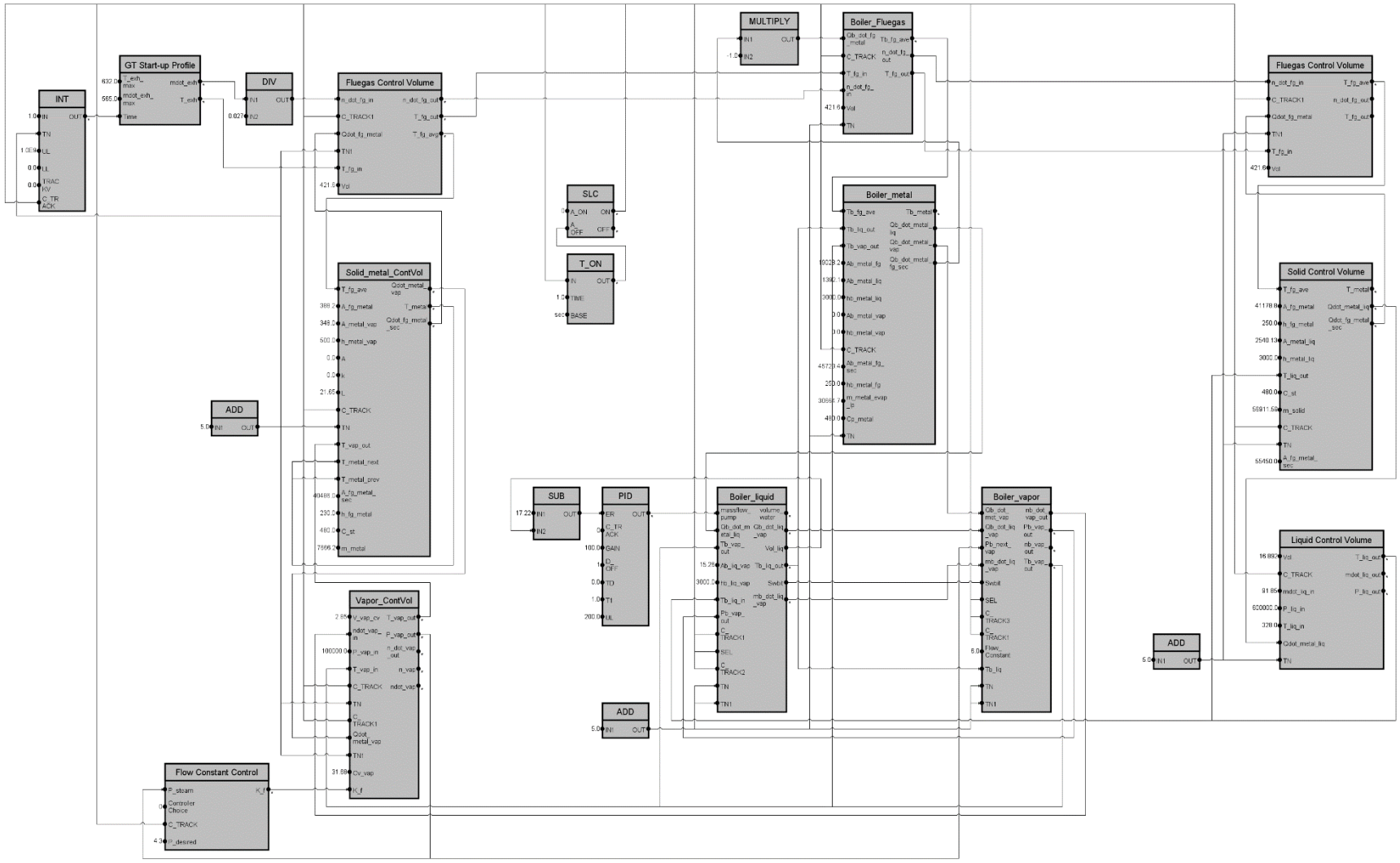

Figure 4.20: SPPA-T3000 model of the low-pressure heat recovery steam generator

CHAPTER 5: MODEL SIMULATION IN T3000

A digital prototype of the heat recovery steam generator is developed in the proceeding chapter. This block-diagram model structurally resembles the HRSG but has not been tested to prove its legitimacy. To confirm that the numeric model will accurately predict real-world performance, it must undergo a series of simulations. In doing so, we can analyze the model and make modifications as needed to rectify errors and improve performance. The T3000 platform has been employed in this chapter to carry out the design validation process.

5.1 Organization of Modeling and Simulation

The HRSG is a large and complicated system that combines elements of fluid mechanics, thermodynamics, heat transfer, and mass transfer among other physical phenomena. To develop a computation model of this caliber, a strategy of how to organize the research was necessary. This plan of action would provide a route to achieving the goals set out in this thesis and avoid becoming overwhelmed with the task at hand.

The HRSG model conceived in Chapter 4 is constructed from three heat exchanger modules, each containing multiple CVs. With every additional block of code comes an increase in the likelihood of bugs. Thus, the methodology behind our development process is to test each component with realistic operating conditions and parameters values before inclusion in a more extensive system. This approach is useful in the early detection of numerical instability and modeling deficiencies within individual modules. Otherwise, it would be difficult to identify and correct these issues when performing tests on the complete system. By doing this, we can prevent the propagation of error throughout the system and reduce time spent debugging. A general overview of the research process that transpired is shown in Table 5.1.

Table 5.1: Organization of Modeling and Simulation

Step No.	Task Type	Task Description
1	Modeling	Develop a liquid control volume block
2	Simulation	Test the liquid control volume for numerical stability
3	Modeling	Develop a vapor control volume block
4	Simulation	Test the vapor control volume for numerical stability
5	Modeling	Develop a metal control volume block
6	Simulation	Test the metal control volume for numerical stability
7	Modeling	Develop a flue gas control volume block
8	Simulation	Test the flue gas control volume for numerical stability
9	Validation	Simulate the liquid control volume with realistic inlet conditions
10	Validation	Simulate the vapor control volume with realistic inlet conditions
11	Validation	Simulate the metal control volume with realistic inlet conditions
12	Validation	Simulate the flue gas control volume with realistic inlet conditions
13	Modeling	Construct a superheater module
14	Simulation	Test the superheater for numerical stability
15	Modeling	Construct an evaporator module
16	Simulation	Test the evaporator for numerical stability
17	Modeling	Construct an economizer module
18	Simulation	Test the economizer for numerical stability
19	Validation	Simulate the superheater using Siemens plant conditions
20	Validation	Simulate the evaporator using Siemens plant conditions
21	Validation	Simulate the economizer using Siemens plant conditions
22	Modeling	Combine economizer, evaporator, and superheater into one model
23	Simulation	Test the combined model for numerical stability
24	Validation	Simulate the combined model using Siemens plant conditions

5.2 Model Validation

Validation of the LP HRSG model was performed by comparing its simulation results to data from an active Siemens combined-cycle power plant. The Panda Stonewall plant in Virginia is the reference plant for this thesis. Geometric parameter values such as pipe diameters, pipe bundle surface areas, and control volume dimensions were obtained or calculated from HRSG

reference drawings for Stonewall. Operating conditions including feedwater inlet conditions, flue gas (FG) inlet conditions, and boiler water level are also based on Stonewall specifications. These geometric parameters and operating conditions were implemented into the T3000 model to allow for an accurate comparison between simulation results and plant data.

5.2.1 Siemens Plant and T3000 Simulation Trends

Validation began by obtaining start-up trends from the Stonewall power plant for the LP system without supplementary firing (duct firing). The transient and steady-state data from this plot would become the baseline for the T3000 simulation. A sample of this information is shown below in Figure 5.1. For this start-up procedure, the plant was ramped up to 50% GT load, held constant, and then increased to base load.

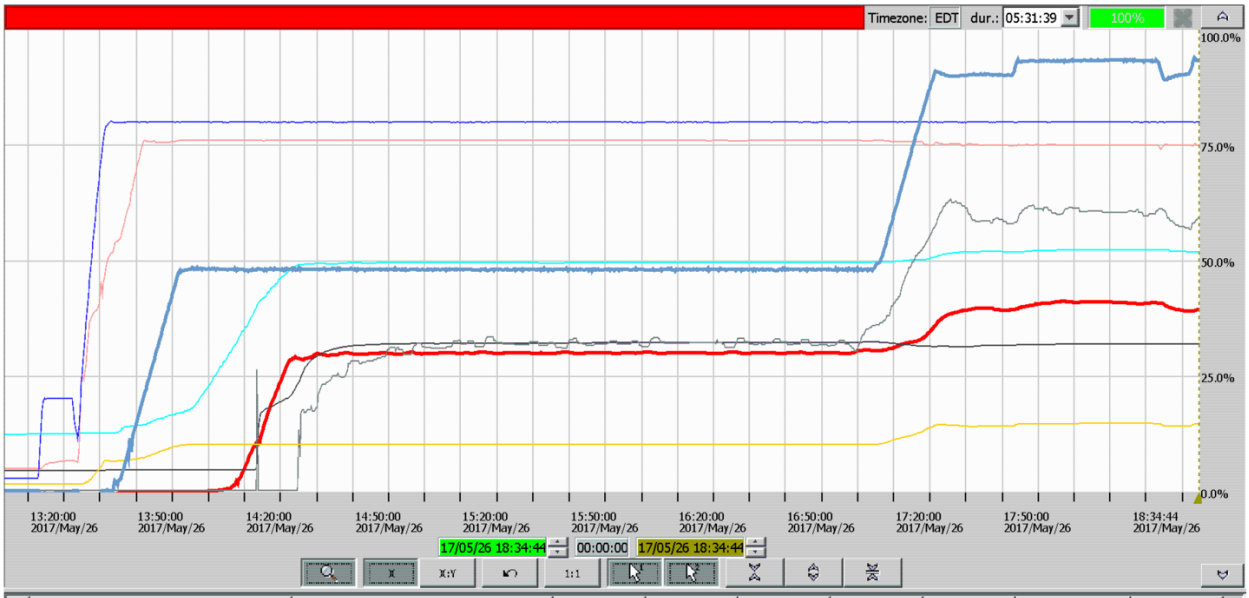

SIGNAL TAG	DESIGNATION	RANGE LOW	RANGE HI	CURSOR 1	CURSOR 2	Y DIFF	UNIT	LAST
11HAD80CP001||XQ01	LP DRUM PRES	0.0000	160.0000	62.9167	62.9167	0.0000	PSIG	62.9167
11HAD80CT001||XQ01	LP EVAP OUT TEMP	0.0000	600.0000	310.8724	310.8724	0.0000	°F	310.8724
11LBA80CT001||XQ01	LP STM TEMP	0.0000	1500	478.0816	478.0816	0.0000	°F	478.0816
11LBA80CF001||XQ01	LP STM FLOW	0.0000	110.0000	65.1513	65.1513	0.0000	KPPH	65.1513
11HSA60EC900||ZQ01	DRY EXHAUST FLOW	0.0000	1.000E6	145076	145076	0.0000	SCFH	145076
11MBA10EU002A||ZQ01	AVERAGE EXHAUST TEMP	0.0000	1500	1125	1125	0.0000	°F	1125
11MBY10CS004SA||OUT	TURB SPEED SELECTED	0.0000	4500	3600	3600	0.0000	RPM	3600
11HAD00EU001||XQ04	CT MEGAWATT SELECT	0.0000	250.0000	233.5239	233.5239	0.0000	MW	233.5239

Figure 5.1: Siemens data for the Stonewall low-pressure system

Subsequently, a T3000 simulation was run using the appropriate geometric parameters and initial conditions considered in the Stonewall LP data. An illustration of the simulation results is shown below in Figure 5.2. In this simulation run, the plant was ramped up to GT baseload without an intermediate hold.

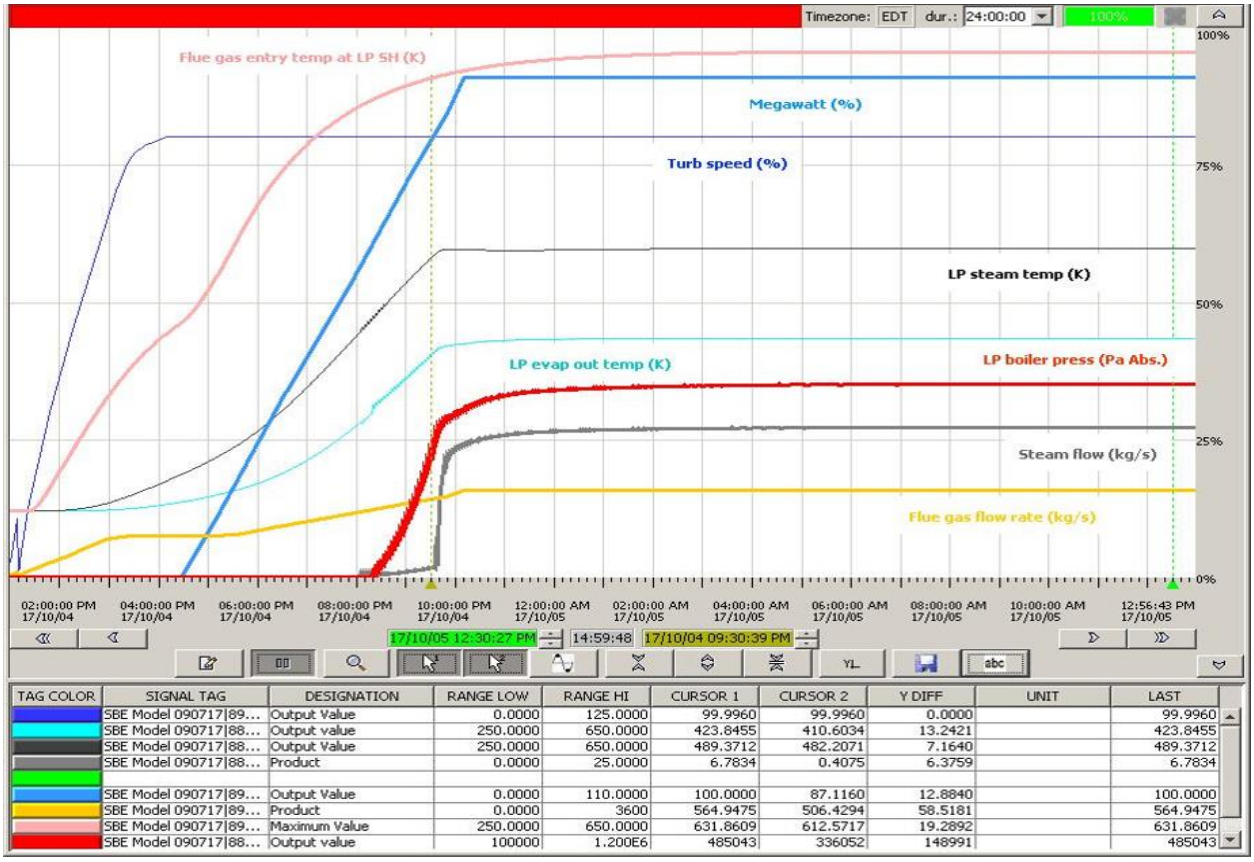

TAG COLOR	SIGNAL TAG	DESIGNATION	RANGE LOW	RANGE HI	CURSOR 1	CURSOR 2	Y DIFF	UNIT	LAST
	SBE Model 090717|89...	Output Value	0.0000	125.0000	99.9960	99.9960	0.0000		99.9960
	SBE Model 090717|88...	Output value	250.0000	650.0000	423.8455	410.6034	13.2421		423.8455
	SBE Model 090717|88...	Output Value	250.0000	650.0000	489.3712	482.2071	7.1640		489.3712
	SBE Model 090717|88...	Product	0.0000	25.0000	6.7834	0.4075	6.3759		6.7834
	SBE Model 090717|89...	Output Value	0.0000	110.0000	100.0000	87.1160	12.8840		100.0000
	SBE Model 090717|89...	Product	0.0000	3600	564.9475	506.4294	58.5181		564.9475
	SBE Model 090717|89...	Maximum Value	250.0000	650.0000	631.8609	612.5717	19.2892		631.8609
	SBE Model 090717|88...	Output value	100000	1.200E6	485043	336052	148991		485043

Figure 5.2: T3000 simulation results for the Stonewall low-pressure system

Both trends are characterized by an x-axis which represents elapsed time, and a y-axis which represents the normalized parameter value in percent. The normalization of these plots is with respect to constant reference values which are typically the upper and lower bounds for that parameter. The purpose of this action is to more easily compare the plant and simulation graphs regardless of the unit system used for each data set.

5.2.2 Siemens Plant and T3000 Simulation Results

When comparing the Siemens Stonewall plant data for their LP system to the simulation results presented in this thesis, the two plots correlate well with one another. Not only do the transient responses match, but the steady-state values also equate to an acceptable degree given the assumptions made during the modeling process. Presented in the following tables are results from the validation process.

The first simulation of the LP system used the operating conditions shown in Table 5.2. While the turbine speed and flue gas flow rate are explicitly known from Siemens data, the flue gas entry temperature at the LP superheater is not. Since there is no temperature sensor at that location within the HRSG, there is no way to precisely know the flue gas inlet temperature into the LP system. However, the upstream flue gas inlet temperature into the entire HRSG is known to be 880 K. Therefore the flue gas entry temperature into the LP superheater is approximated in accordance with HRSG documentation for Stonewall. Thus, the simulation I flue gas entry temperature at the LP superheater is estimated to be 632 K.

Table 5.2: Operating Conditions for Siemens Data and Low-Pressure Simulation I

Variable No.	Variable Description	Steady Values	Units	Comments
1	Turbine Speed	80	%	Given
2	FG Flow Rate	564.95	Kg/s	Given
3	FG Entry Temp. at LP Superheater	632	K	Approx. from given FG inlet temp. of 880 K

Steady-state results from the first low-pressure system simulation are presented in Table 5.3. As shown, the evaporator outlet temperature and steam outlet temperature adequately correlate to Siemens plant data. However, the boiler pressure and steam flow rate are marginally higher than

desired. To increase the correlation between simulation results and Stonewall plant data, we can alter the estimated flue gas entry temperature.

Table 5.3: Siemens Data vs. Low-Pressure Simulation I Results

Variable No.	Variable Description	Siemens Data	T3000 Simulation	Units	Error
1	Boiler Pressure	5.35	4.85	Bar(a)	+0.5 (9%)
2	Evaporator Outlet Temp.	428.08	423.85	K	+4.23 (1%)
3	Steam Temp. at Superheater Outlet	520.93	489.37	K	+31.56 (6%)
4	Steam Flow Rate	8.21	6.95	Kg/s	+1.26 (15%)

In the second simulation, operating conditions for the LP system were slightly altered as shown in Table 5.4. While the turbine speed and flue gas flow rate were kept the same, flue gas entry temperature was increased to 700 K. As previously stated, the approximation of this parameter corresponds to HRSG specifications for Stonewall. Thus, increasing the flue gas entry temperature within reasonable margins is acceptable. The dynamic simulation response caused by a flue gas temperature change is illustrated in Figure 5.3.

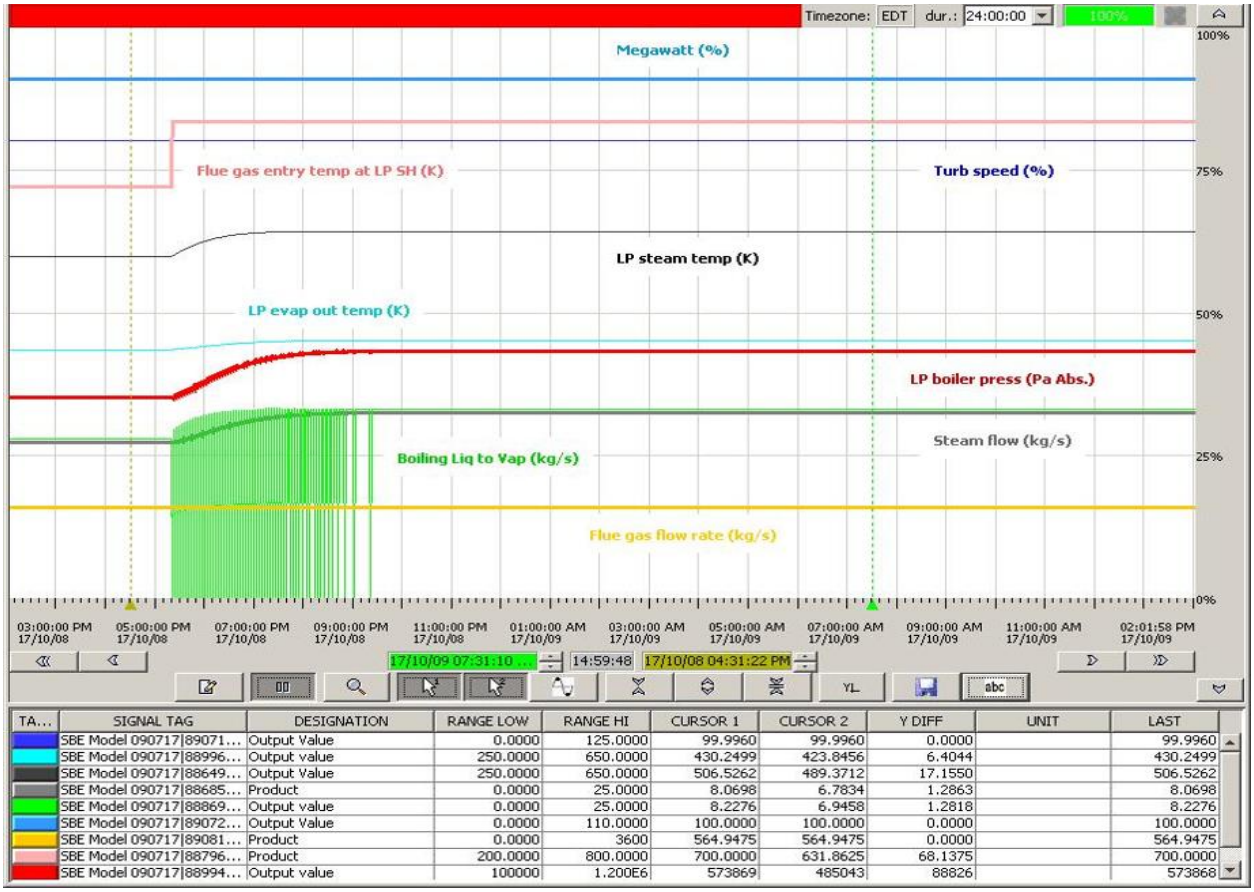

TA...	SIGNAL TAG	DESIGNATION	RANGE LOW	RANGE HI	CURSOR 1	CURSOR 2	Y DIFF	UNIT	LAST
	SBE Model 090717|89071...	Output Value	0.0000	125.0000	99.9960	99.9960	0.0000		99.9960
	SBE Model 090717|88996...	Output value	250.0000	650.0000	430.2499	423.8456	6.4044		430.2499
	SBE Model 090717|88649...	Output Value	250.0000	650.0000	506.5262	489.3712	17.1550		506.5262
	SBE Model 090717|88685...	Product	0.0000	25.0000	8.0698	6.7834	1.2863		8.0698
	SBE Model 090717|88869...	Output value	0.0000	25.0000	8.2276	6.9458	1.2818		8.2276
	SBE Model 090717|89072...	Output Value	0.0000	110.0000	100.0000	100.0000	0.0000		100.0000
	SBE Model 090717|89081...	Product	0.0000	3600	564.9475	564.9475	0.0000		564.9475
	SBE Model 090717|88796...	Product	200.0000	800.0000	700.0000	631.8625	68.1375		700.0000
	SBE Model 090717|88994...	Output value	100000	1.200E6	573869	485043	88826		573868

Figure 5.3: Dynamic effect of a parameter change during the simulation

As shown, the system reenters boiling mode due to an introduction of additional heat content into the HRSG. As a result, the steam temperature, evaporator temperature, boiler pressure, and steam flow rate all increase accordingly and settle at new steady-state values.

Table 5.4: Operating Conditions for Siemens Data and Low-Pressure Simulation II

Variable No.	Variable Description	Steady Values	Units	Comments
1	Turbine Speed	80	%	Given
2	FG Flow Rate	564.95	Kg/s	Given
3	FG Entry Temp. at LP Superheater	700	K	Approx. from given FG inlet temp. of 880 K

Steady-state results from the second low-pressure simulation are displayed in Table 5.5. As shown, each parameter received a drop in error compared to the first simulation. Thus, increasing the flue gas entry temperature improved the correlation between simulation results and plant data. Further trials were conducted to determine which flue gas entry temperature would generate the lowest error values. However, a flue gas entry temperature of 700 K proved to be the optimal value for producing the highest correlation. Thus, the second LP simulation was chosen for the following transient simulation study.

Table 5.5: Siemens Data vs. Low-Pressure Simulation II Results

Variable No.	Variable Description	Siemens Data	T3000 Simulation	Units	Error
1	Boiler Pressure	5.35	5.74	Bar(a)	-0.39 (7%)
2	Evaporator Outlet Temp.	428.08	430.25	K	-2.17 (0.5%)
3	Steam Temp. at Superheater Outlet	520.93	506.53	K	+14.4 (3%)
4	Steam Flow Rate	8.21	8.23	Kg/s	-0.02 (0.2%)

While steady-state results correlate well with plant data, the transient response of the model was also analyzed to complete the validation. Shown below in Table 5.6 are the operating conditions for the transient study conducted on the second LP simulation. The turbine speed rise time and megawatt ramp time are known from Siemens data. However, the rise time of the flue gas temperature at the LP superheater is unknown. As discussed previously, no temperature sensors are located at the LP superheater inlet. Therefore, the flue gas inlet temperature is not explicitly measured and the rise time of the flue gas temperature is once again approximated.

Table 5.6: Transient Conditions for Siemens Data and Low-Pressure Simulation II

Variable No.	Variable Description	Data Time	Simulation Time	Comments
1	Turbine Speed Rise Time (0 to 90 %)	~ 10 min.	~ 2.5 hrs. = 7.5 min.	Simulation time can be tuned
2	Megawatt Ramp Time (0 to 100 %)	~ 40 min.	~ 6 hrs. = 18 min.	Simulation time can be tuned
3	FG Temp. Rise Time at LP Superheater	Not Known	Time Constant: 0, 2, 5 hrs. = 0, 6, 15 min.	FG temp. rise time at inlet is given (time constant is tunable)

Transient results from the low-pressure simulation II study are detailed in Table 5.7. With a time constant of 15 minutes, we were able to achieve an acceptable start time for boiler pressurization. Similarly, a time constant of 6 minutes produced a satisfactory boiler pressurization time in comparison to Siemens data. Further modification to time constants for both the operating conditions and LP system transients are possible to improve the correlation between simulation results and plant data.

Table 5.7: Siemens Data vs. Low-Pressure Simulation II Transients

Variable No.	Variable Description	Siemens Data	T3000 Simulation
1	Start Time for Boiler Pressurization	~ 40 min.	~ 12.5 min. with 0 min. time constant ~ 21 min. with 6 min. time constant ~ 38 min. with 15 min. time constant
2	Boiler Pressurization Time	~ 15 min.	~ 13 min. with 6 min. time constant

5.2.3 Temperature Trends

A plot of the flue gas temperature trends is shown below in Figure 5.4. These simulation results are in agreement with actual plant data and show how flue gas thermal energy is reduced throughout the HRSG.

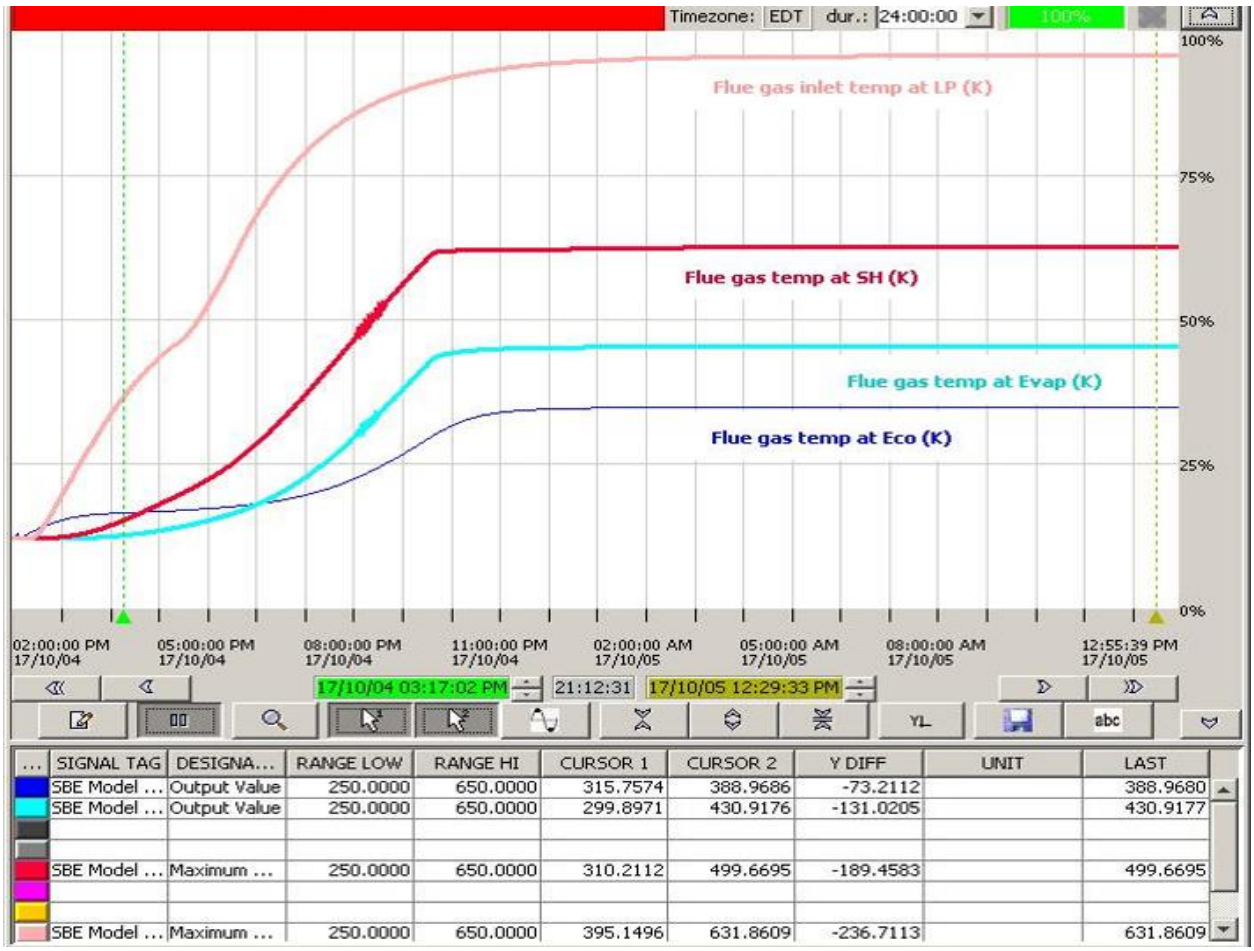

Figure 5.4: Flue gas temperature trends for the low-pressure simulation II

Gas turbine exhaust enters the LP HRSG at its highest temperature before it participates in heat transfer. Once the flue gas hits the superheater section, it will begin to transfer some of its thermal energy to this heat exchanger. As a result, the flue gas temperature will reduce and settle at a value lower than the flue gas inlet temperature. In a similar fashion, the flue gas will then pass through the evaporator and economizer sections. The heat exchange occurring in each of these devices will

cause a further reduction in flue gas temperature. As shown in Figure 5.4, each successive heat exchanger causes a reduction in flue gas temperature which matches the system physics. During simulation startup, there is an initial surge in the economizer flue gas temperature where it exceeds the evaporator and superheater sections. While counterintuitive, the cause is a constant feedwater inlet temperature of 328 K which is higher than ambient conditions of 298 K. Therefore, the initial temperature jump of the economizer section is created by incoming feedwater heating the metal and flue gas CVs. Once the flue gas surpasses the feedwater temperature, this phenomenon will disappear, and the intended heat transfer will resume. A similar anomaly is seen in the metal temperature trends shown below in Figure 5.5.

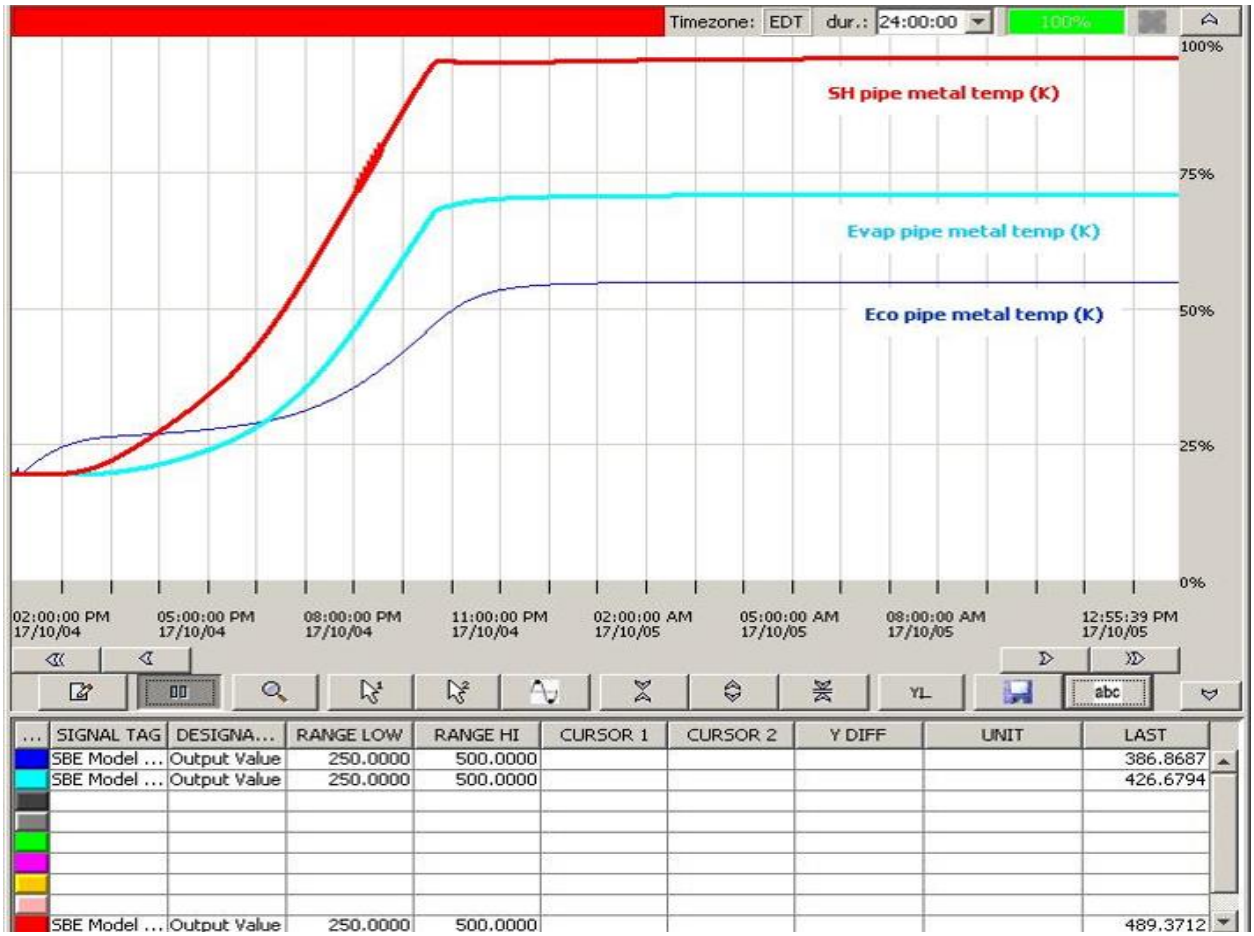

Figure 5.5: Metal temperature trends for the low-pressure simulation II

5.3 Simulation Challenges

With any ambitious endeavor comes challenges that must be surmounted. This project was no different and presented obstacles in multiple facets ranging from thermodynamics to computer science. In the following sections are some of the most problematic obstructions overcome.

5.3.1 Numerical Instability

5.3.1.1 Heating and Boiling Phase Switching

The most prevalent challenge encountered over the course of this research was numerical instability of evaporation. During a plant startup, the liquid control volume is initially in heating mode. As described in Section 3.3.3.3, the liquid CV will remain in heating mode until the liquid temperature surpasses its saturation temperature at the vapor pressure. Since boiling has not begun at this point, the vapor pressure remains constant and produces a constant liquid saturation temperature. The liquid temperature will continue to rise in heating mode until it exceeds its saturation temperature and enters into the boiling mode. In this mode vapor formation occurs, causing a mass transfer from the liquid into the vapor CV. This transfer of evaporated liquid into the vapor CV will cause the vapor temperature and pressure to rise dramatically. At this point is the onset of numerical instability due to the low sampling rate of T3000. When the vapor temperature shoots up, it produces a higher than solvable thermal gradient within the chosen time step. This issue prevents the integration described in Equation (3.89) from accurately capturing the temperature increase. The vapor temperature should dramatically increase until the liquid temperature falls below the new saturation temperature and enters into heating mode. Instead, the vapor temperature overshoots the heating mode condition and continues to rise because of the substantial time step. As a result, the boiler pressure increases past the intended value and produces

a higher than expected saturation temperature for the liquid. Since the liquid temperature is held constant during boiling mode, it will fall below the new saturation temperature and return to heating mode. When this happens, the mass transfer into the vapor CV will cease and cause a drop in the vapor temperature. Since the vapor temperature has overshot its actual value, the temperature drop will be more dramatic than intended and cause another sizeable thermal gradient. The vapor temperature should decrease until the liquid temperature rises above the new saturation temperature and enters into the boiling mode. Instead, the vapor temperature overshoots the boiling mode condition and continues to drop because of the large time step. Consequently, the boiler pressure will reduce past the intended value and produces a lower than expected saturation condition. This inaccuracy will cause the liquid volume to switch rapidly back into boiling mode and generate an even larger vapor temperature thermal gradient. This process of switching from heating to boiling mode will continue to progress more rapidly and produce even greater thermal gradients. Eventually, the system response will grow exponentially, and instability will occur.

The solution to this numerical issue is composed of multiple parts. The first step was to implement a higher integration time constant (TN) which dilates the simulation and artificially slows it down. This change would reduce the thermal gradient of vapor temperature spikes, and allow the integration to become more manageable. The next step was to increase the sample rate of the simulation. This solution involved modifying the software runtime environment (runtime container) and lowering the base cycle time of the simulation. The result is an increase in the simulation sample rate and an increase in the accuracy of calculations. Lastly, a deadband was placed around the saturation temperature to buffer the heating-boiling switching condition. This inclusion would eliminate the possibility of rapid switching between modes and reduce the chance

of instability. The effect of these modifications have resulted in a stable simulation during phase change, and an equilibrium point to be attainable.

5.3.1.2 Integrator Drift

As shown in Equation (3.93), the rate of vapor mass change ($\dot{m}_{vap}$) within the evaporator is based on incoming and outgoing vapor mass flow. More specifically, this is the difference between vapor entering the vapor CV due to evaporation ($\dot{m}_{liq,vap}$), and vapor leaving the CV to enter the superheater ($\dot{m}_{vap,out}$). At equilibrium, vapor should enter and exit the CV at the same rate, causing $\dot{m}_{vap}$ to be zero. This would result in the vapor mass (m_{vap}) remaining constant according to Equation (3.94). With that being said, when the simulation reached equilibrium, it did not produce a constant vapor mass. This was caused by the incoming and outgoing vapor flow rates not being identical. Since these values are calculated independently from each other, their equilibrium values were nearly the same, but not exactly equal. This caused $\dot{m}_{vap}$ to be nonzero and become slightly positive or negative. The consequence is a vapor mass that, over time, would either accumulate infinitely or diminish to zero. The effect of this inaccuracy is felt in Equation (3.88), where vapor mass appears in the denominator of the vapor temperature change calculation. An infinitely large vapor mass would cause the temperature rate to be zero. On the other hand, zero vapor mass would cause the temperature rate to become undefined. Neither occurrence is desired and would produce inaccurate or unstable models respectively.

The solution to this numerical issue was to implement a deadband on the vapor flow rate integrator. Upper and lower limits were established to allow integration during transient operation, but stop integration when equilibrium was reached. If $\dot{m}_{vap}$ fell outside of the deadband limits, its value would be integrated to calculate vapor mass. However, if $\dot{m}_{vap}$ is within the deadband, its

value would be set to zero and thereby halt the vapor mass calculation. Multiple simulations have shown the vapor mass drift to be corrected and a stable steady state to be attainable. In future research, we plan to remove the vapor moles deadband and use the Redlich-Kwong calculation to correct for mass accumulation/reduction.

5.3.2 Peculiarities of a Distributed Control System

5.3.2.1 Low Sample Rate

T3000 is a distributed control system commonly applied to monitor and autonomously control plant processes. Since most plant signals have a gradual response, using a high cycle time of 400 to 800 milliseconds is sufficient. Nevertheless, this thesis used T3000 as a graphical programming environment to model the dynamic and transient behavior of a thermodynamic system. In this capacity, a 400 to 800 millisecond cycle time is incapable of accurately capturing the temperature, pressure, and mass flow fluctuations. Figure 5.6 shows an example of flue gas temperature instability due to a higher than solvable thermal gradient within the chosen time step. As a consequence, vapor temperature instability ensued, and the entire model became numerically volatile. To accurately simulate the model at high cycle times, a few modifications were made to the system.

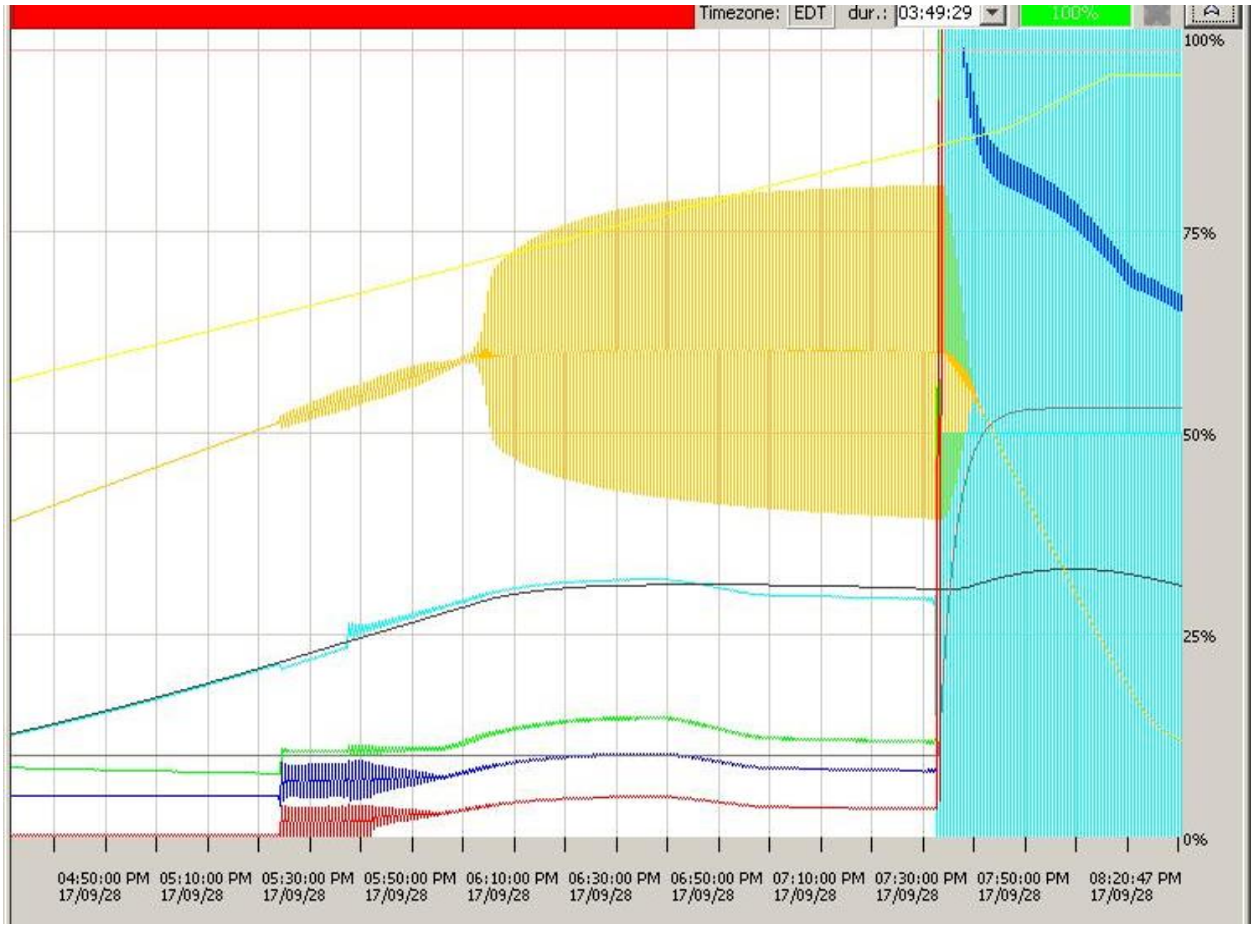

Figure 5.6: Example of flue gas temperature numerical instability

The most straightforward solution is to increase the integration time constant (TN) for all integrators to dilate the simulation time. This change artificially slows down the entire simulation to effectively run the model at a higher sample rate. Reducing computational burden would minimize the erratic behavior of highly fluctuating signals to allow for a more controllable integration. Another alteration made to the model was the application of time delays to volatile parameters. The purpose of this change is to smoothen out the response of highly fluctuating signals to prevent instability in subsequent calculations. An example of this solution is the application of a first-order lag (PT1) to the vapor temperature. During phase change, this vapor temperature rapidly increases and decreases because the liquid CV is quickly switching between

heating and boiling mode. The attenuation of this variable prevented the vapor enthalpy computation from becoming unstable and effecting downstream calculations.

5.3.2.2 Lack of a Restart Feature

Distributed control systems, such as T3000, are designed to continuously run for days, weeks, or even months while the power plant is operational. Thus, it can be a challenge to restart a simulation in T3000 with no included feature to do so. The brute force method is to completely deactivate and reactivate the simulation which is tedious and time-consuming. Once more, this type of system restart causes the loss of overridden port values and data plots. This hindrance was overcome by implementing a manual system restart into the model. This device connected all integrator reset ports to a binary signal generator. When activated, the signal generator would send a Boolean pulse to all integrators for a short amount of time. This signal would cause the integrators to restart integration simultaneously from their initial condition. This action effectively resets the simulation in a seamless manner without the loss of overridden port values or simulation data. The T3000 switch used by the operator to reset the simulation is shown in Figure 5.7. An image of the manual reset which includes the switch (T_ON) and binary pulse generator (SLC) blocks are seen below in Figure 5.8.

Figure 5.7: SPPA-T3000 faceplate for the simulation reset switch

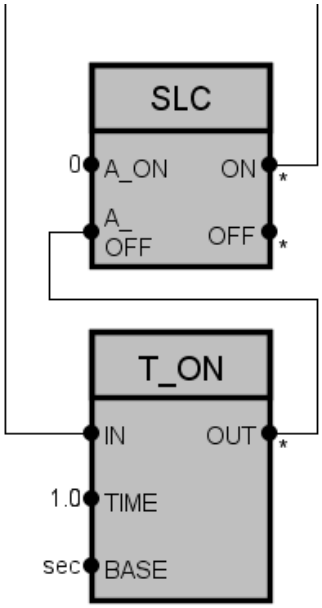

Figure 5.8: SPPA-T3000 simulation restart block diagram

5.3.3 Validation Conditions

During the validation process, operating conditions and geometric dimensions from the Siemens plant were applied to the T3000 model. These input values would allow for an accurate comparison between the Siemens data and simulation results to determine how well they correlate.

Constant parameters such as surface area and volume were explicitly calculated from detailed HRSG drawings. However, variable parameters like flow coefficients and flue gas inlet conditions were more challenging to implement. The proper application of their transient profile in T3000 is imperative to produce an accurate transient response of the system.

5.3.3.1 Flow Coefficient Control

The flow coefficient (K_f) in this model defines the relative measure of a devices ability to allow fluid flow. This is apparent in the evaporator and superheater where steam flow is present within these modules. As vapor exits the evaporator, it is allowed to freely flow without any constraint into the superheater. This corresponds to a higher flow coefficient which denotes a lower flow restriction. However, as steam leaves the superheater, it does not freely travel to the steam turbine at all times. During plant startup, the superheated steam conditions are not initially met. Therefore, a ST bypass valve between these two systems regulate how much, if any steam flow is allowed to enter the turbine. This valve will initially be wide open, and divert steam flow away from the ST until satisfactory superheat conditions are achieved. Once steam conditions are satisfactory, the valve will gradually close to allow steam flow into the ST. The flow coefficient in this scenario is not fixed, and required additional effort to correctly model the bypass valve actuation in T3000. A demonstration of the ST bypass valve actuation and the resulting flow and pressure evolution is shown in Figure 5.10.

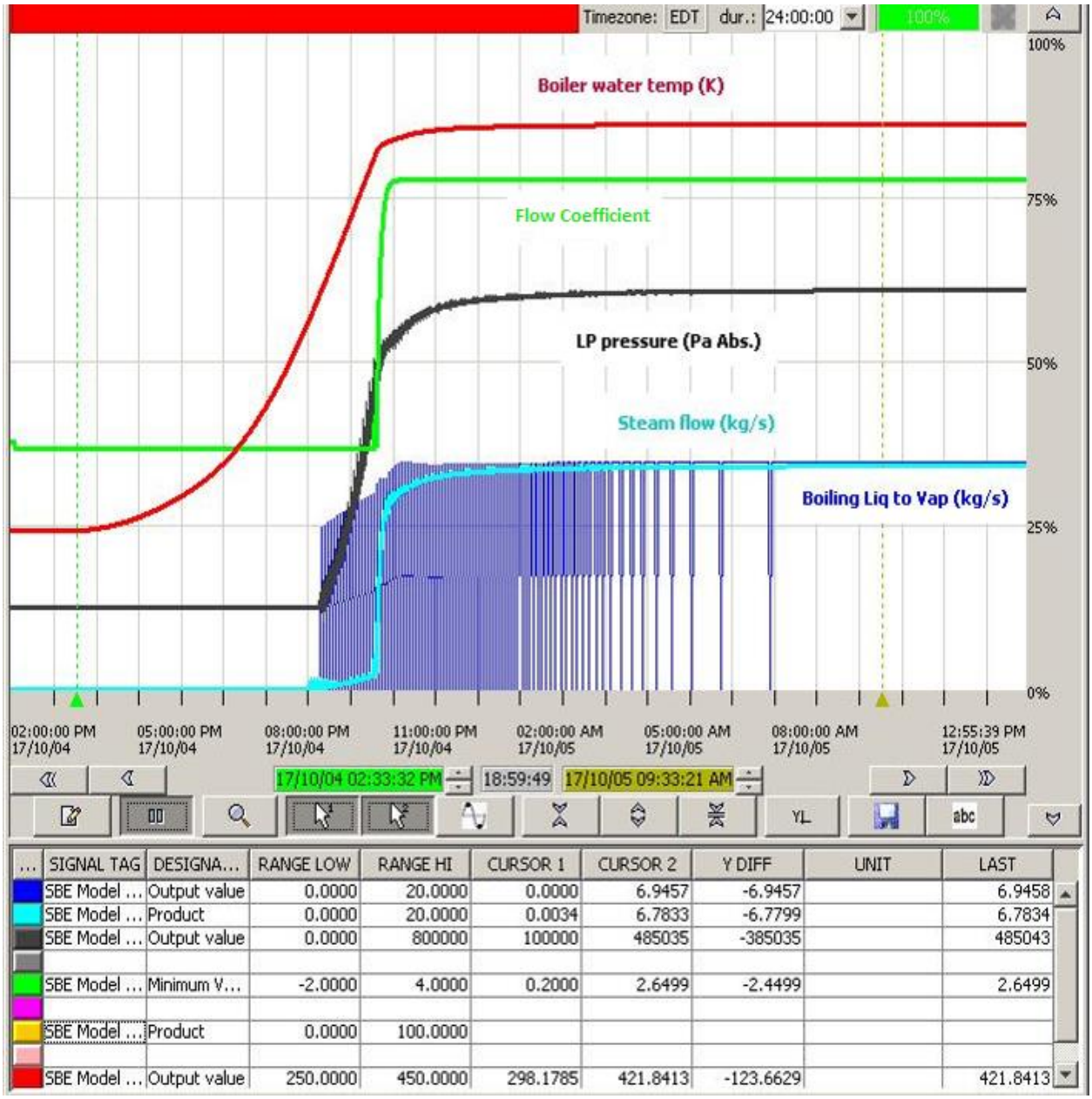

...	SIGNAL TAG	DESIGNA...	RANGE LOW	RANGE HI	CURSOR 1	CURSOR 2	Y DIFF	UNIT	LAST
	SBE Model ...	Output value	0.0000	20.0000	0.0000	6.9457	-6.9457		6.9458
	SBE Model ...	Product	0.0000	20.0000	0.0034	6.7833	-6.7799		6.7834
	SBE Model ...	Output value	0.0000	800000	100000	485035	-385035		485043
	SBE Model ...	Minimum V...	-2.0000	4.0000	0.2000	2.6499	-2.4499		2.6499
	SBE Model ...	Product	0.0000	100.0000					
	SBE Model ...	Output value	250.0000	450.0000	298.1785	421.8413	-123.6629		421.8413

Figure 5.9: Flow and pressure trends for the low-pressure simulation II

Modeling the ST bypass valve was accomplished by first determining the flow coefficient range. A wide open bypass valve corresponds to complete flow restriction into the ST and a flow coefficient of (nearly) zero. A fully closed bypass valve is related to an unimpeded steam flow into the ST and was calculated using a mass balance shown in Equation (5.1).

$$\dot{m} = K_f \sqrt{\rho} \sqrt{\Delta P} \tag{5.1}$$

In the equation above, $\dot{m}$ is mass flow rate, ρ is density, and ΔP is the pressure drop across the valve. By rewriting this expression to solve for the flow coefficient, we get the following.

$$K_f = \frac{\dot{m}}{\sqrt{\rho} \sqrt{\Delta P}} \tag{5.2}$$

Using steady-state design parameters for the low-pressure HRSG, we determined the flow coefficient for this system to be 2.65 when the valve is fully closed.

Two control theories were considered for the implementation of the bypass valve flow coefficient. As shown in Figure 5.11, a bang-bang controller (box A) and proportional-integral (PI) controller (box B) were created to determine which would be the most appropriate.

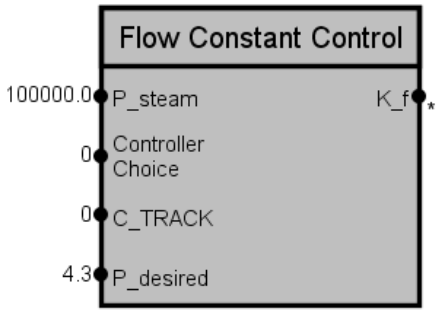

Figure 5.10: SPPA-T3000 block for the flow coefficient control

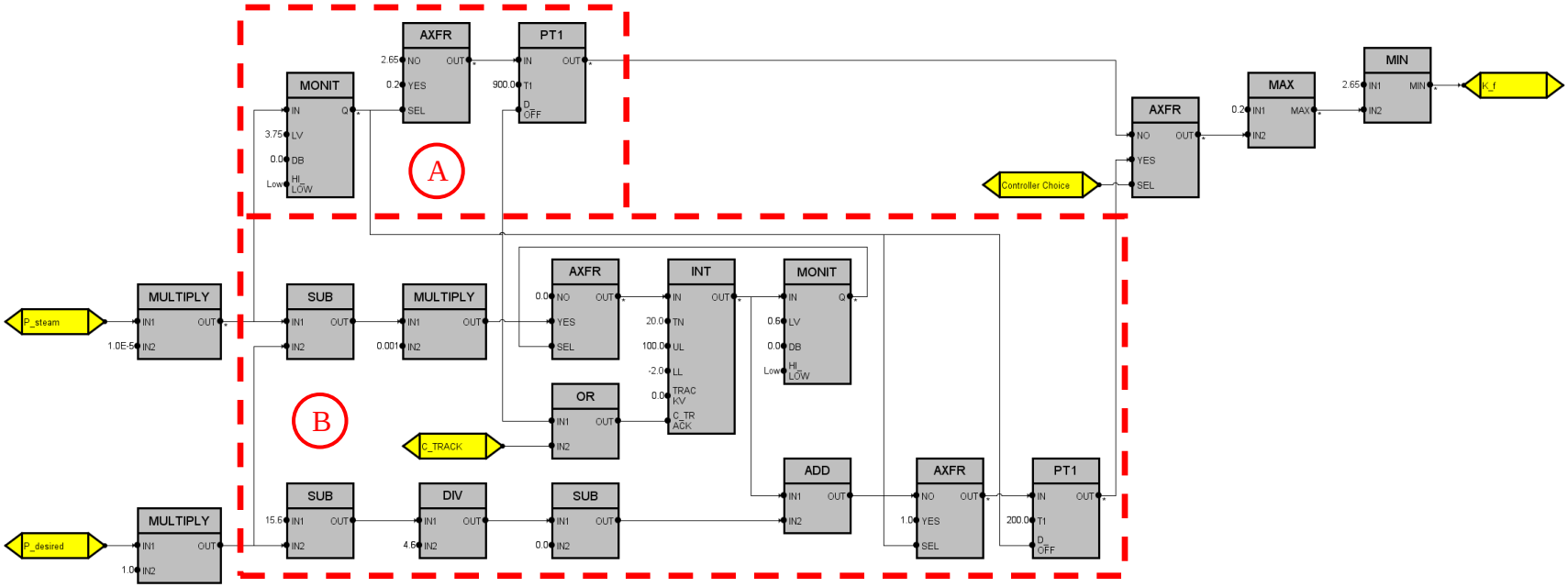

Figure 5.11: SPPA-T3000 block diagram of the flow coefficient control

While both control approaches functioned adequately, the bang-bang controller more closely resembled the actual plant bypass valve and was therefore chosen. This type of controller behaves like a simple on-off switch. The flow coefficient value is initially set to zero which describes the bypass valves fully open position during plant startup. Once the steam has reached acceptable superheated conditions, the valve will begin to close to direct steam flow to the ST. When the steam pressure reaches this acceptable level, the controller will switch the flow coefficient to 2.65 which represents the valve in a fully closed position. In reality, the valve does not switch from a wide open to an entirely closed state instantaneously. This process happens more gradually to prevent significant pressure fluctuations or steam hammer from occurring. A first-order time delay (PT1) was applied to the flow coefficient value to correct this inaccuracy. The time lag will enable the bypass valve to close more steadily to a fully sealed state. Furthermore, the time delay is tunable which will allow the flow coefficient to mimic the steam flow rise time accurately. Future research on this topic is needed to develop a more robust control scheme and more closely model the turbine bypass system [15].

5.3.3.2 Flue Gas Inlet Conditions

Incoming exhaust from the GT provides the thermal energy necessary to boil water and produce steam. However, the heat content of the flue gas entering the HRSG is not constant and ramps up during GT startup. In the Panda Stonewall energy facility, the Siemens SGT6-5000F gas turbine is employed to generate electricity and consequently produce exhaust. To represent this GT's flue gas transient behavior, we modeled a generic start-up profile for this gas turbine in T3000. This data was utilized to provide a link between the GT start-up behavior and the inlet conditions to the HRSG. The rotor speed and megawatt load largely define the GT start-up

conditions. These two parameters were plotted versus time in T3000 to correlate them to the simulation time. Next, the exhaust temperature and flow rate were related to rotor speed and megawatt load. This correlation was done to connect GT start-up behavior to the HRSG inlet conditions during a plant startup. As GT rotor speed and load increases over time, the exhaust temperature and flow rate will also increase correspondingly. Furthermore, if the rotor speed and load are held constant, the exhaust temperature and flow will respond accordingly like in an actual plant startup.

The gas turbine profile modeled in T3000 is a normalized plot with respect to reference values. This diagram is a function of time and percentage which makes the GT start-up profile modular. While these curves will remain identical in shape, we can increase or decrease their reference values to produce different transient results. For instance, we can raise the maximum exhaust temperature and flow rate so that this profile can be applicable in future intermediate-pressure and high-pressure HRSG models. Since the SGT6-5000F start-up profile used in this thesis is confidential, below in Figure 5.12 [16] is an example of a typical GT start-up curve.

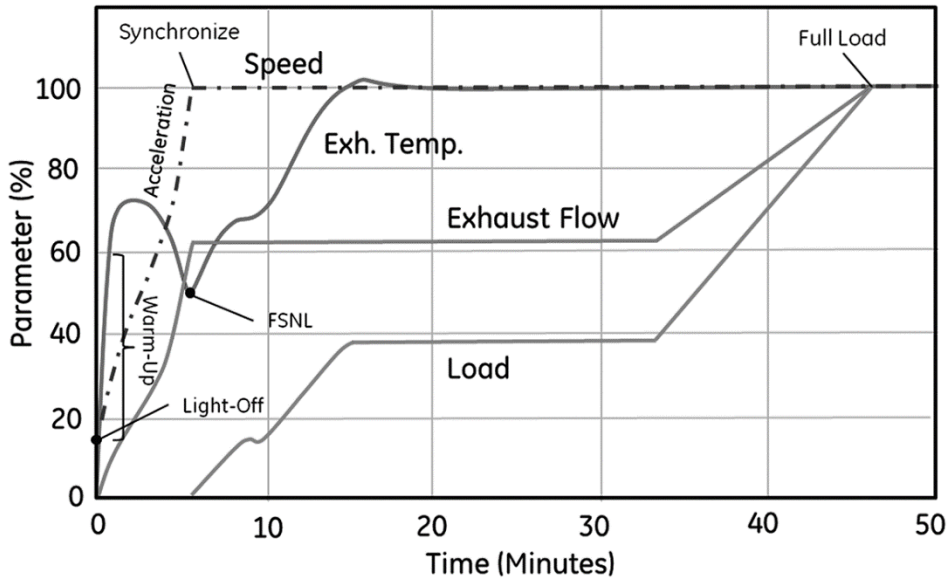

Figure 5.12: Example of a normalized gas turbine start-up profile

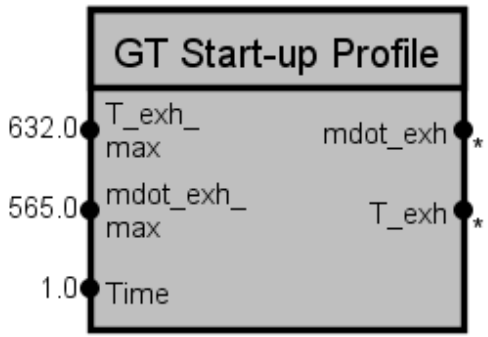

Figure 5.13: SPPA-T3000 block for the gas turbine start-up profile

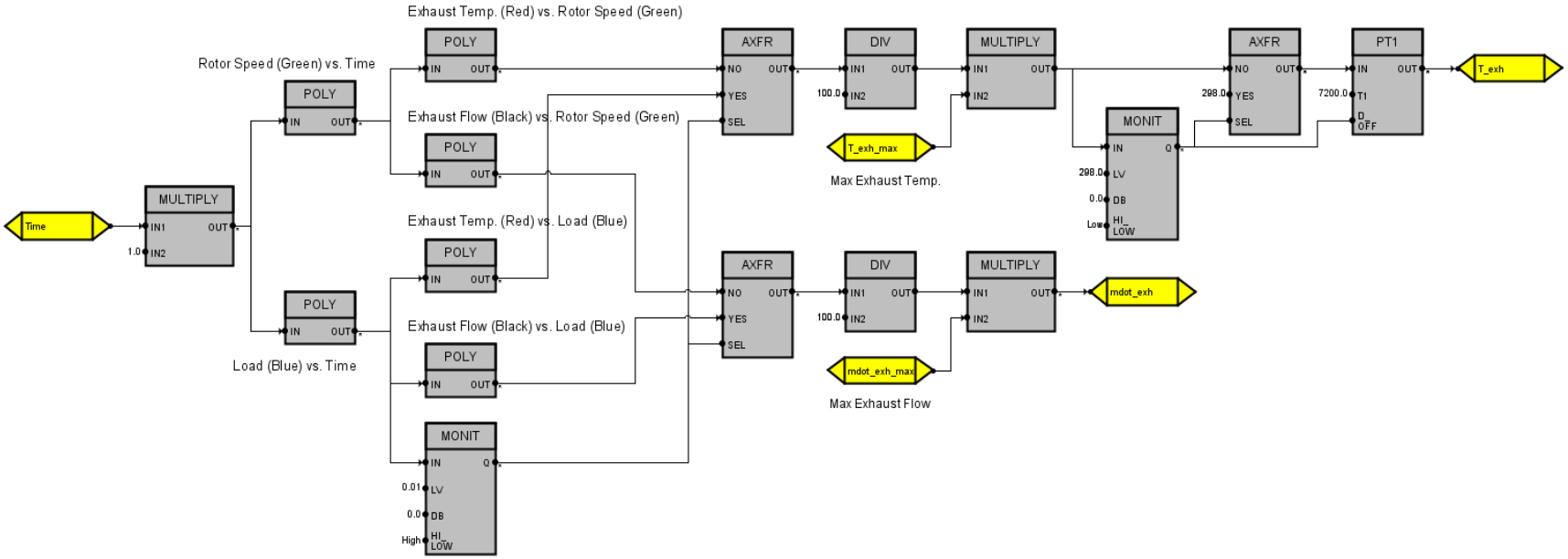

Figure 5.14: SPPA-T3000 block diagram of the gas turbine start-up profile

5.3.3.3 Boiler Level Control

Maintaining an appropriate boiler drum level is central to the proper operation of a heat recovery steam generator. If the water level is too low, there will not be enough liquid in the evaporator piping to extract the flue gas heat. The pipe bundles will overheat and rupture resulting in plant downtime for repairs. Inversely, if the water level is too high, the moisture separation process within the drum will become impaired. The boiler efficiency will reduce, and the water content within the vapor can damage downstream components such as the superheater piping or steam turbine. In order to avoid these expensive and hazardous issues, boiler level control is implemented. The goal of this control scheme is to raise the drum up to the desired level during plant startup and maintain this drum level throughout steady-state operation. A depiction of the level control system for a boiler drum is shown in Figure 5.15 [17].

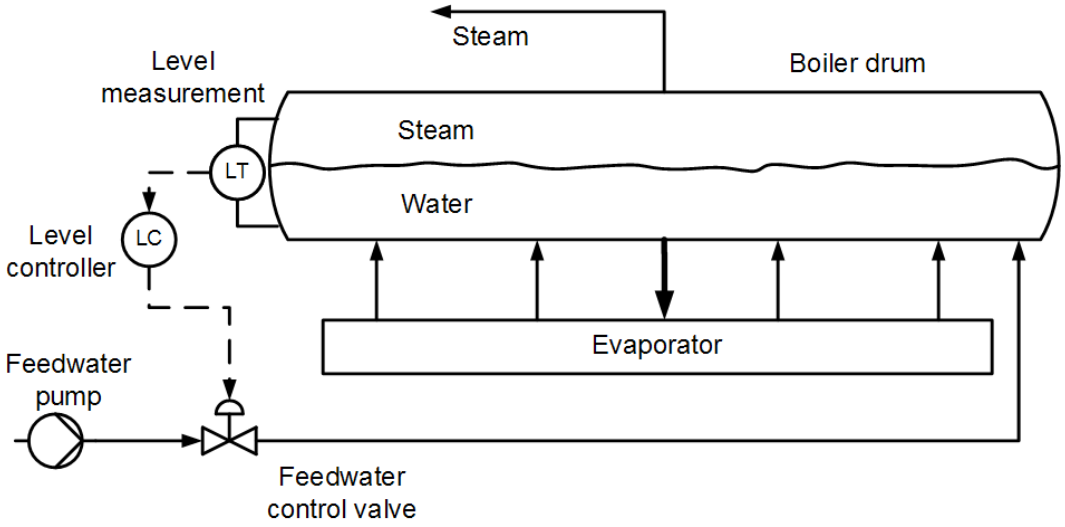

Figure 5.15: Diagram of a boiler drum level control system

As shown in Figure 4.16, the boiler level is managed by a proportional-integral-derivative (PID) controller. This continuous control mechanism first calculates the difference between the desired setpoint and the measured boiler level. Based on this error, the corresponding correction

is made to either allow more or less feedwater mass flow into the boiler. The resulting change in mass flow rate causes a recalculation of the boiler drum level. Thus, the updated drum level is measured, and the closed-loop feedback system repeats. During plant startup, the difference in desired and actual drum level is vast which produces a proportionately large controller response. The feedwater mass flow rate into the evaporator will fluctuate in an attempt to meet the desired drum level. PID controller gains were conservatively chosen and tuned to minimize mass flow rate overshoot and prevent boiling instability. A more aggressive approach to control loop tuning may be considered in future research to more quickly reach the desired drum level and steady-state mass flow. Boiler swell and shrink is another area of future research that would dramatically improve the boiler model. The work of Karl Åström and Rodney Bell in [18], [19], and [20] will considerably aid in the implementation of these, as well as other boiler phenomena. Hence, providing to a more realistic test bench for the development of boiler level control algorithms [21]. Figure 5.16 shows the PID controller used to manage boiler flow level during T3000 simulations.

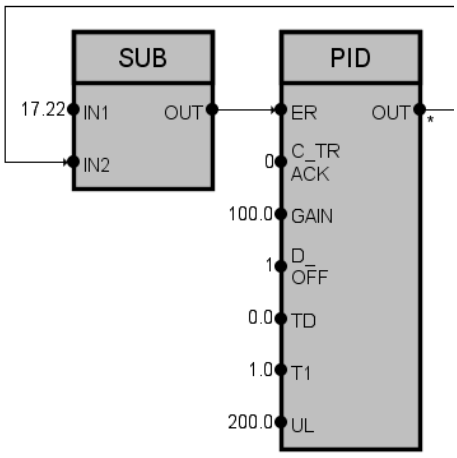

Figure 5.16: SPPA-T3000 block for boiler level control

CHAPTER 6: CONCLUSION

6.1 Overview of Research

Even though nonrenewable energy resources are dwindling, fossil fuel power stations remain the primary producer of electricity worldwide. To economically utilize the remaining nonrenewable fuel sources, we look to the advancement of combined-cycle power plant technology. The heat recovery steam generator is essential to the operation and efficiency of a CCPP. To that end, this thesis discussed the thermodynamic modeling of a HRSG to deepen our comprehension of their dynamic and transient behavior. The thermodynamic model was developed from fundamentals of heat transfer, phase change, fluid dynamics, conservation laws and unsteady flow energy equations. These physical phenomena were characterized using mathematical equations to capture the essential system dynamics. This network of expressions was implemented on the SPPA-T3000 platform which proved to be a feasible programming environment. The resulting model aimed to accurately simulate the transient and steady-state response of a heat recovery steam generator. The T3000 model was validated by comparing simulation results to start-up data from the low-pressure system of a Siemens power plant using the same operating conditions and geometric parameters. Simulation results correlated well with plant data regarding transient behavior and equilibrium conditions to prove the model's legitimacy. Thus, the comprehensive LP HRSG model will allow for further research to transpire and support the progression of steam power system technology.

6.2 Assumptions and Future Research

With an acceptable model operational, the goal of future research is to remove some of the assumptions and simplifications made during the modeling process. In doing so, the system will

more closely resemble a HRSG and hopefully produce more accurate results. With that being said, the model will not be able to correlate to Siemens plant data flawlessly. The lumped modeling approach taken in this thesis simplifies the model, which consequently reduces its accuracy. Regardless, the model was never expected to correlate with plant data perfectly. A significantly more extensive and intricate model would be necessary for that ambition to be attainable. Furthermore, it was not our desire to over tune model parameters to match plant data so that they exactly corresponded. This model intends to provide a better understanding of transient and steady-state behavior. To accomplish this, we did need to adjust specific parameters such as heat transfer coefficients and flow coefficient. However, we ultimately wanted to let the physics dictate the system response. This would allow the model to be easily modifiable when attempting to simulate different plant configurations.

6.2.1 Lumped Capacitance Analysis

Heat transfer coefficients (HTCs) were estimated and turned during model validation in relation to Siemens data. While this was a useful procedure in creating a baseline for the heat transfer coefficients, it is not the most precise method. Once more, the heat transfer coefficients in this model are set as constants which represented an average HTC. In reality, this parameter is not fixed and evolves during phase change throughout the thermodynamic cycle. A convective HTC depends on the flow regime, fluid-to-solid temperature difference, and fluid thermo-physical properties (viscosity, density, etc.) among other various parameters. These properties will vary during vaporization which would cause the HTC also to fluctuate. In future work, we plan to remove the constant HTC assumption and consider using an inverse lumped capacitance method. As described in [22] and [23], this approach can be applied to back-calculate the heat transfer

coefficients for industrial-sized heat exchangers. Thus, it may also be applicable to the HRSG model and provide a more accurate simulation of heat transfer during transient operation.

6.2.2 Logarithmic Mean Temperature Difference

As hot exhaust gas passes through the HRSG, it transfers a portion of its thermal energy to the metal pipe bundles. This heat transfer is captured within the low-pressure HRSG model inside each flue gas control volume. Initially, we used the outlet flue gas temperature in the convective heat transfer equation to compute the metal temperature. However, we felt that the outlet flue gas would be at a lower temperature than the actual exhaust gas heating the metal. Therefore, we took the inlet and outlet temperatures of the flue gas control volume and used their average to calculate the metal temperature. This change improved simulation results and was retained during the validation process in this thesis. In future research, we plan to investigate the feasibility of using a logarithmic mean temperature difference (LMTD) in place of the mean temperature calculation. Since temperature change along a heat exchanger is exponential, a linear temperature average may not be sufficient in adequately describing the model. Thus, the arithmetic mean can be replaced with a logarithmic mean to accurately describe the heat transfer in the flue gas control volume.

6.2.3 Evaporative Cooling Mode

As described in Section 5.3.1.1, the liquid will remain in heating mode until it exceeds the saturation temperature deadband. Once this happens, the liquid will enter boiling mode and transfer mass to the vapor. Boiling will continue until the liquid temperature falls outside of the saturation temperature deadband. Typically, the vapor temperature will dramatically increase while the liquid temperature remains constant. This phenomenon causes the vapor pressure to rise, and a

recalculation of the saturation temperature to ensue. As the liquid temperature falls beneath the new saturation temperature deadband, it returns into heating mode. However, an alternative thermodynamic process called evaporative cooling can occur. This phenomenon can take place if the system cools down due to a reduction of input thermal energy. The consequence is a rapid decrease of the vapor temperature which lowers the liquid saturation temperature. If the saturation temperature deadband were to drop below the liquid temperature, evaporative cooling would occur. During evaporative cooling, the liquid temperature is allowed to change, and mass transfer is present between the liquid and vapor. This combination can provoke the liquid temperature to cool, and decrease below the saturation temperature, and return to boiling mode. An increase of input thermal energy could also cause the saturation temperature to surpass the liquid temperature and cause boiling to resume. With the addition of a cooling mode, this would allow for boiler depressurization during plant startup and shutdown procedures. Including this feature would lead to a more comprehensive model and a deeper understanding of the HRSG. A visual depiction of the heating, boiling, and cooling mode switching conditions is shown in Figure 6.1.

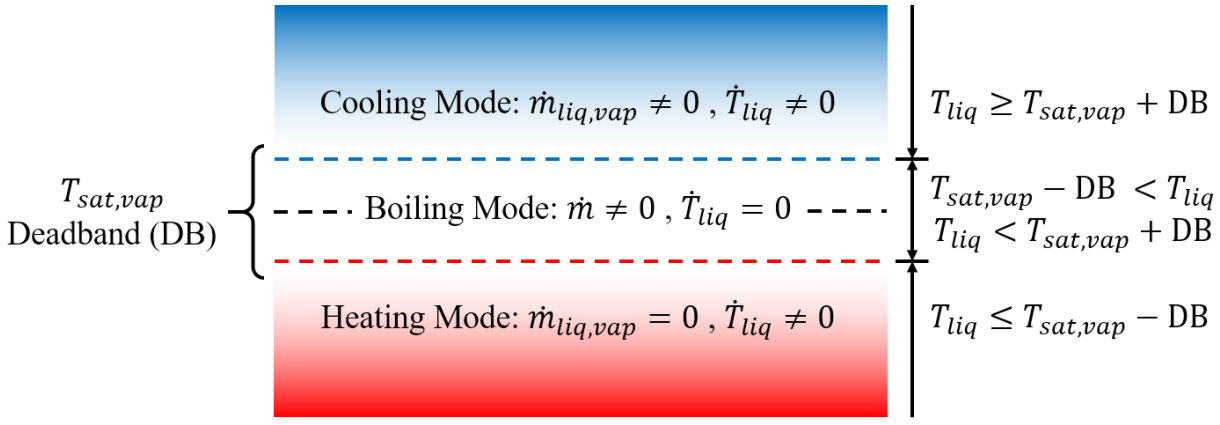

Figure 6.1: Heating, boiling, and cooling mode switching conditions

6.2.4 Thermodynamically Closed System

Throughout this research, we considered the HRSG to be an isolated system. This idealization meant there was no exchange of energy or matter between the system and its surrounding environment. In reality, the HRSG is well insulated to prevent heat loss and enhance combined-cycle efficiency. However, the system it is not perfectly isolated and does dissipate a small amount of heat to its surroundings. In future research, we can consider lifting this idealization and model the system as closed. This condition will allow the HRSG to exchange energy with its environment, but prevent the transfer of matter. One way this idea can be realized is by modifying the flue gas control volume. This domain expands to fill the interior volume of the HRSG and encompasses the metal and medium CVs. Currently, the flue gas only participates in heat transfer with the metal pipe bundles. To simulate heat loss, we can allow a small portion of flue gas thermal energy to partake in heat transfer with the insulated HRSG casing. While the decrease in flue gas temperature would be small, it will capture the imperfect nature of heat transfer within the system. This change will improve the model's authenticity and lead to an improved correlation with Siemens plant data.

6.2.5 Complete HRSG Model

The next major objective of this research is to model the intermediate-pressure (IP) and high-pressure (HP) systems of the HRSG. Since an acceptable model of the low-pressure side is already available, we have a design template for the other two systems. The IP and HP sections of the HRSG also contain economizer, evaporator, and superheater modules. We can use these modular elements from the existing LP system to construct the remaining portions of the HRSG. Once the IP and HP systems are invented, we can integrate them with the existing LP model to

create a fully functioning three-pressure HRSG. With a complete HRSG model constructed, we can remove some assumptions and simplifications made for each system.

A necessary assumption that can be lifted is the approximate flue gas temperature at the LP system inlet. As described in Section 5.2.2, the flue gas entry temperature at the LP superheater is an estimated value. Since Siemens had no temperature information at that location, we made an educated guess. Based on HRSG documentation for the Stonewall power plant, we assumed the flue gas inlet temperature to be 700 K. Now that all three pressure systems are combined, this assumption can be abolished. We know the flue gas inlet temperature into the complete HRSG is 880 K. With this inlet condition known, the model physics will determine flue gas temperatures throughout the system.

Another assumption made in the LP model is considering pressure variation along the flue gas path to be negligible. For the low-pressure system, this simplification was viable. Initial experiments showed the pressure change within the flue gas control volumes to be insignificant. However, this notion may be removed for the complete HRSG model. As shown in Figure 2.5, flue gas will enter at the HP superheater, and exit after the feedwater heater (LP economizer). Due to the large temperature gradient between these locations, the pressure drop may be substantial. Therefore, it would be inappropriate to ignore pressure variation along the flue gas path. Future studies of the complete HRSG model will need to be carried out. However, it is likely that removing the previously stated assumption would lead to an improved correlation between simulation results and plant data.

In addition to exploring the challenge of modeling a triple-pressure HRSG, there lie other opportunities beyond the scope of this thesis to improve our understanding of combined-cycle power plants. Another area of research would involve developing a comprehensive, physics-based

model for the steam turbine, gas turbine, and condenser similarly to the HRSG. These three components, along with the HRSG, form the basis of a combined-cycle plant. Integrating these elements into a singular system would form a rudimentary model capable of simulating the transient and steady-state response of a combined-cycle power plant. The work presented in this thesis hopefully serves as a stepping stone on the path to accomplishing this objective, for an even greater goal of improving plant efficiency is in mind. This advancement in power generation technology would secure the prosperity of society today, and enhance the welfare of future generations.

APPENDIX: THESIS DEFENSE ANNOUNCEMENT

Announcing the Final Examination of Andres Caesar for the degree of Master of Science

Time & Location: June 18, 2018 at 10:30 AM in ENGR2 202A
Title: Thermodynamic Modeling and Transient Simulation of a Low-Pressure Heat Recovery Steam Generator Using Siemens T3000

With world energy consumption rising, and nonrenewable energy resources being quickly depleted, it is important to design more efficient power plants and thereby economically utilize fossil fuels. To that end, this work focuses on thermodynamic modeling of steam power systems to enhance our understanding of their dynamic and transient behavior. This thesis discusses the physical phenomena behind a heat recovery steam generator (HRSG) and develops a mathematical description of its system dynamics. The model is developed from fundamentals of fluid dynamics, phase change, heat transfer, conservation laws and unsteady flow energy equations. The resulting model captures coupled physical phenomena with acceptable accuracy while achieving fast, and potentially real-time, simulations. The computational HRSG model is constructed in the Siemens T3000 platform. This work establishes the dynamic modeling capability of T3000, which has traditionally been used for programming control algorithms. The validation objective of this project is to accurately simulate the transient response of an operational steam power system. Validation of the T3000 model is carried out by comparing simulation results to start-up data from the low-pressure system of a Siemens power plant while maintaining the same inlet conditions. Simulation results are well correlated with plant data in terms of transient behavior and equilibrium conditions. With a comprehensive HRSG model available, it will allow for further research to take place, and aid in the advancement of steam power system technology. Some future research areas include the extension to intermediate and high-pressure system simulations, combined simulation of all three pressure stages, and continued improvement of the boiler model. In addition to enabling model-based prediction and providing further insight, this effort will also lead to controller design for improved performance.

Major: Mechanical Engineering

Educational Career:
Bachelor’s of Mechanical Engineering, BS, 2015, University of Florida

Committee in Charge:
Tuhin Das, Chair, Mechanical & Aerospace Engineering
Shawn Putnam, Mechanical & Aerospace Engineering
Samik Bhattacharya, Mechanical & Aerospace Engineering

Approved for distribution by Tuhin Das, Committee Chair, on June 11, 2018.

The public is welcome to attend.

REFERENCES

[1] (2017, 17-June-2018). *How It Works - Renaissance Energy Center*. Available: https://www.renaissanceenergycenter.com/how-it-works/

[2] (2015, 16-June-2018). *TVA - Caledonia Combined Cycle Plant*. Available: https://www.tva.gov/Energy/Our-Power-System/Natural-Gas/Caledonia-Combined-Cycle-Plant

[3] J. Dahl, "Jet Engine," ed. Wikimedia Commons: Wikimedia Commons, 2007.

[4] "GE THERMOELECTRIC GENERATOR WILL GENERATE POWER TO SUPPLY EXTRA DEMAND FOR THE RIO 2016 OLYMPIC AND PARALYMPIC GAMES," *DINO News Discloser*, p. 2, 08-02-2016. Accessed on: 27-June-2018Available: http://www.dino.com.br/releases/termeletrica-com-turbinas-ge-vai-gerar-energia-para-suprir-demanda-extra-dos-jogos-olimpicos-e-paralimpicos-rio-2016-dino89093768131

[5] HRSG Inspection Tools, TesTex, ed.: TesTex, 2015, p. 8. [Online]. Available: http://www.testexndt.co.uk/wp-content/themes/_testex%202.0/resources/HRSG-NDT-Brochure-Spring-15-rev1.pdf. Accessed on 17-June-2018.

[6] Precious Power Plants, D. o. P. S. Engineering, ed.: University of West Bohemia, 2012, p. 51. [Online]. Available: https://kke.zcu.cz/export/sites/kke/old_web/_files/projekty/enazp/24/MMP/174_Soucasne_elektrarny_Prezentace_Sliva.pdf. Accessed on 17-June-2018.

[7] SST-900 Industrial Steam Turbines, Erlangen: Siemens AG, 2009, p. 4. [Online]. Available: https://www.energy.siemens.com/ru/pool/hq/power-generation/steam-turbines/SST-900/downloads/SST-900_en.pdf. Accessed on 5-June-2018.

[8] (2018, 25-June-2018). *Utility steam turbines - proven technology*. Available: https://www.siemens.com/global/en/home/products/energy/power-generation/steam-turbines/utility-steam-turbines.html

[9] "Siemens delivers steam turbine-generator sets and I&C components to India," ed: Siemens AG, 2013.

[10] Water Management Program Workshop, Pittsburg: National Energy Technology Laboratory, 2016, p. 33. [Online]. Available: https://www.netl.doe.gov/File%20Library/Events/2016/Proceedings/Water%20Workshop/6-Carney-NETL-2016-Water-Workshop.pdf. Accessed on 16-June-2018.

[11] (2016, 16-June-2018). *Surface Condenser*. Available: http://www.dh.co.kr/surface-condenser/?ckattempt=2

[12] Kelvion, "Kelvion Vacuum Steam Condensers - MASH Design," ed: Kelvion, 2016.

[13] (2017, 25-June-2018). *Kahnooj project*. Available: https://www.mapnamd1.com/Mapna/General/DisplayProject/cc28d942-ec70-4988-9287-8685bb83d481

[14] E. Coale. (2017, 16-June-2018). *GAS TURBINE HEAT RECOVERY STEAM GENERATORS: 101*. Available: https://www.victoryenergy.com/articles/gas-turbine-heat-recovery-steam-generators-101/

[15] F. Alobaid, R. Postler, J. Ströhle, B. Epple, and H.-G. Kim, "Modeling and investigation start-up procedures of a combined cycle power plant," *Applied Energy*, vol. 85, no. 12, pp. 1173-1189, 2008/12/01/ 2008.

[16] S. Can Gülen and K. Kim, "Gas Turbine Combined Cycle Dynamic Simulation: A Physics Based Simple Approach," *Journal of Engineering for Gas Turbines and Power*, vol. 136, no. 1, pp. 011601-011601-15, 2013.

[17] J. F. Smuts, "Inverse Response," in *Control Notes - Reflections of a Process Control Practitioner* vol. 2018, ed: OptiControls Inc., 2013.

[18] K. J. Åström and R. D. Bell, "Drum-boiler dynamics," *Automatica*, vol. 36, no. 3, pp. 363-378, 2000.

[19] K. J. Åström and R. D. Bell, "Simple drum-boiler models," in *Power Systems: Modelling and Control Applications*: Elsevier, 1989, pp. 123-127.

[20] R. D. Bell and K. J. Åström, "A fourth order non-linear model for drum-boiler dynamics," *IFAC Proceedings Volumes*, vol. 29, no. 1, pp. 6873-6878, 1996.

[21] G. Pellegrinetti and J. Bentsman, "Nonlinear control oriented boiler modeling-a benchmark problem for controller design," *IEEE Transactions on Control Systems Technology*, vol. 4, no. 1, pp. 57-64, 1996.

[22] Y. Y. Kim, K. S. Kim, G. H. Jeong, and S. Jeong, "An experimental study on the quantitative interpretation of local convective heat transfer for a plate fin and tube heat exchanger using the lumped capacitance method," *International Journal of Heat and Mass Transfer*, vol. 49, no. 1-2, pp. 230-239, 2006.

[23] I. Mohamed, "An inverse lumped capacitance method for determination of heat transfer coefficients for industrial air blast chillers," *Food research international*, vol. 41, no. 4, pp. 404-410, 2008.